Winter 12-15-2018

Molecular Basis of Class Ib Drug Interactions with the NaV Channel Macromolecular Complex: A Route to Personalized Medicine for Cardiac Arrhythmia

Wandi Zhu
Washington University in St. Louis

WASHINGTON UNIVERSITY IN ST. LOUIS

School of Engineering and Applied Science

Department of Biomedical Engineering

Dissertation Examination Committee:
Jonathan Silva, Chair
Jianmin Cui
Jeanne Nerbonne
Stacey Rentschler
Yoram Rudy

Molecular Basis of Class Ib Drug Interactions with the Na_V Channel Macromolecular Complex: A Route to Personalized Medicine for Cardiac Arrhythmia

by
Wandi Zhu

A dissertation presented to
The Graduate School
of Washington University in
partial fulfillment of the
requirements for the degree
of Doctor of Philosophy

December 2018
St. Louis, Missouri

Table of Contents

List of Figures

List of Tables

Acknowledgments

The completion of my dissertation will not be possible without my mentor Dr. Jonathan Silva. Beyond his guidance in research, he has helped me to develop skills for becoming an independent scientist. He inspired me to remain curious and enjoy the excitement of every small finding. His optimism and enthusiasm have influenced me personally. I want to thank him for his continuous support and inspiration. I simply cannot imagine having a better mentor.

I am also very grateful to have such a dedicated and supportive committee. Each committee member helped me tremendously throughout my PhD. training. Particularly, Dr. Jeanne Nerbonne for her generously support in many of my projects, Dr. Jianmin Cui for his guidance in ion channel biophysics, Dr. Stacey Rentschelar for giving me many valuable clinical insights, Dr. Rudy for his intelligent advices and encouragements.

I would also like to thank the entire Silva lab, present and past, not only for their help in terms of research, but also for their encouragement and company as some of my best friends. I had a wonderful time working in lab because of them.

Many of my projects would not be completed without resources and help from our collaborators. Particularly, I want to thank Dr. Kristen Naegle for inspiring me and guiding me through the field of system biology. Dr. Silvia Priori, Dr. Andrea Mazzanti for sharing their precious clinical data. Dr. Jeanne Nerbonne and Dr. David Wang, Rebecca Mellor for helping us with mouse electrophysiology and biochemistry. Dr. Jianmin Cui and the rest of Cui lab for collaborating with us for the frog surgeries. I want to give special thanks to my collaborator and friend Dr. Panpan Hou for his kindness and generous support throughout all these years. I also want to

thank other collaborators that I co-authored with, for making the publication process easy and pleasant.

I want to thank the BME department chair, staff and faculties. They have made many tedious processes easy for us, so we can focus on research.

None of the research would be possible without our funding support. Personally, I want to thank the CBSE center and the American Heart Associations for giving me fellowships.

Finally, I want to give special thanks to my family, friends and my dog Rizzo. They are the reasons that I got through my hardest days and had my greatest days.

Wandi Zhu

Washington University, December 2018

This dissertation is dedicated to my dear parents.

You have supported every decision I made in my life.

I am more than lucky to have both of you.

ABSTRACT OF THE DISSERTATION

Molecular Basis of Class Ib Drug Interactions with the NaV Channel Macromolecular Complex: A Route to Personalized Medicine for Cardiac Arrhythmia

by

Wandi Zhu

Doctor of Philosophy in School of Engineering and Applied Science

Department of Biomedical Engineering

Washington University in St. Louis, 2018

Professor Jonathan Silva, Chair

The heart rhythm is precisely controlled by the electrical impulse that propagate in the cardiac tissue. In single cardiomyocytes, the electrical activity generated by action potentials (AP). Cardiac Na_V channels ($Na_V1.5$) carry a large influx of Na^+ that mediates the initiation and propagation of the AP in both atria and ventricles. Disruption of $Na_V1.5$ function by genetic variants or external factors can result in deadly arrhythmias, such as long QT syndrome and Brugada syndrome. Thus, Na_V channels are import therapeutic targets. The class I antiarrhythmics are the modulators of the Na_V channels. Although they have been used clinically for over 100 years, detailed mechanisms of their action are not well understood. The Na_V channel co-assembles with many regulatory and accessory proteins to form a macromolecular complex that tailor channel function to different cells. The complicated multi-molecular interactions add another level of complexity in dissecting the drug mechanisms.

The pore-forming $Na_V1.5$ α-subunit contains four domains (DI-DIV), each with a voltage sensing domain (VSD). The voltage clamp fluorometry (VCF) method probes the conformational changes of each VSD by attaching a fluorophore on it. Here, we utilized VCF to measure how the accessary β-subunits and Class Ib antiarrhythmics affect the conformational dynamics of the $Na_V1.5$.

We found that the non-covalently linked β1 and β3 subunits regulate channel gating by altering the DIII and DIV-VSD dynamics. Moreover, results from multiple experiments provided compelling evidence that β1 and β3 bind proximally to the DIII-VSD.

The DIII-VSD also plays an important role in channel's interaction with Class Ib antiarrhythmics, such as lidocaine, ranolazine and mexiletine. Recent clinical studies showed that mexiletine is effective in treating patients with LQT3 syndrome. However, the patient response is variable, depending on the genetic mutation in Na_V 1.5. We showed that mexiletine altered the conformation of the DIII-VSD, which is the same VSD that many tested LQT3 mutations affect. Analysis of 15 LQT3 variants showed a strong correlation between the activation of the DIII-VSD and the strength of the inhibition of the channel by mexiletine. Based on this improved molecular-level understanding, we generated a systems-based model that successfully predicted the response of 7 out of 8 patients to mexiletine in a blinded, retrospective clinical trial. The new model can be used to personalize treatment for LQT3 patients, and improving therapeutic decision making.

As the non-covalently linked β subunits and the Class Ib antiarrhythmics both interact with the same part of the Na_V channel. We further investigated how β expression affects the Class Ib drug effectiveness. We found that β1 differentially modulates lidocaine and ranolazine blockade of

$Na_V1.5$. The molecular mechanism underlying this phenomenon is due to altered drug interaction with the DIII-VSD. In human hearts, β1 expresses at levels that are 3-fold higher in the atria compared to ventricles. Thus, this molecular difference can be targeted to develop chamber specific antiarrhythmic therapies.

In conclusion, we demonstrated the essential role of the DIII-VSD dynamics in modulating Na_V channel response to the Class Ib antiarrhythmics. This molecular interaction is regulated by the accessary β subunits. We hope to apply this mechanistic insight to improve current antiarrhythmic therapeutic approaches.

Chapter 1

Introduction

1.1 $Na_V1.5$ macromolecular signaling complex

The heart is an electrical and mechanical organ that pumps blood to the circulation system to maintain constant blood flow of the body. The activity of the heart is delicately controlled by the electrical signal that travels through the tissue. The electrical rhythm is first initiated by a group of cells called pacemaker cells in the SA node, which is then conducted through cells known as cardiomyocytes in the atrium and ventricle to cause contraction of the heart (Zipes & Jalife, 2013). In individual cardiomyocyte, the electrical activity is reflected as action potentials (AP), as the cell membrane potential depolarizes and repolarizes. The AP is controlled by varies well-balanced ionic currents through the membrane, which are carried by the ion channels (Nerbonne & Kass, 2005). When electrical impulse reaches the cardiomyocyte, it depolarizes the membrane to reach the threshold for opening the Na_V channels. Then, Na_V channels rapidly open, carrying a large influx of Na^+ ions that greatly depolarizes the membrane (Bertil Hille, 2001). Thus, Na_V channel controls the upstroke of AP and propagation of electrical signal in both atria and ventricles.

Since the Na_V channel are essential for regulating cardiac excitability, any disturbance of channel function, either by inherited genetic mutations or external factors can lead to serious diseases. Cardiac arrhythmia is a pathological condition where the heart loses its regular rhythm and stops

pumping blood efficiently. Na_V channel dysfunction can cause arrhythmias such as Long QT syndrome (Schwartz et al., 2001), Brugada syndrome (Brugada & Brugada, 1992) and atrial fibrillation (Morten S Olesen, Nielsen, Haunsø, & Svendsen, 2014). All those types of arrhythmias are extremely dangerous, as they can result in sudden cardiac death if not terminated in time. Hence, Na_V channel are important therapeutic targets.

1.1.1 Voltage-gated Na_V Channel Structure and Gating

The eukaryotic Na_V channels all share common structures. They are formed by four homologous domains connected by intracellular linkers. Each domain consists of six transmembrane segments (S1-S6) (Ganetzky, Robertson, Wilson, Trudeau, & Titus, 1999; Gellens et al., 1992b; Itoh et al., 1998; Qin, Yagel, Momplaisir, Codd, & D'Andrea, 2002). The fourth segment (S4) has several positive charged residues (Arginine and Lysine) that drive the S4 segment up cell membrane depolarization. Therefore, the S1-S4 segments are called voltage sensing domain (VSD). The S5-S6 segments of all four domains form the pore, where Na^+ ions pass through. When membrane depolarizes, the VSDs changes their conformations, which are coupled to the pore through the S4-S5 linker and other mechanisms to make the pore open (Aggarwal & MacKinnon, 1996; Bezanilla, 2008; Liman, Hess, Weaver, & Koren, 1991; Seoh, Sigg, Papazian, & Bezanilla, 1996). Their structure is domain-swapped, which means that VSD of one domain is adjacent to the pore of the other domain. This unique assembly mediate the complex couplings of each parts of the channel.

The intracellular linkers and domains also paly an essential role in channels gating. In particular, the DIII-DIV linker contains the IFM motif that is known as the inactivation gate (West et al., 1992). Quickly after channel opens, the inactivation gate moves to interact proximal to the pore. This action occludes the Na^+ flux and cause the channel to inactivate. Inactivation almost

diminishes all the I_{Na}, except a very small portion (~1-2%), which is called the late or sustained I_{Na} (Maltsev, Kyle, & Undrovinas, 2009a). Previous studies suggest that an increase in late INa by signaling molecules, mutations, and drugs can be very arrhythmogenic, because it competes with the repolarizing Ik that results in prolongation of the AP (Zipes & Jalife, 2013).

Unlike potassium channel, which is a tetramer formed by four identical subunits, Na_V channel has an asymmetrical structure, because it is formed by four different domains. Each domain contributes to channel gating distinctively. The DIV-VSD has been shown to associate with channel inactivation, and other three VSDs are more related to channel activation (Albert Cha, Peter C., Alfred L., Esther, & Francisco, 1999). However, more recent literatures suggest that DIII-VSD plays multiple roles in regulating channel activation, inactivation and recovery from inactivation (Hsu et al., 2017a).

1.1.2 Accessary β Subunits Regulate Na_V Channel Function

Na_V channels form macromolecular signaling complexes in cardiomyocytes (Abriel, 2010), whose parts work in concert to regulate channel function. The Nav channel β subunit members of this complex have been shown to regulate cell adhesion (Isom, Ragsdale, et al., 1995b; Jyoti Dhar Malhotra, Kazen-Gillespie, Hortsch, & Isom, 2000a; Yu et al., 2003) and signaling in addition to affecting NaV channel density (Calhoun & Isom, 2014), gating kinetics (Fahmi et al., 2001; H. Watanabe et al., 2009), and pharmacology (Lenkowski, Shah, Dinn, Lee, & Patel, 2003; Uebachs et al., 2010).

The Nav channel β1 and β2 subunits were first to be identified and were purified together with the pore-forming NaV α subunit, from the rat brain (Hartshorne & Catterall, 1984; Messner & Catterall, 1985). Subsequently, three additional members of the family, β1b (Kazen-Gillespie et

al., 2000), β3 (Morgan et al., 2000b) and β4 (Yu et al., 2003) were identified based on homology. β2 and β4 form covalent disulfide bonds with the α subunit (Isom, Ragsdale, et al., 1995a), while β1 and β3 interact non-covalently (Isom, Scheuer, et al., 1995; Morgan et al., 2000b). With the exception of the β1b splice variant (Patino et al., 2011), the β subunits comprise a single transmembrane-spanning domain that is tethered to an extracellular Immunoglobulin (Ig) loop and a cytoplasmic C-terminus (Calhoun & Isom, 2014). Very recently, the covalently bound β2 and β4 were crystallized (Das, Gilchrist, Bosmans, & Van Petegem, 2016; Gilchrist, Das, Van Petegem, & Bosmans, 2013), and a crucial disulfide bond formed by 55Cys in β2 and 910Cys in the DII pore loop was localizing β2 to the DII pore domain (Das et al., 2016). However, 910Cys is not present in Nav1.5, and instead the homologous position is Leu.

The β subunits are widely expressed in many tissues, including the central and peripheral nervous system, the heart, and skeletal muscle (Calhoun & Isom, 2014). Intriguingly, even in the same organ, β subunit localization can differ (Calhoun & Isom, 2014; Fahmi et al., 2001; Yuan et al., 2014). For example, the β1 and β3 subunits have been shown to differentially express in the atria and ventricles (Fahmi et al., 2001; H. Watanabe et al., 2009; Yuan et al., 2014), suggesting that they may specifically tailor NaV channel function according to cell type. The physiological role of the β-subunits is highlighted by the recent linkage between β subunit mutations and epilepsy (Calhoun & Isom, 2014), Dravet syndrome (Calhoun & Isom, 2014), and cardiac arrhythmias, including Brugada Syndrome (Hu et al., 2012; Hiroshi Watanabe et al., 2008), Long QT Syndrome (Medeiros-Domingo et al., 2007; Riuró et al., 2014), Sudden Infant Death Syndrome (Calhoun & Isom, 2014) and atrial fibrillation (Li et al., 2013; M S Olesen et al., 2011) (AF). Further, since β subunits can co-assemble with more than one type of Nav channel, mutations in β subunits can lead to multi-organ diseases. For example, the β1 subunit R85H

variant has been linked to both epilepsy (Xu et al., 2007) and atrial fibrillation (AF) (H. Watanabe et al., 2009). These myriad findings suggest that significant insight into the molecular basis of the many pathologies and drug interactions could be gained via a deeper understanding of the mechanisms of NaV channel regulation by the β subunits.

1.2 Voltage clamp fluorometry

1.2.1. Introduction to voltage-clamp fluorometry

Despite much progress in understanding how channels sense voltage and selectively allow ions to cross into and out of the cell, the conformational changes that determine AP dynamics are not well-defined. A method known as voltage-clamp fluorometry (VCF) allows simultaneous observation of changes in channel conformation and ionic current kinetics, and very recently, VCF protocols have been established for major cardiac ionic currents including the cardiac Na+ current (INa), the L-type Ca2+ current ($I_{Ca,L}$), the rapid and slow components of the delayed rectifier K+ currents (IKr and IKs), and the Na+/K+ ATPase (I_{NaK}).

1.2.2 The VCF protocol

VCF was first used to observe the prototypical Shaker K+ channel VSD with a fluorophore tethered to the S4 segment (Mannuzzu, Moronne, & Isacoff, 1996). As the environment surrounding the S4 was altered by VSD movement in response to changes in membrane potential, the fluorescence emission from the tethered fluorescent molecule was also altered (**Fig. 1.1A**). Thus, the change in fluorescence emission could be used to observe the voltage-dependent kinetics of the VSD.

Fluorophore tethering for VCF is typically accomplished by introducing a cysteine residue into the area of interest and labeling it with a thiol-reactive fluorophore. Native cysteines are often

removed in order increase the specificity of labeling and reduce background fluorescence (Gandhi & Olcese, 2008). To track VSD conformation, the fluorophore is usually conjugated to a cysteine into the S3–S4 linker (Fig. 1A).

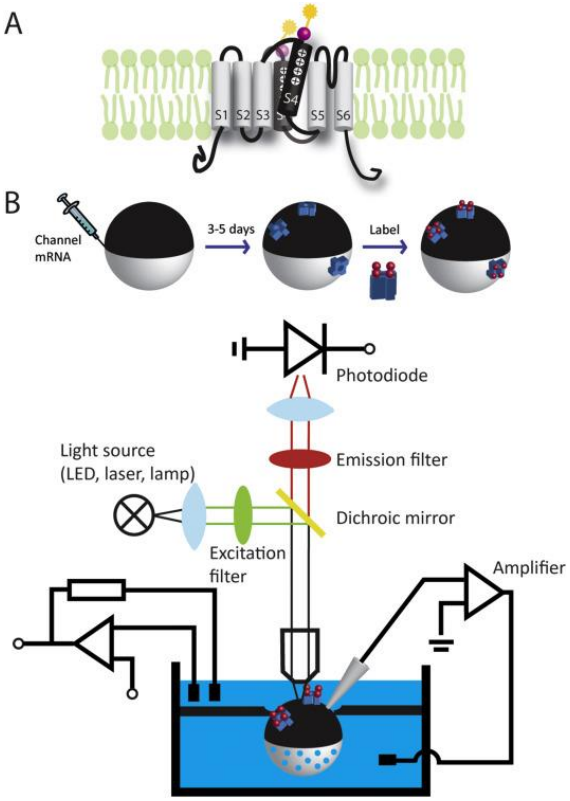

Figure 2.1 A) K_v channel VCF construct under resting (transparent) and activated (solid) states. The pink dot represents the engineered cysteine residue and yellow star denotes the tethered fluorophore. The movement of the S4 segment causes fluorophore displacement. As a result of quenching by surrounding residues, and changes in fluorophore environment, fluorescence emission is altered. B) Above: mRNA encoding VCF channel constructs are injected into *Xenopus* oocytes. Channels express at high levels after several days. Channels are then labeled with a fluorophore, which conjugates to the introduced cysteine residues. Below: An example highlighting cut-open oocyte recording, which allows resolution of fast kinetics by clamping a small membrane patch. The upper chamber filled with external solution is clamped to the command voltages, while the bottom channel filled with internal solution is connected to ground. Membrane currents are measured using the electrode filled with 3 M KCl. Fluorescence emission is separated from excitation light by a dichroic mirror and filtered by the emission filter. Finally, it is collected with a photodiode that is connected to a low noise current amplifier.

The fluorescence signal created by the change in channel conformation is usually quite small, so large numbers of channels must be expressed to observe a useful signal. The Xenopus oocyte is often used as it is well-known to express large numbers of channels from mRNA that is injected into the cytoplasm. The oocyte also has a dark pigmented layer directly beneath the membrane of the animal pole, which eliminates most of auto-fluorescence from cell, allowing for resolvable fluorescence signals (Gandhi & Olcese, 2008). In mammalian cells, the whole-cell patch clamp configuration has been combined with semiconfocal epifluorescence microscopy to observe Shaker K+ channel conformations (Blunck, Starace, Correa, & Bezanilla, 2004). However,

cardiac channels have not been successfully studied using this method. One challenge to studying these channels is much lower channel density, in comparison to Shaker.

In the oocyte protocol, channels typically express at high levels 3–7 days after RNA injection, and they are subsequently labeled with a thiol-reactive fluorophore, which binds to the introduced cysteine (**Fig 1.1B**). Then, ionic currents and fluorescence emission can be recorded using the two-electrode or cut-open oocyte Vaseline gap (COVG) voltage-clamp configuration. The COVG configuration provides faster clamping and lower noise, and is commonly applied to observe Ca2+ and Na+ channel currents whose fast kinetics are physiologically pertinent (Fig. 1B)(Antonios Pantazis & Olcese, 2013; Siefani & Bezanilla, 1998). Changes in fluorescence emission are tracked simultaneously with a photodiode (Albert Cha et al., 1999; Rudokas, Varga, Schubert, Asaro, & Silva, 2014) that is coupled to a patch clamp amplifier or by a photomultiplier tube (Mannuzzu et al., 1996).

There are multiple physical mechanisms that could underlie the observed changes in fluorescence. First, displacement of the fluorophore upon VSD activation could enable the fluorophore to move from a lipid environment to the extracellular solution, resulting in fluorescence quenching and a right shift in the emission spectrum (Blunck, 2015). Second, changes in fluorescence emission can also be caused by photo-induced electron transfer, a quenching mechanism where electrons are transferred between two molecules via a non-radiative path could reduce fluorescence emission as the fluorophore approaches a quenching molecule (Doose, Neuweiler, & Sauer, 2005, 2009; Marmé, Knemeyer, Sauer, & Wolfrum, 2003; Vaiana et al., 2003). This transfer typically occurs within the van der Waals radius (10 Å), and the amount of quenching varies between amino acids. Tryptophan and tyrosine are usually the most potent quenchers (Chen, Ahsan, Santiago-Berrios, Abruña, & Webb, 2010). In support of the

latter mechanism, VCF in Shaker K+ channels showed no shift in the spectrum of fluorescence emission, implying that a change in solvent environment is not responsible for the fluorescence signal in these experiments (A Cha, Snyder, Selvin, & Bezanilla, 1999). As it is currently not possible to reliably predict how a fluorophore at a particular position will be quenched, development of VCF DNA constructs often requires cysteine scanning of multiple positions for fluorophore labeling. If multiple labeling sites produce usable signals, the labeled cysteine that minimally perturbs the channel function is typically chosen. Further, the location of the optimal labeling site can depend on the fluorophore's properties, including its solubility, the length of the carbon chain that connects the fluorophore to the thio-reactive group, and its charge content (Hughes, Rawle, & Boxer, 2014).

1.2.2. Overview of the Cardiac sodium channel $Na_V1.5$ VCF Results

VCF was first applied to skeletal muscle Na_V channels ($Na_V1.4$) and has been used to probe VSD interaction with inactivation (Albert Cha et al., 1999; Silva & Goldstein, 2013b), local anesthetics (Arcisio-Miranda, Muroi, Chowdhury, & Chanda, 2010b; Muroi & Chanda, 2009a), 2009), and toxins (Campos, Chanda, Beirão, & Bezanilla, 2007, 2008). To probe similar phenomena in the cardiac channel, we recently developed VCF protocols to track each of the VSDs of $Na_V1.5$. Out of 16 positions attempted, we observed robust signals with DI-V215C, DII-S805C, DIII-M1296C, and DIV-S1618C (Varga et al., 2015). Each of the VSDs displayed unique voltage-dependent kinetics. The DI, DII, and DIII VSDs each activated much more rapidly than DIV (**Fig 1.2**). Deactivation of DI and DII were also rapid, while DIII- and DIV-VSD deactivation was markedly slower than activation (**Fig 1.2**). To quantify voltage dependence, VSD activation is typically measured by recording peak fluorescence after stepping to various depolarizing potentials, the fluorescence-voltage (F–V) curve. We observed that the

V1/2 of the F–V curves for each NaV1.5 VSD is more negative than channel activation (G-V curve) (**Fig 1.2**), suggesting that activation of the VSDs occurs prior to pore opening. The DII-VSD stands out, by completing its activation at higher potentials than the channel conductance, which could suggest that the DII-VSD is a facilitator channel activation whose transition is not absolutely required to open the channel pore (**Fig 1.2**).

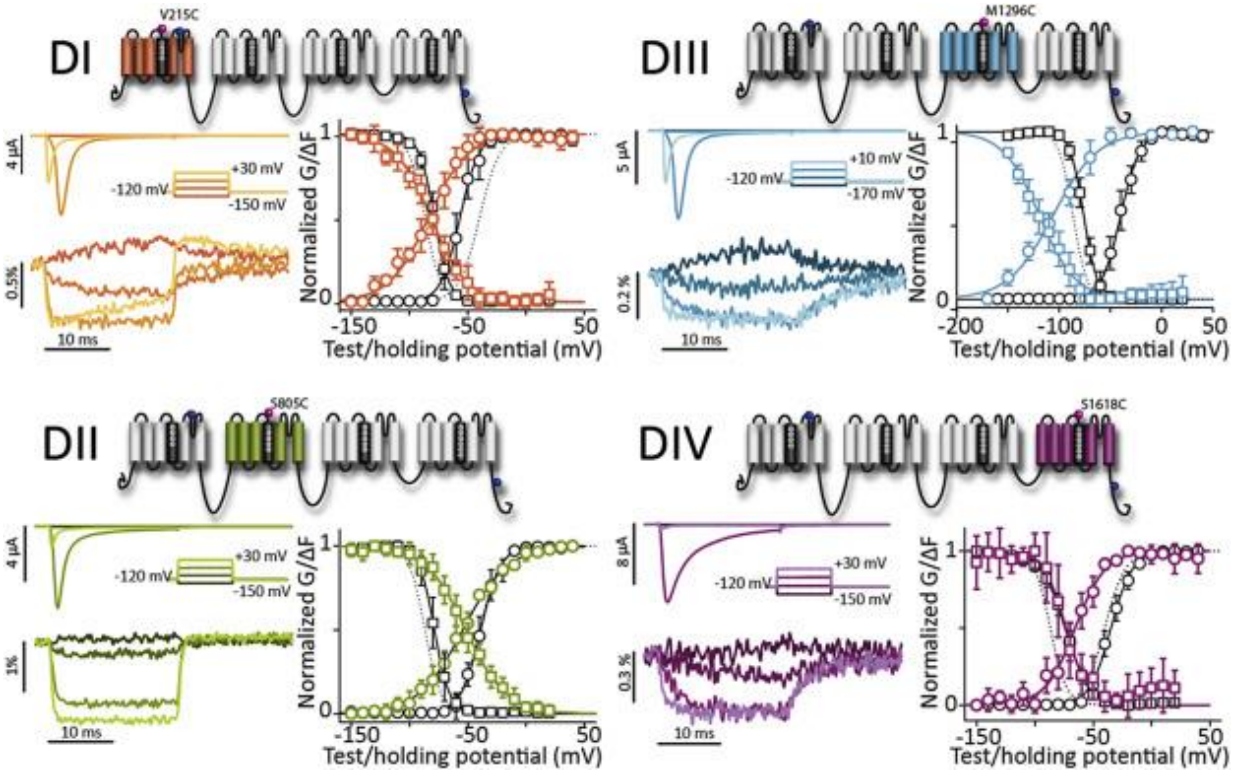

Figure 1.2. Representative current and fluorescence traces of four Nav1.5 VCF constructs, describing four VSDs, in response to voltage pulses from −100 mV, a 50ms step to −120 mV preceded by 20ms-long test pulses to −150, −90, −30, +30 mV. These steps were then followed by a 50ms step to −120 mV before returning to the holding potential. G-V curve (black circles), SSI (black squares), and the corresponding fluorescence voltage relationship F–V curve (color circles and squares, respectively).

VSD activation can also be observed during protocols that measure channel inactivation. A typical steady-state inactivation protocol measures peak Na^+ current during a test pulse that follows 200 ms long inactivation-inducing pulses. Significant inactivation occurs at negative potentials during these pulses, before the channel opens. Thus, the protocol is primarily

measuring closed-state inactivation. Tracking DIV-VSD conformation during the steady-state inactivation protocol reveals a striking correlation between DIV-VSD activation and closed-state inactivation (**Fig 1.2**), similar to previous findings in Nav1.4, where DIV-VSD activation was found to be the rate limiting step of channel inactivation (Capes, Goldschen-Ohm, Arcisio-Miranda, Bezanilla, & Chanda, 2013).

1.2.2. Future applications of the VCF technique

In later chapters, we showed using these $Na_V1.5$ VCF constructs to reveal details of α subunit interaction with accessory β subunits, the molecular pathology of inherited mutations, how class I anti-arrhythmic drugs interact with the VSDs, and mechanisms whereby post-translational modifications control channel gating. VCF data will also be tremendously useful for creating computational AP models. For example, traditional, Hodgkin–Huxley type, models imply that each of the channel "gates" must be open before the channel is able to conduct ionic current. This requirement has persisted to date, even in modern Markov type models that simulate complex drug interactions (Moreno et al., 2011). In contrast, the above DII-VSD results imply that the NaV1.5 pore may open even if the DII-VSD gate remains in the resting conformation, which would require an allosteric model. Moreover, the VCF data also provides a molecular connection, revealing specific channel domains that are responsible for the transitions that are represented in the model. Thus, by parameterizing computational models with VCF data, it will be possible to explicitly represent experimentally measured channel conformational dynamics within models of the AP. Such models will be able to connect the molecular dynamics of $Na_V1.5$ channel gating, drug interaction and post-translational modification to the cell and tissue dynamics.

1.3: Antiarrhythmic drug therapy

Antiarrhythmic therapy was first used in clinical practice over 100 years ago (Zimetbaum, 2012). The concept of antiarrhythmic is to modulate one or more ion channels functions or signaling pathways in cardiomyocytes, which counterbalance the disturbance of regular rhythm due to arrhythmias. Normally, the electrical impulse generates in the SA node, and travels down the atrium and AV node, then quickly spreads through the purkinje fibers to excite the whole ventricle, which causes a synchronized contraction (Zipes & Jalife, 2013). The electrical signal only propagates unidirectional because the myocytes that just got excited cannot fire another action potential immediately, a phenomenon called refractory (Burton & Cobbe, 2001). The time that a myocyte remains in refractoriness is defined as effective refractory period (ERP). In some cases of arrhythmia, the electrical signal fails to travel down the normal pathway, rather it circles back to the tissue that has been already excited, a phenomenon termed reentry, which will result in unsynchronized contractions that are not able to pump blood efficiently. The reentry can happen due to numerous reasons. Some common causes are shortening of ERP, prolongation and shortening of action potential duration (APD), or slowing of conduction velocity (CV). Altering the I_{Na} alone can result in changes in all three parameters, as the channel recovery from inactivation determines the ERP, late I_{Na} affects the APD, and peak I_{Na} modulates the CV. Given the intricacy of how ionic currents influence reentry circuit, we can imagine that antiarrhythmic requires precise control of currents.

The lack of understanding in antiarrhythmic mechanisms resulted in catastrophic failures in the clinical trials. One example is the cardiac arrhythmia suppression trial (CAST) trial of Class Ic drug flecainide (Greene et al., 1992), on patients post myocardium infarction. The trial showed that patients under flecainide therapy showed lower survival rate compared to patients under

placebo (Echt et al., 1991). This depressing outcome is because flecainide blocks the peak I_{Na}, which resulted in great slowing in the CV that was arrhythmogenic. This examples shows that Antiarrhythmic therapy can have adverse effects if not used properly.

1.3.1 Classification of Antiarrhythmia Drugs

The most commonly used classification for antiarrhythmic agents are Vaughan Williams and Singh's classification, which categorizes drugs based on their effects on the AP morphology. It separates antiarrhythmics into four classes, Na_V channel blockers (Class I), beta adrenergic pathway blocker (Class II), K_V channel blockers (Class III), and Ca_V channel blockers (Class IV) (Vaughan Williams, 1970). Each class is further separated into subclasses. For example, the Class I agents have subclasses of Ia, Ib, and Ic, where Ia drugs slows down upstroke and prolongs duration of AP, Ib drugs shorten the AP duration, and Ic drugs delay upstroke without affecting the AP duration (Vaughan Williams, 1970).

The Vaughan Williams and Singh's classification is still being used in clinics. However, this classification is greatly limited by the fact that it was based on outcomes, but not mechanisms. To prevent the adverse effects of antiarrhythmics, it is essential to develop mechanism-based therapy for different diseases, or even different patients.

1.3.2 Class Ib Antiarrhythmic

Class Ib agents, such as lidocaine, are also used as local anesthetics to treat pain. As local anesthetics, they have been extensively studies in the past. Over 40 years ago, Bertil Hille proposed that lidocaine has two ways to enter the channel pore, the hydrophobic and hydrophilic pathways (B Hille, 1977). The binding actions were further described by the modulated receptor theory (Hondeghem & Katzung, 1984). It emphasized that lidocaine binding to the channel pore stabilized the channel inactivation, and an inactivated channel has higher affinity for lidocaine.

This theory was able to explain the two different types of blocks induced by lidocaine, tonic block (TB) and use-dependent block (UDB). However, as we gained more knowledge of the NaV channel structure, it is clear that the modulated receptor is a much simplified view of Class Ib drug action. The detailed allosteric changes in channel conformation needs to be incorporated into the model.

Chapter 2

Mechanisms of noncovalent β subunit regulation of Na_V channel gating

Large portions of this chapter is adapted from

Zhu, W., Voelker, T. L., Varga, Z., Schubert, A. R., Nerbonne, J. M., & Silva, J. R. (2017). Mechanisms of noncovalent β subunit regulation of NaV channel gating. The Journal of General Physiology. http://doi.org/10.1085/jgp.201711802

2.1 Summary

Voltage-gated Na+ (NaV) channels comprise a macromolecular complex whose components tailor channel function. Key components are the non-covalently bound β1 and β3 subunits that regulate channel gating, expression, and pharmacology. Here we probe the molecular basis of this regulation by applying voltage-clamp fluorometry to measure how the β-subunits affect the conformational dynamics of the cardiac NaV channel (NaV1.5) voltage-sensing domains (VSDs). The pore-forming NaV1.5 α-subunit contains four domains (DI-DIV), each with a VSD. Our results show that β1 regulates NaV1.5 by modulating the DIV-VSD, whereas β3 alters channel kinetics mainly through DIII-VSD interaction. Introduction of a quenching tryptophan into the extracellular region of the β3 transmembrane segment inverted the DIII-VSD fluorescence. Additionally, a fluorophore tethered to β3 at the same position produced voltage-dependent fluorescence dynamics strongly resembling those of the DIII-VSD. Together these results provide compelling evidence that β3 binds proximally to the DIII-VSD. Molecular-level

differences in β1 and β3 interaction with the α subunit lead to distinct activation and inactivation recovery kinetics, significantly affecting NaV channel regulation of cell excitability.

2.2 Introduction

In electrically excitable organs, such as the heart, brain, and skeletal muscle, voltage-gated Na^+ (Na_V) channels cause the initiation and propagation of action potentials by conducting a large and rapid inward Na^+ flux. Within the cells of these tissues, Na_V channels form macromolecular signaling complexes (Abriel, 2010), whose parts work in concert to regulate channel function. The Na_v β subunit members of this complex have been shown to regulate cell adhesion (Malhotra et al. 2000; Isom et al. 1995; Yu et al. 2003) and signaling, in addition to affecting channel density (Calhoun & Isom, 2014), gating kinetics (Calhoun & Isom, 2014; Fahmi et al., 2001; Hiroshi Watanabe et al., 2009), and pharmacology (Lenkowski et al., 2003; Uebachs et al., 2010). However, the mechanisms whereby the β subunits interact with the Na_V channel α-subunit to exert their influence on gating remain undiscovered.

Five types of Na_v β subunits have been identified, β1, β2, β3, β4, and β1b (Hartshorne & Catterall, 1984; Kazen-Gillespie et al., 2000; Messner & Catterall, 1985; Morgan et al., 2000b; Yu et al., 2003). β2 and β4 form covalent disulfide bonds with the α subunit (Isom et al. 1995; Yu et al. 2003), while β1 and β3 interact non-covalently (Isom et al. 1992a; Morgan et al. 2000a). With the exception of the β1b splice variant (Patino et al., 2011), the β subunits comprise a single transmembrane domain that is tethered to an extracellular Immunoglobulin (Ig) loop and a cytoplasmic C-terminus (Calhoun & Isom, 2014). Very recently, the covalently bound β2 and β4 were crystallized (Das et al., 2016; Gilchrist et al., 2013), and a crucial disulfide bond formed by ^{55}Cys in β2 and ^{910}Cys in the DII pore loop was identified (Das et al., 2016). However, ^{910}Cys is not present in $Na_v1.5$, and instead the homologous position is ^{868}Leu.

The β subunits are widely expressed in many tissues, including the central and peripheral nervous system, the heart, and skeletal muscle (Calhoun & Isom, 2014). Despite the sequence homology between non-covalently associated β1 and β3 subunits, their expression profile across organs differs. For instance, β1 is highly expressed in skeletal muscles, but not β3 (The Human Protein Atlas). Intriguingly, even in the same organ, β subunit localization can differ (Calhoun & Isom, 2014; Fahmi et al., 2001; Yuan et al., 2014). For example, the β1 and β3 subunits have been shown to differentially express in the atria and ventricles (Fahmi et al., 2001; Hiroshi Watanabe et al., 2009; Yuan et al., 2014), suggesting that they may specifically tailor Na_V channel function according to cell type. Moreover, β1 and β3 also have a varied temporal expression profile during heart development. β1 expression was shown to increase (Domínguez et al., 2005), whereas β3 was shown to decrease through embryonic development (Okata et al., 2016). The dynamic expression patterns of β1 and β3 suggest that these two subunits play distinct roles in regulation of Na_V channel function and the action potential.

The pore-forming Na_V channel α-subunit is composed of four homologous domains (DI-DIV) connected by cytoplasmic linkers (Gellens et al., 1992a). Each domain is formed by six α-helical transmembrane segments (S1-S6). The fourth segments (S4) contain multiple positively charged residues that move across the membrane in response to changes in membrane potential. S4, together with S1-S3, form the voltage sensing domains (VSDs) and are coupled to the S5 and S6, which form the channel pore. Upon membrane depolarization, the S4 segments within the VSDs of DI-DIII are propelled outward to open the channel within a millisecond, known as channel activation (Chanda & Bezanilla, 2002). Shortly thereafter, channels rapidly close, a process termed ‘fast inactivation’ that is mediated by the intracellular DIII-DIV linker and the DIV-VSD (West et al., 1992). Both activation and inactivation gating have been previously shown to be

modulated by the β1 and β3 subunits (Calhoun & Isom, 2014; Fahmi et al., 2001; Morgan et al., 2000a; Hiroshi Watanabe et al., 2009).

Much mechanistic insight into Na_V channel gating has been recently provided by applying the voltage clamp fluorometry (VCF) protocol, used to fluorescently track VSD conformation and correlate VSD kinetics with ionic current gating. For many years, this protocol has been applied to study the skeletal muscle isoform $Na_V1.4$, and it has provided great insight into the VSD roles in determining activation and inactivation gating kinetics (Cha et al., 1999; Chanda & Bezanilla, 2002; Silva & Goldstein, 2013a, 2013b), the mechanisms of local anesthetic regulation of the VSDs (Arcisio-Miranda et al., 2010; Muroi & Chanda, 2009), and details of how toxins pathologically affect VSD activation (Campos et al., 2007, 2008). We have recently broadened this approach by developing voltage clamp fluorometry (VCF) constructs to track VSD conformations of all four domains in the cardiac paralog, $Na_v1.5$ (Varga et al., 2015; Zhu et al., 2016), whose ionic current modulation by β subunit in oocytes mirrors the mammalian cell phenotype.

We hypothesized that the non-covalently bound β1 and β3 subunits modulate $Na_V1.5$ ionic current kinetics by altering the activation of one or more VSDs. In this study, we test this hypothesis by applying VCF to observe the β subunit effects on the VSD of each $Na_V1.5$ domains.

2.3 Results

β1 regulates channel inactivation by altering voltage-dependent DIV-VSD transitions

We co-expressed the human β1 subunit with the pore-forming hNav1.5 α subunit in *Xenopus* oocytes by co-injecting β1 and α subunit mRNA at a molar ratio of 3:1. β1 co-expression had no

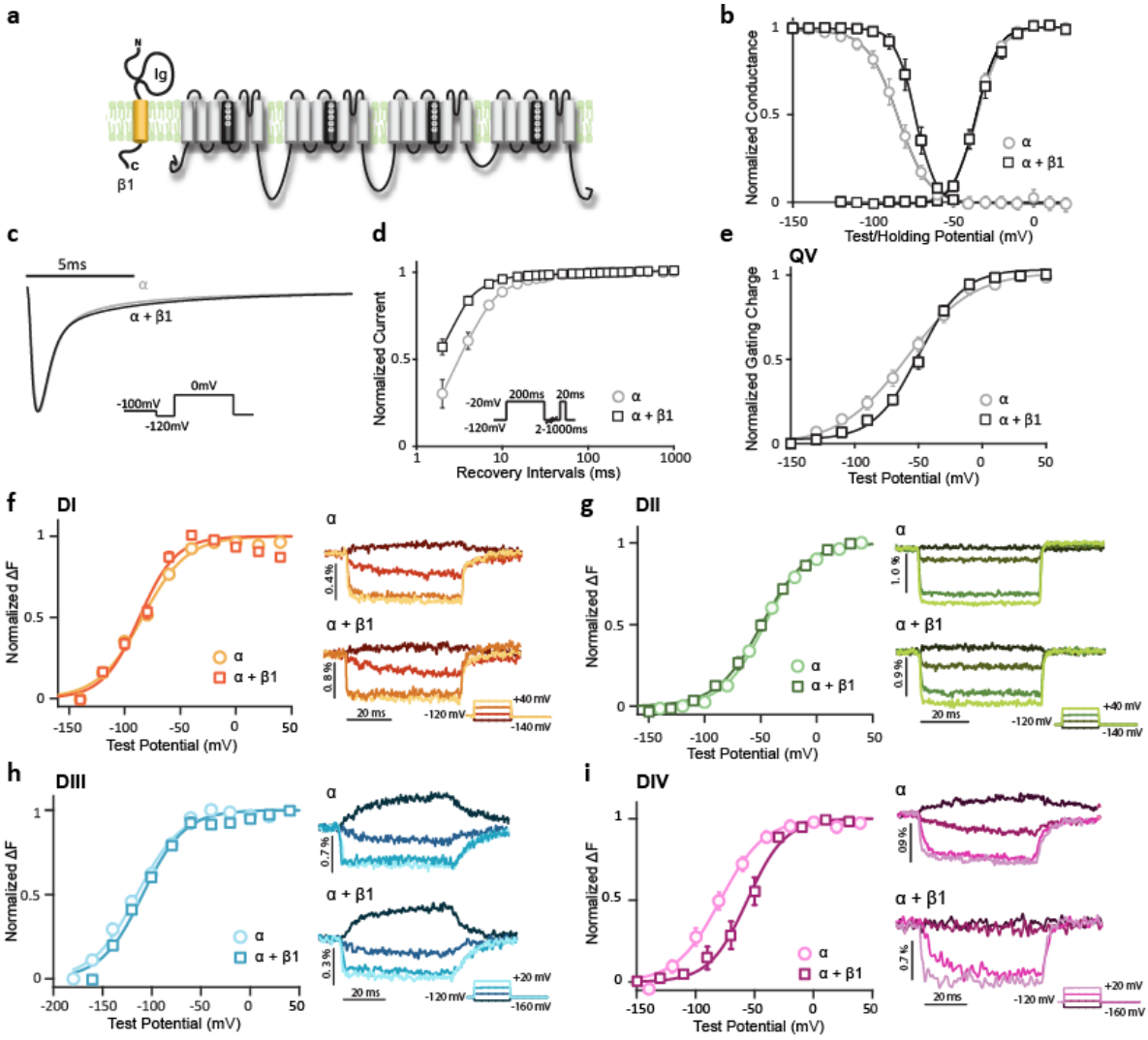

Figure 2.1 Nav β1 regulates Nav1.5 inactivation by altering DIV-VSD activation. Nav1.5 ionic currents were measured using the cut-open voltage clamp technique to resolve fast Na+ channel kinetics. Changes in site-specific fluorescence of Nav1.5 are reported by four VCF constructs (V215C, S805C, M1296C, and S1618C) after conjugating to MTS-TAMRA (Varga et al., 2015). The mean ±SEM is reported for groups of 3-8 cells. The error bars represent the SEMs. Some error bars are not visible due to small SEMs.

a) Topology of Nav1.5 and Nav β1 subunits on plasma membrane. b) Voltage-dependence of activation (G-V) and steady state inactivation (SSI) for WT Nav1.5 with β1 (α+β1, square), or without β1 (α, circle). c) Representative current traces of WT channel with β1 (black), or without β1 (grey) in response to depolarizing pulse to 0mV from -120mV. d) Time dependence of fraction of current recovered for channels with β1 (α+β1, square), or without β1 (α, circle). (f-i) Left panel, Voltage dependence of steady-state fluorescence (F-V curve) from all four domains f) DI-S216C, g) DII-S805C h) DIII-M1296C, and i) DIV-S1618C co-expressed with (α+β1, squares), or without β1 subunit (α, circles).

significant effect on the voltage-dependence of WT channel activation, as shown by the conductance-voltage (G-V) curve (**Fig 2.1b**), but caused a depolarizing shift in the channel steady-state inactivation (SSI) curve, compared to WT alone ($\Delta V_{1/2}$=12.2 ±1.4 mV, p=0.02) (**Fig 2.1b**). The right-shifted SSI curve implies that more channels are available to open at higher potentials. Moreover, β1 further increased channel opening by accelerating channel recovery from inactivation (**Fig 2.1d**). To ensure that the changes in the β1 regulation mechanism that we observed were consistent across different expression systems, we also used identical protocols to assess β1 effects on $Na_v1.5$ currents in HEK 293T cells, and observed similar behavior. The β1-induced depolarization of SSI we observed is also consistent with previous results in HEK 293 and HEK 293T cells (Malhotra et al. 2001; An et al. 1998; Maltsev et al., 2009).

We investigated how β1 modulates inactivation by first measuring gating currents, which reflect charge translocation of all four VSDs. To be able to measure the gating current for the $Na_V1.5$ channel, we used the WT-LFS construct, which contains C373Y mutation that increases channel sensitivity to TTX, and the Y1977A mutation that prevents ubiquitination of the channels to increase expression (Varga et al., 2015). Comparison between the gating charge voltage-dependence (Q-V) of WT-LFS channels co-expressed with and without the β1 subunit (**Fig 2.1e**) revealed that β1 caused a depolarizing shift in the Q-V curve at negative potentials, resulting a steeper Q-V relationship (Δk=-10.1±4.2 mV, p=0.04). This result suggests that in the presence of the β1 subunit, one or more of the VSDs requires higher potentials to activate. To identify which VSD(s) was affected, $Na_V1.5$ VCF constructs were co-expressed with the β1 subunit. We have previously shown that MTS-TAMRA-labeled $Na_v1.5$ channels activate and inactivate similarly to WT channels (Varga et al., 2015). Co-expression of the β1 subunit with the VCF constructs caused a shift in the SSI curves that is similar to the shift caused by β1 in WT channels. The

voltage-dependence of activation of each VSD can be described by plotting steady-state fluorescence against voltage (F-V curve). In comparison to α alone, the β1 subunit did not significantly alter the DI, DII, or DIII F-V curves (**Fig 2.1f-h**), but induced a strong depolarizing shift in the DIV F-V curve ($\Delta V_{1/2}$=31.3±1.7mV, p=0.02) (**Fig 2.1i**). Thus, in the presence of the β1 subunit, the DIV-VSD requires higher potentials to accomplish its activation transition, consistent with the gating charge shift (**Fig 2.1e**).

Previously, DIV-VSD activation was shown to be more closely linked to Na_V channel inactivation, than activation (Capes, Goldschen-Ohm et al., 2013; Cha et al., 1999). Specifically, the DIV-VSD was observed to be immobilized by fast inactivation (Cha et al., 1999), and DIV-VSD activation was shown to be the rate-limiting for fast inactivation (Capes et al., 2013). Hence, changes in the voltage dependence of DIV-VSD activation or DIV-VSD kinetics would be expected to cause correlated changes in channel steady-state inactivation (SSI) or inactivation kinetics. Notably, DIV-VSD deactivation kinetics are also faster with β1 ($t_{100\%-10\%}$ =4.5±0.6ms at -160mV after 0mV pulse), compared to α alone ($t_{100\%-10\%}$ =13.2±0.4ms at -160mV after 0mV pulse, p=0.0003). Thus, our results imply that the β1 subunit regulates inactivation by altering DIV-VSD transitions. This mechanism is consistent with previous studies suggesting that β1 binds to the C-terminus of $Na_v1.1$ (Spampanato et al., 2004b) and the S5-S6 linker of DIV of $Na_v1.4$ (Makita et al., 1996). Our results build on these previous findings by connecting VSD regulation to altered inactivation kinetics.

Even though β1 does not affect the voltage dependence of DIII-VSD activation, comparison of DIII-VSD deactivation kinetics in the presence of β1, shows that DIII-VSD recovery to the resting position upon repolarization is faster and more complete ($t_{100\%-10\%}$=16.5±1.6ms at 0mV), in contrast to α alone ($t_{100\%-10\%}$=23.9±2.3ms at 0mV, p=0.05) (**Fig 2.1h, right panel**). In

previous studies, fast inactivation was shown to immobilize the gating charge displaced by DIII and DIV (Armstrong & Bezanilla, 1977; Cha et al., 1999), in particular DIII-VSD (Sheets & Hanck, 2005; Varga et al., 2015). Our result suggests that β1 allows the DIII and DIV VSDs to recover to the resting state more quickly. Given the link to inactivation, this more rapid recovery of the VSDs will allow channels to recover more quickly from inactivation (**Fig 2.1d**), and become available for excitation in a shorter amount of time.

β3 alters channel activation and inactivation by modulating DIII- and DIV-VSD kinetics

We co-expressed the β3 subunit with $Na_v1.5$ using the same protocols that were used for β1 (**Fig 2.2a**). As with the β1 subunit, β3 had no apparent effect on voltage dependence of channel activation (G-V) (**Fig 2.2b**), but slowed ionic current activation and inactivation kinetics (**Fig 2.2c**). It also caused a depolarizing shift ($\Delta V_{1/2}$=8.7±1.5mV, p=0.02) in SSI (**Fig 2.2b**), implying that β3 expression increases $Na_v1.5$ channel availability at higher potentials. A similar β3-induced SSI shift was also present in HEK cells, recorded with identical protocols. Unlike β1, β3 does not significantly alter channel recovery kinetics (**Fig 2.2d**). When we co-expressed β3 with the four VCF constructs, the gating effects of β3 were preserved, except with the DII-LFS construct, where the shift in SSI induced by β3 is less pronounced. Our observations of the ionic current changes induced by β3 co-expression are consistent with the gating effects shown previously in oocytes (Fahmi et al., 2001) and the *scn3b* knock-out mouse phenotype (Hakim et al. 2008).

Like β1, β3 caused a depolarizing shift in the Q-V curve at negative potentials and a steeper Q-V relationship (Δk=8.6±3.0 mV, p=0.05), showing that β3 also alters the voltage-dependence of VSD activation. Considering the homology between the β1 and β3 subunits, the similar Q-V curves are not surprising. However, comparison of the F-V curves of α alone and α with β3

shows that β3 induces a depolarizing shift in the DIII F-V curve (DIII F-V: $\Delta V_{1/2}$ =20.7± 3.9mV, p=0.01), in addition to its depolarizing effect on the DIV F-V (DIV F-V: $\Delta V_{1/2}$ =25.0± 7.7mV, p=0.01) (**Fig 2.2h, i**), causing both the DIII and DIV-VSDs to activate at higher potentials. The DIV F-V depolarizing shift occurs over the same potential range as the shift in SSI, consistent with the findings that DIV-VSD activation strongly correlates with channel inactivation, and with the above experiments with β1.

Channel opening is known to be regulated by DIII-VSD activation (Muroi et al., 2010; Wang et al., 2016). Yet, β3 induced depolarization of DIII-VSD activation without affecting channel voltage-dependence of activation (G-V), which may be due to DIII-VSD activation at very negative potentials in the $Na_V1.5$ paralog. Still, β3 slowed ionic current activation kinetics (α alone: dI/dt_{max}=1.6±0.1 ms^{-1}; α+β3: dI/dt_{max}=1.1±0.1 ms^{-1}, p=0.04) (**Fig 2.2c**), suggesting that when channels are co-expressed with β3, DIII-VSD activation becomes a rate-limiting factor for pore opening. We note that slower inactivation rates can also result in slower activation kinetics when normalized currents are compared, since channel activation and inactivation are tightly coupled. Thus, the slowed activation kinetics we observed with β3 could alternatively be caused by slowed inactivation kinetics. In contrast to β1, β3 only accelerates DIII-VSD deactivation (α+β3: $t_{100\%-10\%}$ =9.2±1.3ms, α alone: $t_{100\%-10\%}$ =23.9±2.3ms, p=0.005), but not DIV-VSD deactivation (**Table 4**). In the $Na_V1.5$ channel, the DIII-VSD activates at very negative potentials (~160mV). Thus, it is a technical challenge to acquire the negative baseline of the DIII F-V for the more hyperpolarized shifted constructs (α alone and α+β1). Despite this limitation, we expect the hyperpolarized shifted constructs would have more negative $V_{1/2}$ if we were able to record to the baseline, suggesting that the DIII depolarizing shift induced by β3 is even larger than reported.

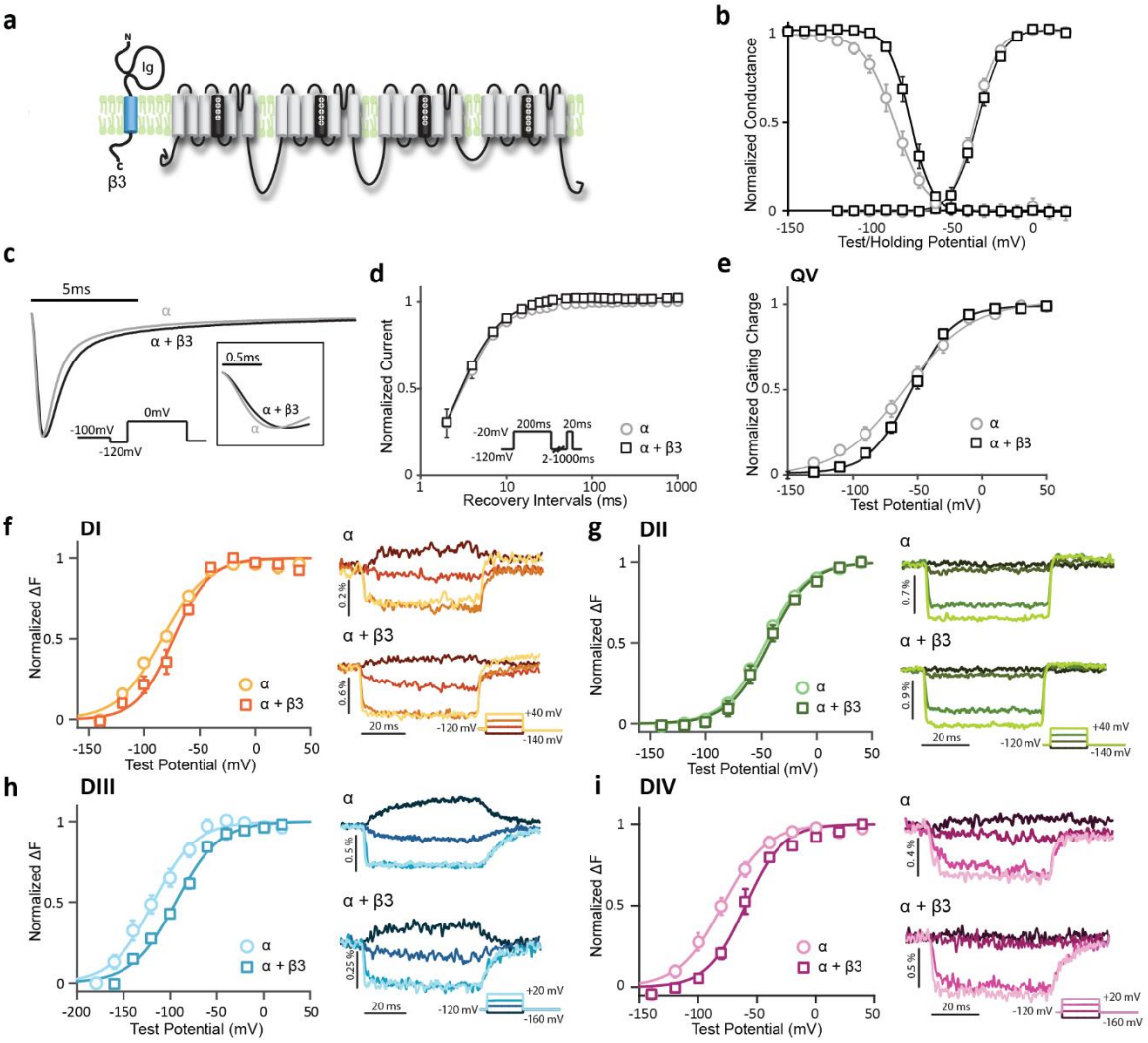

Figure 3.2 Nav β3 subunit affects Nav1.5 inactivation by modifying both DIII and DIV-VSD activation.
Nav1.5 ionic currents and site-specific fluorescence changes are measured as described in Figure 1. Groups of 3-10 cells are reported as mean ± SEM.

a) Topology of Nav1.5 and NaV β3 subunits on plasma membrane. The NaV β3 subunit structure is homologous to the β1 subunit, and it also has been shown to express in the myocardium (Hu et al., 2012). b) Voltage-dependence of activation (G-V), and steady-state inactivation (SSI) for WT Nav1.5 with β3 (α+β3, squares), or without β3 (α, circles). c) Representative current traces of WT channel with β3 (black), or without β3 (grey) in response to depolarizing pulse to 0mV from -120mV. Channels with β3 show slower activation and deactivation kinetics, compared to α alone. d) Time dependence of fraction of current recovered for channels with β3 (α+β3, black square), or without β3 (α, grey circle). The same protocol was used as described in Fig.1. e) Gating charge-voltage curve (Q-V) for WT-LFS Nav1.5 with β3 (α+β3, squares), or without β3 (α, circles). (f-i) Left panel, Voltage-dependence of Fluorescence (F-V curve) from four VCF constructs f) DI-V215C, g) DII-S805C, h) DIII-M1296C, and i) DIV-S1618C co-expressed with (α+β3, square), or without β3 subunit (α, circle). F-V curves are constructed and recorded as in Fig. 1. β3 co-expression causes depolarizing shifts in DIII and DIV F-V, without significantly affecting the other two domains. Right panel, Representative fluorescence signals representing the kinetics of each VSD activation.

		DI	DI+B1	DI+B3	DII	DII+B1	DII+B3
G-V	**$V_{1/2}$**	-42.3±1.7	-50.2±1.0	-37.1±1.8	-33.9±2.2	-38.9±3.0	-43.5±2.2
	k [n]	8.16±0.7 [5]	8.3±0.6 [4]	9.7±0.5 [4]	9.5±0.2 [4]	8.5±1.2 [9]	-7.0±0.5 [4]
SSI	**$V_{1/2}$**	-96.3±4.55	-78.6±2.1	-79.6±2.4	-88.8±1.3	-79.2±4.5	-86.4±0.7
	k [n]	-11.0±1.1 [4]	-6.4±0.2 [8]	-7.0±0.4 [4]	-8.2±0.4 [4]	-6.5±0.9 [7]	-6.1±0.1 [4]
F-V	**$V_{1/2}$**	-111.5±1.0	-92.1±11.4	-75.7±4.6	-48.4±2.7	-51.1±3.5	-45.5±5.0
	k [n]	21.3±2.4 [4]	18.6±2.3 [4]	15.3±2.5 [4]	19.4±0.7 [4]	23.1±2.2 [6]	19.3±0.8 [4]
		DIII	**DIII+β1**	**DIII+β3**	**DIV**	**DIV+β1**	**DIV+β3**
G-V	**$V_{1/2}$**	-43.7±1.9	-40.0±4.4	-39.2±1.4	-36.8±1.6	-34.6±3.4	-38.2±1.3
	k [n]	7.8±0.6 [5]	9.4±0.7 [13]	7.4±0.5 [6]	8.9±0.9 [4]	9.2±0.6 [19]	7.2±0.5 [5]
SSI	**$V_{1/2}$**	-94.7±1.9	-76.2±2.5	-86.0±1.6	-91.7±3.4	-74.2±3.1	-78.0±1.6
	k [n]	-9.8±0.7 [4]	-6.7±0.4 [7]	-7.6±0.4 [4]	-12.6±0.9 [5]	-10.3±0.9 [13]	-9.2±0.5 [5]
F-V	**$V_{1/2}$**	-120.7±4.8	-122.1±1.4	-98.0±2.6	-88.2±5.3	-56.8±6.6	-63.2±4
	k [n]	25.6±0.7 [4]	24.3±1.3 [5]	26.4±2.0 [5]	23.6±3.1 [4]	14.5±2.5 [6]	14.4±0.3 [4]
		DIII+β1+β3	**DIV+ β1+β3**				
G-V	**$V_{1/2}$**	36.5±0.8					
	k [n]	7.9±0.3 [3]					
SSI	**$V_{1/2}$**	-80.4±1.1					
	k [n]	-6.6±0.1 [3]					
F-V	**$V_{1/2}$**	-79.8±3.2	-59.2±0.8				
	k [n]	29.7±1.8 [5]	13.2±1.1 [3]				

Table 2.1 Parameters of Boltzmann fit to G-V, SSI and F-V curves for WT Nav1.5 or VCF constructs expressed with or without WT β1 or β3.

Despite being highly homologous to β1, β3 is unique in altering the VSD transitions of both DIII and DIV. The DIV-VSD effects induced by β3 are similar to β1, causing a depolarizing steady-state inactivation shift. The β3 effect on the DIII-VSD, which shifts DIII-VSD's activation to higher potentials, slows ionic current activation and inactivation kinetics. Two α-β3 interaction mechanisms could explain the changes in the VSD movements that we observed. One possibility is that β3 can interact with both DIII and DIV. A second plausible mechanism is that β3 mainly interacts with the DIII-VSD, which can allosterically modify the adjacent DIV-VSD activation.

Below, results from β1/β3 chimera and α-β3 quencher fluorophore pair experiments support the latter mechanism.

High expression of β3 separates DIII-VSD activation into two steps

To ensure that the VSD alterations we observed were truly caused by expression of β subunits, and the amount of β subunits expressed on membrane saturated their modulation effects of $Na_V1.5$ channels, we tested different expression levels of β subunits. We altered β subunit expression levels by injecting mRNAs encoding α and β subunits at different molar ratios, observing their effects on ionic current and VSD activation.

For the β1 subunit, as we increased the mRNA molar ratio from 1:1 to 1:2, the DIV F-V shifted to more depolarized potentials (1:1 α:β1: $V_{1/2}$ =-70.1± 5.2mV, 1:2 α:β1: $V_{1/2}$ =-56.8± 5.0mV). Further, when the α:β1 mRNA molar ratio was increased to 1:4, the DIV F-V curve overlaps with F-V of a 1:2 α:β1 mRNA molar ratio (**Fig 2.3a**), suggesting that β1 modulation of DIV-VSD saturated at 1:2 α:β1 ratio. Consistently, the β1 alteration of channel SSI followed a similar saturation pattern (**Fig 2.3b**). This result further supports the idea that β1 regulates channel inactivation by altering DIV-VSD activation, an effect that saturates at a 1:2 ratio.

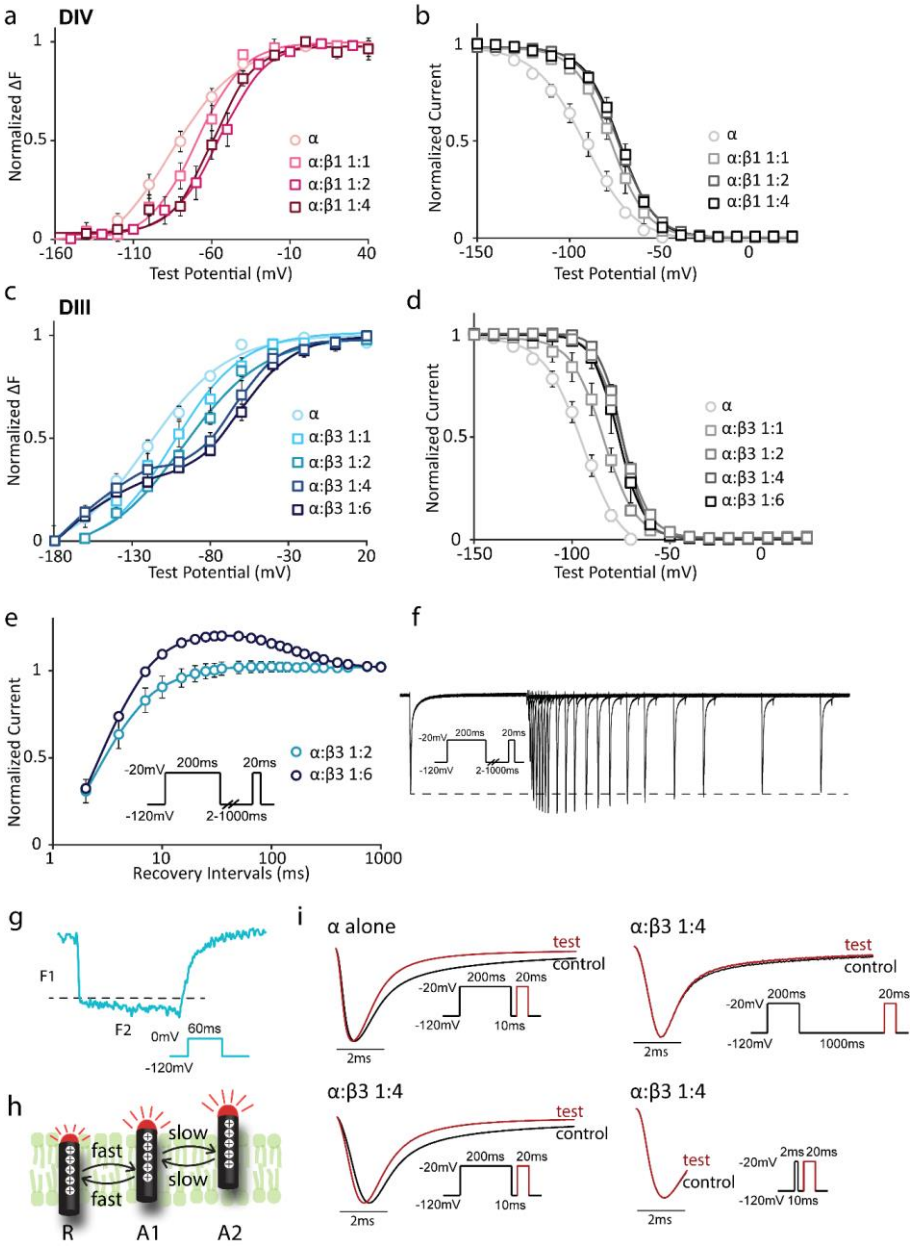

Figure 2.4 High expression of β3 subunits separate DIII-VSD movements into two components. a-b) DIV VCF construct (α) was co-injected with β1 mRNA at molar ratios of 1:1, 1:2, 1:4, or without β. c-d) DIII VCF construct (α) was co-injected with β3 mRNA at molar ratios of 1:1, 1:2, 1:4, 1:6, or without β. e) Comparison between channel recovery from inactivation curves for α: β3 at 1:2 and 1:6. f) Representative channel recovery from inactivation current traces at 1:6 α: β3 molar ratio. Dotted line represents the first pulse peak amplitude. g) DIII fluorescence trace at 1:6 α: β3 molar ratio, in response to 0mV depolarizing potential. In parallel to DIII fluorescence voltage dependence, the DIII fluorescence activation kinetics also display two components F1 and F2. h) Schematic model of DIII-VSD movements when channels are co-assembled with high expression level of β3. i) Comparison of the current activation kinetics show that with high expression of the β3 subunit, the second current pulse after short recovery time has faster activation kinetics.

For β3, the saturation behavior was more complex. When we increased the mRNA molar ratio from 1:1 to 1:2, the DIII F-V curve shifted to depolarized potentials (1:1 α:β3: $V_{1/2}$ =-108.6± 5.6mV, 1:2 α:β3: $V_{1/2}$ =--97.9± 2.6mV) (**Fig 2.3c**). Intriguingly, when the molar ratio of α:β3 is increased to 1:4 or higher, the DIII F-V curve started to exhibit two components, which could no longer be fit with a single Boltzmann function (**Fig 2.3c**). The curve was well-fit with two Boltzmann curves, one at very negative potentials (-180mV to -80mV), and the other within the channel activation voltage range (-80mV to 20mV). Correspondingly, the DIII fluorescence kinetics also followed two steps, which were also not well-fit with a single exponential. The first rapid transition occurred within 2ms after depolarization, denoted by F1, followed by a very slow component, denoted by F2 over 60ms time course (**Fig 2.3g**).

The separation of two components in DIII-VSD activation caused unusual recovery from inactivation, where the peak current magnitude during the test pulse was larger than the control pulse following recovery times of 10 to 300 ms (**Fig 2.3e, f**). After 500-1000ms recovery at -120mV, the peak current during the test pulse returned to the magnitude of the control pulse. Typically, Na^+ currents exhibit monotonic behavior during this protocol.

We assessed the relationship between the two DIII-VSD activation components and channel recovery from inactivation by aligning current during the first control pulse with that of the second test pulse after 10 ms or 1000 ms recovery (**Fig 2.3i bottom left, top right**). For channels expressed without the β subunit, current during the test pulse after 10ms recovery activated at the same rate as the control pulse (**Fig 2.3i top left**). For channels co-expressed with β3 subunit at 1:4 molar ratio, current during the test pulse after 10 ms recovery activated more quickly in comparison to the control pulse (**Fig 2.3i bottom left**). In contrast, the current during the test pulse after 1000 ms recovery rose at the same rate as that of the control pulse (**Fig 2.3i top**

right). Faster channel activation kinetics can significantly increase peak current. High β3 expression causes faster activation kinetics during a test pulse that follows a short recovery interval (10-300ms), resulting in peak current that exceeds the control pulse current.

To account for this behavior, we first suppose that the DIII-VSD activates in two steps from resting (R) to intermediate activated (A1), and activated states (A2) (**Fig 2.3h**). We then assume that the transition between R to A1 is fast, and is described by F1 component, while A1 to A2 is slow, as shown by F2 component. In this model, pore opening is facilitated by the transition of the DIII-VSD to the A1 state and further encouraged by entry into the A2 state. During the first 200 ms pulse, most DIII-VSDs are brought to A2. Since the transition from A2 to A1 state is slow, when channels were given 10-300ms to recover at -120mV, the time was too short for DIII-VSD to recover to A1, resulting most of the DIII-VSDs being trapped in the A2 state. As most of DIII-VSDs were still in A2 state and it greatly facilitates pore opening, channel activation was faster for the second pulse. If this scheme is correct, we would predict that if we only allow the DIII-VSD to enter A1 by applying a short 2ms depolarizing pulse as the control pulse, the second pulse will not have faster rising kinetics compared to the control pulse. Indeed, comparison of the control and test pulses show that both pulses completely overlap (**Fig 2.3i bottom right**).

It is unlikely that the physiological assembly of α-β3 will reach such high ratio to separate DIII-VSD movement into two components (Yuan et al., 2014). It is possible that overexpression of β3 forces some of the β3 subunits in a secondary low-affinity binding site. Consequently, if β3 is locally expressed at very high levels, this group of cells will have a relatively short refractory period and become particularly excitable, because of the unique channel recovery behavior.

β1 and β3 do not regulate VSD activation from the Nav1.5 pore via the S4-S5 linkers

By probing the VSD dynamics, we discovered that β1 and β3 modulate channel current by altering DIII and DIV VSD activation. However, the mechanism by which the β1 and β3 subunits interact with the Na_V channel to alter VSD activation remains unclear. The recent Cryo-EM structure of eukaryotic Na_V channel shows that the pore loops of Na_V channel have bulky extracellular structures, making them good candidates for β subunit binding (Shen et al., 2017). To test if β1 and β3 subunits allosterically modulate the VSDs by interacting with the DIII and DIV pore domains, we assessed β1 and β3's effects on mutant channels where DIII or DIV-VSD is decoupled from the pore. The interaction between the S4-S5 linker and the S6 is known to be essential for canonical coupling between the VSD to the pore of each domain. We utilized mutations that were previously found to disrupt this type of coupling.

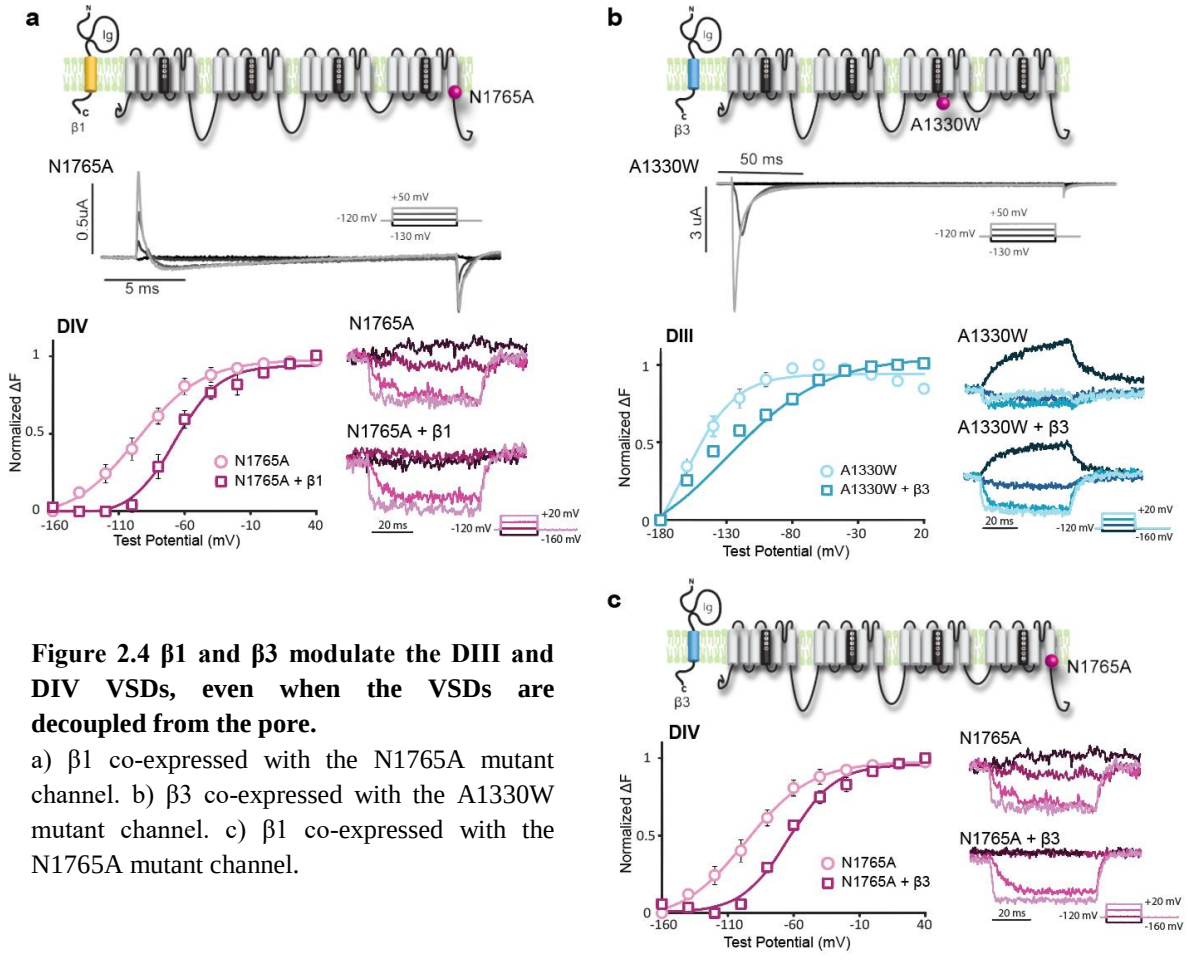

Figure 2.4 β1 and β3 modulate the DIII and DIV VSDs, even when the VSDs are decoupled from the pore.
a) β1 co-expressed with the N1765A mutant channel. b) β3 co-expressed with the A1330W mutant channel. c) β1 co-expressed with the N1765A mutant channel.

Residue N1765, which is on the S6 of DIV, was previously shown to be essential for coupling the DIV-VSD to the pore (Sheets et al., 2015). Mutating N1765 to Alanine (A) abolishes most of the ionic current (**Fig 2.4a**) without affecting DIV-VSD movement and gating currents, suggesting that the DIV-VSD is decoupled from the pore. Co-expressing β1 with the N1765A channel still depolarized the Q-V curve and the DIV F-V (**Fig 2.4a**), similar to the β1 effect on WT channels. If β1 interacts with the DIV-pore domain to allosterically modulate the DIV-VSD through the S4-S5 linker, decoupling of the DIV-VSD from the DIV-pore domain should abolish most of the β1 effect on the DIV-VSD. Instead, we found that the DIV-VSD of the N1765A is still modulated by β1, suggesting that β1 does not regulate the DIV-VSD via pore coupling through the DIV S4-S5 linker, but instead interacts with the DIV-VSD directly or via an alternative pore-VSD coupling mechanism.

Since β3 was shown to alter DIV-VSD activation (**Fig 2.2**), we also tested the β3 effect on the N1765A channel. Like β1, β3 still causes depolarizing shifts in the DIV F-V curve (**Fig 2.4c**) and voltage dependence of gating charges (Q-V) of the N1765A channel, suggesting that β3 does not interact with the DIV pore domain to regulate DIV-VSD activation via the S4-S5 linker. In addition to the DIV effect, we also showed that DIII-VSD is significantly affected by β3. We assessed the β3 effects on channels that contain a mutation that decouples the DIII-pore from its VSD. A1149, located on the DIII S4-S5 linker of $Na_V1.4$, is one of the key residues on the gating interface (Muroi et al., 2010). Mutating A1149 to W in the $Na_V1.4$ stabilizes the activated DIII-VSD, but not the pore, suggesting that the coupling between the DIII-VSD to the DIII-pore is reduced (Muroi et al., 2010). The homologous residue in the $Na_V1.5$ isoform is A1330. Consistent with previous studies, A1330W greatly hyperpolarized the DIII F-V curve, compared to WT. However, ionic current activation (G-V) was not significantly affected. When co-

expressed with β3, the DIII F-V was still significantly depolarized ($\Delta V_{1/2}$=22.6±6.7, p=0.03), compared to A1130W alone (**Fig 2.4b**). This result suggests that β3 does not regulate DIII-VSD activation via S4-S5 linker coupling to the DIII-pore domain. However, there are alternate means to compule the pore to the VSD, including the DIII-DIV linker, and these alternative mechanisms could possibly be in play.

Assessing β subunit localization

Since we observed that β1 and β3 modulate channel gating by affecting the DIII and DIV VSDs, we hypothesized that β1 and β3 are proximally located to these VSDs. To test this hypothesis, we introduced a fluorophore or a quenching tryptophan into the β subunit. This method was previously applied to other proteins, such as T4 lysozyme (Mansoor et al., 2010; Mansoor, Mchaourab, & Farrens, 2002) and the BK channel (A. Pantazis & Olcese, 2012) to map distances within proteins. We reasoned that if β1 or β3 resides near one of the channel's VSDs, introducing a tryptophan residue to the top of the transmembrane segment of β1 or β3 would quench the fluorophore attached to the S3-S4 linker of that VSD.

We first introduced a tryptophan mutation to the extracellular region of the β1 transmembrane segment, S156W. Compared to WT β1, S156W β1 only slightly depolarizes the DI and DIV F-V curves, but none of the domains' fluorescence signal was significantly quenched. This result suggests that the β1 transmembrane segment is not within detectable quenching distance to the S4s of any domain.

We then introduced a tryptophan mutation into the extracellular region of the β3 transmembrane segment, S155W. S155W β3 did not affect DI, DII or DIV F-V curves or fluorescence compared to WT β3, but the fluorescence of the DIII-VSD was completely reversed (**Fig 2.5a**). In the DIII-

LFS construct, the DIII-VSD fluorescence signal moves downward upon membrane depolarization (**Fig 2.2h**). This reduction in fluorescence is consistent with local environment quenching of the fluorophore attached to the S3-S4 linker of DIII upon activation. In contrast, when S155W β3 is present, its tryptophan strongly quenches the fluorophore on the DIII S3-S4 linker when S4 is at resting position. When S4 activates, the fluorophore moves away from the tryptophan, resulting in an increase in fluorescence. This result shows that the β3 subunit resides very near to the DIII-VSD at a distance that is within the van der Waals contact distance (5-15 Å) (Mansoor et al., 2002). Notably, the DIII fluorescence kinetics with S155W β3 are greatly slowed, and the F-V curve has similar voltage dependence ($V_{1/2}$=-67.2±3.5mV) as the second component of DIII F-V with high β3 expression (**Fig 2.3c**). Thus, the DIII fluorescence with S155W β3 tracks a slower component of the DIII-VSD that occurs at higher potentials, a component which is observed but not prominent with the LFS construct.

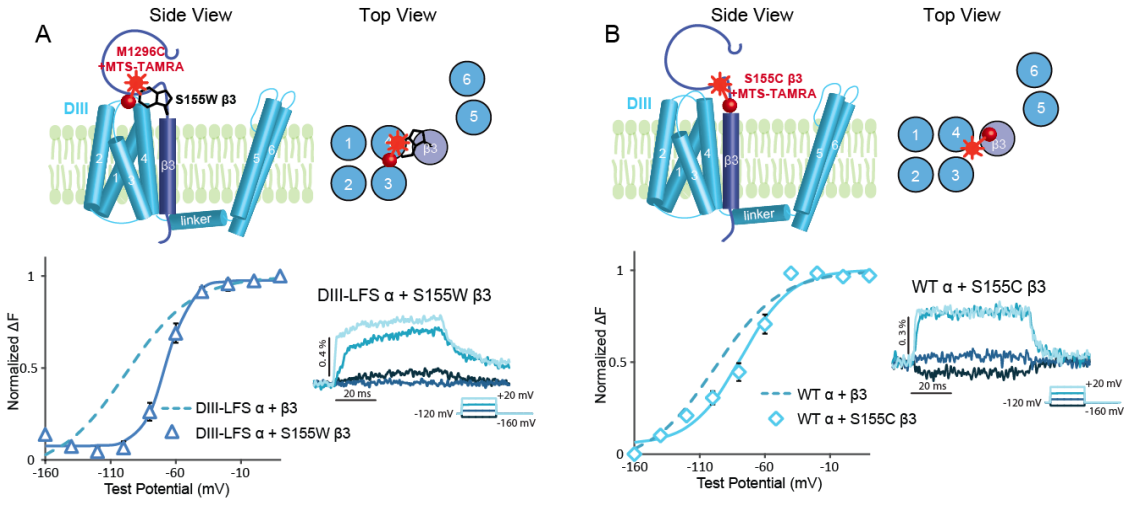

Figure 2.5 tryptophan-induced quenching of the fluorophore method reveals β3 proximity to the DIII-VSD
a) Side view and top view showing the proposed location of the β3 subunit with respect to the channel. A tryptophan mutation is made on of the extracellular β3 domain. Fluorescence-voltage (F-V) curve of DIII-LFS co-expressed with S155W β3(triangles), in comparison to F-V curve of DIII-LFS co-expressed with WT β3 (dotted line). b) Side and top view showing WT α subunit co-expressed with S155C β3 that is labeled with MTS-TAMRA. F-V curve of WT α co-expressed with the labeled S155C β3 (diamond), compared to the DIII-LFS co-expressed with WT β3 (dotted line).

If β3 and the DIII-VSD are close in proximity, we would also expect to track DIII-VSD conformational changes by labeling the β3 subunit. To test this hypothesis, we introduced a cysteine into the extracellular β3 segment, S155C. We co-expressed S155C β3 with the WT $Na_V1.5$ α subunit in *Xenopus* oocytes. We then labeled the S155C β3 with a fluorophore (MTS-TAMRA). A voltage-dependent fluorescence signal was detected (**Fig 2.5b**). Changes the local environment of the fluorophore attached to β3 when DIII-VSD changed conformation likely produced this signal. The F-V curve of WT α subunit with labeled S155C β3 is comparable to the F-V curve of labeled DIII-LFS α subunit with WT β3 subunit (**Fig 2.5b**). This result suggests that the fluorescence signal generated by the labeled β3 represents the conformational changes of DIII-VSD.

Using the tryptophan-induced fluorophore quenching method (Mansoor et al., 2010, 2002; A. Pantazis & Olcese, 2012), we demonstrated β3's proximity to the DIII-VSD. Given that β3 still affects the DIII-VSD that is decoupled from the pore by the A1330W mutation, and the location of the β3, we conclude that β3 modulates DIII-VSD by direct interaction. Taking advantage of β3 proximity to the DIII-VSD, we are now able to track the DIII-VSD conformation without directing labeling the α subunit.

β1 and β3 chimeras show that both the extracellular and transmembrane domains of β3 are essential for its interaction with the DIII-VSD

We observed that β1 and β3 have distinct interactions with channel VSDs, especially the DIII-VSD. In response, we sought to further understand which part of the β subunit is essential for these interactions. We created 3 chimera β1 and β3 subunits (**Fig 2.6a**), one with the β3 extracellular domain and β1 transmembrane and intracellular domain (β3-N β1-TMC), one with

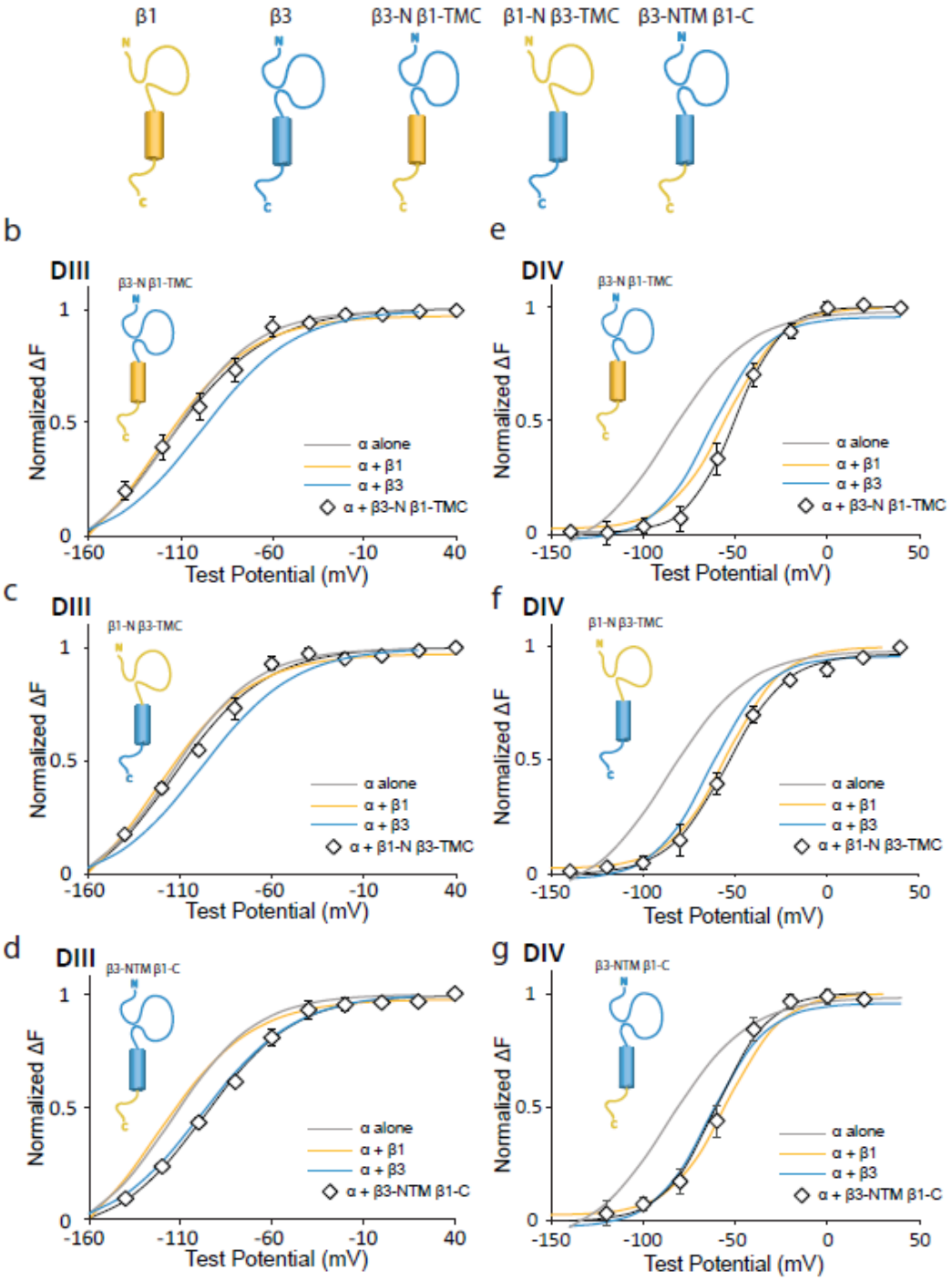

Figure 2.6 β1/β3 chimeras reveal that both extracellular and transmembrane domains of β3 are essential for its modulation of DIII-VSD a) Three β1/β3 chimeras were created, β3-N β1-TMC, β1-N β3-TMC, β3-NTM β1-C, based on predicted extracellular, transmembrane, and intracellular sequences from Uniprot. mRNA encoding β1/β3 chimeras and DIII or DIV VCF constructs were co-injected at a molar ratio of 3:1. b-d) DIII F-V curve with β1 (yellow line), β3 (blue line), β1/β3 chimera (black diamond), or without β (grey line). e-g) DIV F-V curve with β1 (yellow line), β3 (blue line), β1/β3 chimera (black diamond), or without β (grey line).

the β1 extracellular domain and β3 transmembrane and intracellular domain (β1-N β3-TMC), and one with both extracellular and transmembrane domains of β3 and the β1 intracellular domain (β3-NTM β1-C). Comparison of the DIII F-V curves for all three chimeras illustrates that both the extracellular and transmembrane domains of β3 are necessary for its modulation of the DIII-VSD activation, since only the chimera that contains both extracellular and transmembrane domains of β3 (β3-NTM β1-C) caused a depolarizing shift in DIII F-V (**Fig 2.6d**) compared to α alone ($\Delta V_{1/2}$ =22.9±5.0mV, p=0.003), resembling the shift induced by WT β3 subunit ($\Delta V_{1/2}$ =20.7± 3.9mV, p=0.01). The other two β1/β3 chimeras caused no shift in DIII F-V curve compared to α alone, resembling the β1 subunit effects (**Fig 2.6b, c**).

The DIV-VSD response to these β1/ β3 chimeras is more difficult to interpret, because both WT β1 and β3 cause comparable depolarizing shifts in the DIV F-V (**Fig 2.1, 2.2**). Notably, the β3-N β1-TMC chimera causes a larger depolarizing shift of the DIV-VSD ($\Delta V_{1/2}$ =32.7± 1.2mV, p=0.001) than β1 or β3 (**Fig 2.6e**). Both β1-N β3-TMC and β3-NTM β1-C cause DIV F-V depolarization that is similar to WT β1 or β3 (**Fig 2.6f, g**). This result suggests that the interaction of the β3 extracellular domain with the channel can cause additional modulation of the DIV-VSD, and induce an interaction mechanism that is distinct from the transmembrane and C-terminus of the β1 subunit. Previously, we observed that the WT β1 subunit causes the DIV-VSD to deactivate more quickly (**fig 2.1**). Comparing DIV-VSD deactivation kinetics of these chimeras, we note that both β3-N β1-TMC and β3-NTM β1-C chimeras that contain β1 C-terminus, resemble the fast DIV deactivation induced by WT β1 (β3-N β1-TMC: $t_{100\%-10\%}$=3.9±0.6ms, p=0.0002 compared to α alone; β3-NTM β1-C: $t_{100\%-10\%}$=3.7±0.3ms, p=0.0004, compared to α alone), suggesting that the β1 C-terminus is important for speeding DIV-VSD deactivation upon membrane repolarization.

By monitoring DIII- and DIV-VSD conformations in the presence of β1/ β3 chimeras, we found that the extracellular and transmembrane domains of β3 subunit are essential for depolarizing DIII-VSD activation, which controls channel current activation kinetics. The C-terminus of β1 is essential for speeding DIV-VSD deactivation kinetics upon membrane repolarization, which will affect channel recovery from inactivation.

β1 and β3 effects on the DIII- and DIV-VSDs are not independent

Both β1 and β3 have been shown to express in the ventricular myocardium (Fahmi et al., 2001; M S Olesen et al., 2011), to modify $Na_v1.5$ gating in concert. To assess the molecular consequences when both β1 and β3 subunits are expressed, we co-injected mRNA of the α, β1, and β3 subunits at a molar ratio of 1:3:3 (**Fig 2.7a**). As with co-expression of β1 or β3, simultaneously co-expressing the channel with both causes a depolarizing shift in the SSI curve (**Fig 2.7b**), compared to the α subunit alone. The magnitude of this shift is not significantly different to the shifts induced by β1 or β3 (**Fig 2.7b**), raising two possible mechanisms. One explanation is that only one of the β1 and β3 subunits can co-assemble with the α subunit at a time, so that the shift is an average of the shifts induced by either β1 or β3. The other possibility is that β1 and β3 binding to the α subunit is not exclusive, and there might be some cooperation and interaction between the β1 and β3 that are bound to the same α subunit. The latter mechanism appears more likely, as we also observe a depolarizing shift in the G-V curve caused by co-expression with both β1 and β3 subunits ($\Delta V_{1/2}$ =7.2± 2.3 mV, p=0.02) (**Fig 2.7b**), which was not seen in α with only β1 or β3.

To gain insight into potential interaction mechanisms between β1 and β3, we assessed the co-expression of both β1 and β3 on the activation of each VSD. Co-expression of β1 and β3 have minimal effects on DI- and DII-VSD activation, as no significant shift was observed in DI and

DII F-V (**Fig 2.7c, d**), consistent with previous observation that β1 and β3 do not perturb DI- or DII-VSDs. Compared to α alone, co-expression with both β1 and β3 caused a depolarizing shift in the DIII-VSD (**Fig 2.7e**). The magnitude of this shift was greater than the linear addition of the shifts induced by β1 only, and β3 only (dotted line), suggesting that when both β1 and β3 were present, they produced additional depolarization of DIII-VSD activation, corresponding to the depolarizing shift in channel activation. Thus, we infer that there must be cooperation between β1 and β3 that causes a greater effect on the DIII-VSD when both are interacting with the channel.

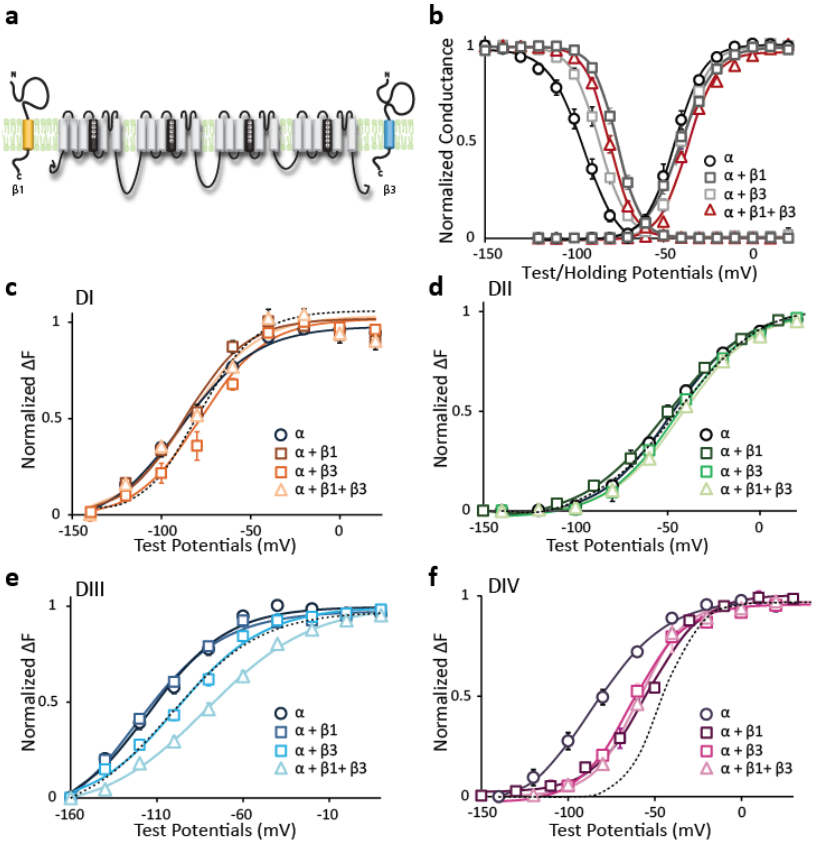

Figure 2.7 Simultaneous co-expression of the β1 and β3 reveals cooperativity between these two subunits.
a) Both β1 and β3 subunits are co-expressed with Nav1.5 by co-injecting mRNAs encoding Nav1.5, β1, and β3 at a molar ratio of 1:3:3. b) Voltage-dependence of activation (G-V), and steady-state inactivation (SSI) for LFS-DIII Nav1.5 co-expressed with β1 (square), β3 (square), β1+ β3 (triangles), or without β (circle). c-f) DI-DIV F-V curve with β1 (square), β3 (square), β1+ β3 (triangles), or without β (circle) co-expressed. The dotted line represents the sum of the shifts induced by β1 and β3, with respect to no β.

In contrast, expressing β1 and β3 together caused a DIV F-V depolarizing shift that most closely resembles the shift produced by β1 or β3 only (**Fig 2.7f**), and also corresponds to the SSI shift (**Fig 2.7b**). If β1 and β3 act independently, the DIV F-V shift should resemble the linear addition of β1 and β3-induced shifts (**Fig 2.7f dotted line**). Thus, this result suggests that β1 and β3's modulation of DIV-VSD is not additive.

Together, these results show that β1 and β3 binding to the $Na_V1.5$ channel is not exclusive, and when both β subunits are present, their cooperativity further depolarizes DIII-VSD activation, which leads to additional modifications of channel activation. The physiological impact of this result is limited, because this experiment was conducted in the condition of overexpressing β subunits, which may cause additional binding that may not happen in native cells. More information regarding the stoichiometry of α, β1, and β3 in native cells is required to infer the physiological consequences of β1 and β3 subunit cooperativity.

2.4 Discussion

The non-covalently bound Na_v channel β1 and β3 subunits were first identified in 1985 (Messner & Catterall, 1985) and 2000 (Morgan et al., 2000a). Despite recent findings showing that these subunits play a critical role in regulating neuronal and cardiac electrophysiology (Calhoun & Isom, 2014), the precise mechanisms that they use to modulate channel gating have not been described. In this study, we utilized VCF to test the hypothesis that the β1 and β3 subunits regulate Na_V channel kinetics via the VSDs. We discovered that WT β1 subunit co-expression shifts DIV-VSD activation to depolarized potentials, consistent with the shift in SSI. β1 subunits also relieve the immobilization of the DIII- and DIV-VSDs by fast inactivation, which potentially contributes to the increased rate of channel recovery from inactivation induced by β1.

The WT β3 subunit also regulates channel inactivation with a corresponding shift in DIV-VSD activation. However, in contrast to β1, there is a prominent WT β3 interaction with the DIII-VSD. We believe β3 modulation of DIII-VSD is primary, since we showed that the transmembrane domain of β3 is very close to the DIII S4 by tryptophan-induced fluorophore quenching. Moreover, β1/β3 chimeras mainly affect the DIII-VSD without changing DIV-VSD activation. Recently, we showed that DIII-VSD deactivation strongly correlates with channel recovery from inactivation, a phenomenon that is determined by the DIII S4-S5 linker's interaction with the inactivation gate after ~100ms pulses (Hsu et al., 2017b). Here, we observed that β3 does not affect channel recovery from inactivation, even though it speeds DIII-VSD deactivation, suggesting that β3 possibly disrupts the interaction between the DIII S4-S5 linker and the inactivation gate, abolishing DIII-VSD regulation of recovery from inactivation.

Despite the β1 and β3 subunits being homologous, we demonstrate that they have distinct interactions with the Na_V channel VSDs, resulting different current kinetics and rates of inactivation recovery. Consistently, our results from the tryptophan induced quenching experiment showed that β1 and β3 assemble with the channel at different locations. As β1 and β3 have very different spatial and temporal expression patterns in heart (Domínguez et al., 2005; Okata et al., 2016), the molecular interactions that we have observed will significantly affect their regulation of tissue excitability. For regions that have higher β1 expression, for example Purkinje fibers in heart (Domínguez et al., 2005), we would expect cells to be more excitable because β1 causes Na_V channels recover more quickly and increase channel availability, consistent with the Purkinje fiber role of fast conduction of cardiac excitation. During heart development, β1 expression increases, while β3 decreases (Domínguez et al., 2005; Okata et al., 2016). This dynamic temporal expression pattern suggests that β1 contributes more to mature

Na_V channel properties, such as increased excitability. Thus, we expect that molecular-level differences in β1 and β3 regulation of the DIII- and DIV-VSDs will affect organ level behavior.

β1 and β3 localization within the $Na_V1.5$ channel complex

The β1 subunit has been found to express and co-assemble with both neuronal and cardiac Na_v channels (Isom et al. 1992b). There is a general consensus that when β1 co-assembles with $Na_V1.5$, it regulates steady-state inactivation (Calhoun & Isom, 2014). However, the direction and magnitude of the inactivation shift varies depending on the expression system used and protocols applied (Calhoun & Isom, 2014). This variability may be linked to the interaction between β1 and other members of the macromolecular Na_V channel complex in native cells, such as Ankyrin G (Malhotra et al. 2002). Thus, the nature of β1-α interaction may vary by expression system, precluding the identification of a universal phenotype.

Several α-β1 interaction sites have been proposed. On the α subunit, a C-terminal mutation was able to eliminate β1 regulation of $Na_V1.1$ current kinetics (Spampanato et al., 2004a), and $Na_V1.4$/$Na_V1.5$ chimeras show that the S5-S6 linker of DIV plays a role in α-β1 interaction (Makita et al., 1996). Both results suggest that binding occurs near the DIV domain. Aside from the consequences of direct binding, the β1 subunit has also been shown to introduce the surface charges that electrostatically affect channel gating (Ferrera & Moran, 2006). We observed that WT β1 mainly affects the voltage dependence of DIV-VSD activation and its deactivation kinetics through possible direct interaction with the DIV-VSD, which suggests β1 proximity to the DIV-VSD. Together, these results support the hypothesis that β1 modulates inactivation by altering DIV-VSD activation. We infer that β1 most likely resides in the cleft between the DIII and DIV-VSD (**Fig 2.8a, b**).

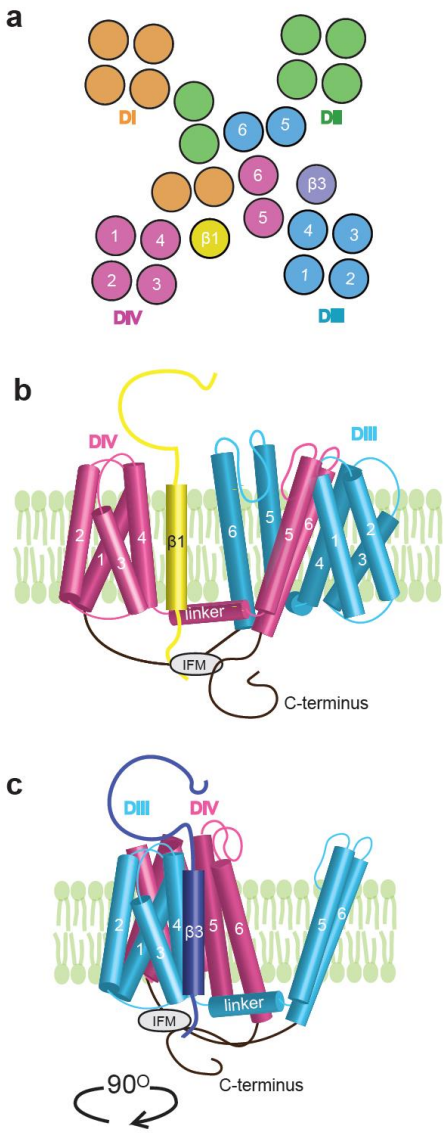

Figure 2.8 Proposed model for β1 and β3 assembly with NaV1.5 channel a) Extracellular view of the Nav1.5 channel based on the Navab structure (Payandeh, Scheuer, Zheng, & Catterall, 2011). b) Side view of NaV1.5, co-assembled with β1 subunit. Only DIII (blue), and DIV (pink) are shown for clarity. Our model suggests β1 locates in the cleft between the DIII-VSD and DIV-VSD, allowing it to interact with the DIV VSD, C-terminus, and potentially S4-S5 linker of DIV, to modify DIV-VSD movements. c) Side view of Nav1.5 (rotated 90^{O}), co-assembled with β3 subunit. Our model suggests β3 locates in the cleft between the DIII-VSD and DII-VSD, next to S4 of DIII, allowing it to strongly modify DIII-VSD activation, and affecting DIII-VSD to pore coupling by interacting with the hinge connecting S4 and S4-S5 linker of DIII.

The β3 subunit is homologous to β1, and also interacts with Na_v channels non-covalently. Less is known about the α-β3 interaction. Because the β1 and β3 subunits are homologous (50%), it has

been generally supposed that β3 interacts with the channel via the same mechanism as β1 (Namadurai et al., 2015). In contrast, we found that the WT β3 subunit caused a large depolarizing shift in DIII-VSD activation, in addition to the DIV shift. The depolarization of DIII-VSD activation slowed down ionic current activation and inactivation kinetics, allowing the DIII-VSD to play a more prominent role in regulating this gating over a physiological range of potentials. Further, we demonstrated β3 proximity to the DIII S4 segment, as we observed that a tryptophan mutation on the top of β3 subunit strongly quench the fluorophore attached to the DIII S3-S4 linker. It is most likely that β3 is adjacent to the DIII S4 segment, in the cleft between the DII and DIII VSDs, which allows β3 to directly interact with the DIII-VSD. Altered DIII-VSD activation can then allosterically affect DIV-VSD activation. Yet, we observed that β3 still depolarized the DIV-VSD when the DIV-VSD to pore coupling via the S4-S5 linker was abolished by the N1759A mutation, suggesting that this coupling to the DIV-VSD takes place via alternative mechanisms, such as the DIII-DIV linker.

The importance of β3 in maintaining normal cardiac function has been highlighted by *scn3b* knock-out mice. These mice exhibit slowed sino-atrial and atrioventricular conduction, burst-pacing-induced atrial tachycardia, fibrillation, and ventricular tachycardia (Hakim et al. 2010; Hakim et al. 2008). Consistent with our results (**Fig. 2.2**), knocking out β3 shifts Na_v SSI to negative potentials, reducing peak Na^+ current in the ventricle, which causes slowed conduction and decreased action potential duration in the endocardium and epicardium. Given the consistency of the knockout mouse phenotype with our results, we infer that β3 regulation of the $Na_V1.5$ DIII and DIV-VSDs significantly determines action potential morphology and conduction.

When we expressed β1 and β3 together, we observed enhancement of the depolarizing DIII-VSD shift and an exclusive effect of β1 on the DIV-VSD (**Fig. 2.6**). These results imply that the subunits do not interact with the channel independently. Consistently, previous work has shown that heterophilic interaction between the β1 and β3 subunits can occur via their respective Ig domains (Yereddi et al., 2013), which could possibly alter their interaction with each VSD. β3 binding to β1 may affect its interaction with the DIII-VSD. Our proposed localization of β1 and β3 would bring the extracellular domains of both subunits near to the DIII-S4 (**Fig 2.8**). In sum, our results show that both the β1 and β3 subunits are likely able to co-assemble with a single $Na_v1.5$ channel complex and that this co-assembly significantly affects channel function.

Each domain of β1 and β3 has distinct interactions with $Na_V1.5$ channel

By measuring VSD conformation in the presence of β1/β3 chimeras, we showed that both the extracellular and transmembrane domains of β3 are necessary for β3 depolarization of the DIII-VSD. When channels were co-expressed with β1/ β3 chimeras containing the β3 extracellular domain and the β1 transmembrane and intracellular domain, DIII-VSD activation was not depolarized, suggesting that the transmembrane domain of β3 is critical for localizing the β3 subunit to this location in $Na_V1.5$, allowing the extracellular Ig domain of β3 to interact with the DIII-VSD. We also showed that the C-terminus of the β1 subunit is necessary for relieving DIV-VSD immobilization, and the β3 C-terminus is important for relieving DIII-VSD immobilization from fast inactivation. Previously, we showed that the interaction between the fast inactivation gate (IFM) and the N1659 residue on DIV S4-S5 linker plays important role in immobilizing DIII and DIV-VSD. It is plausible that the β1 C-terminus can interact with the intracellular DIV-S5 segment, altering this interaction. These results show that β1 and β3 could interact with the

Na_V channel through multiple interaction sites, and that both the extracellular domain and C-terminus play important roles in determining their gating properties.

Two step movements of DIII-VSD revealed by high expression of β3.

Like K_V channels, two step transitions of Na_V channel VSDs have been proposed, based on previous observations that pulses of increasing duration alter the DIII-VSD deactivation rate (Hsu et al., 2017b; Varga et al., 2015). Our results support this suggestion by showing that high levels of β3 subunit expression cause two prominent components of DIII-VSD activation. This phenomenon is similar to KCNQ1 channels that show two step activation in the presence of KCNE1 that stabilizes the activated-VSD closed-pore state and slows ionic current activation (Barro-Soria et al., 2014). Similarly, the activation of Na^+ current is slower when β3 separates the DIII-VSD transition into two components. Additionally, since Na_V channels have very fast and prominent inactivation, the separation of DIII-VSD movement will increase the amplitude Na^+ current as the channels are excited repetitively at relatively high frequency (>3Hz).

Our study shows that β1 and β3's differential interactions with the DIII and DIV VSDs determine their regulation of Na^+ current and cell excitability. These distinct regulatory mechanisms are essential for understanding how β subunits regulate excitable cells and how mutant β subunits cause disease.

2.5 Materials and Methods

Molecular Biology

cDNA encoding the human Nav β3 (UniProtKB/Swiss-Prot accession no. Q9NY72) subunit was custom-synthesized by Life Technologies and inserted into the pBSTA plasmid. cRNAs for the human β1 subunit (UniProtKB/Swiss-Prot accession no. Q07699.1) and α-subunit NaV1.5 (accession no. Q14524.1) were produced from the pBSTA and pMAX vectors respectively. All mutagenesis was accomplished using the QuikChange II site-directed mutagenesis kit (Agilent), with primers from Sigma-Aldrich. Multiple colonies were picked and plasmids were isolated using the NucleoSpin plasmid miniprep kit (Macherey-Nagel). After samples were confirmed with sequencing (Genewiz), a single clone was selected for a Midiprep preparation (NucleoBond Xtra Midi, Macherey-Nagel). Each plasmid was then linearized with the NotI or EcoRI restriction enzyme, and purified with the NucleoSpin Gel and PCR Clean-up kit (Macherey-Nagel). Finally, capped mRNA was synthesized in vitro using mMessage mMachine T7 Transcription Kit (Life Technologies), purified via phenol-chloroform extraction and reconstituted to a concentration of ~1 μg/μL.

Cut-open oocyte recording

mRNAs for the human α-subunit Nav1.5 and β1 or β3 subunits were injected at a 3:1 molar ratio (50-56 ng per cell total) into Xenopus oocytes. Oocytes were then incubated at 18°C in ND93 solution (mM: 93 NaCl, 5 KCl, 1.8 CaCl2, 1 MgCl2, 5 HEPES, and 2.5 Na-pyruvate, and 1% penicillin-streptomycin, pH 7.4). 3-7 days after injection, cut-open recordings(Rudokas et al. 2014; Stefani and Bezanilla 1998) were performed using a cut-open amplifier (CA-1B, Dagan Corporation) coupled to an A/D converter (Digidata 1440; Molecular Devices). Clampex

software (v10, Molecular Devices) was used for data acquisition. During records the temperature was maintained at 19°C with a controller (HCC-100A, Dagan Corporation). The internal recording solution was composed of (mM): 105 NMG-Mes, 10 NaMes, 20 HEPES, and 2 EGTA, pH 7.4, and the external solution was (mM): 25 NMG-Mes, 90 Na-Mes, 20 HEPES, and 2 Ca-Mes2, pH 7.4.

Prior to recording, the membrane capacitance compensation and P/–8 leak subtraction were applied. The ionic currents were recorded using the standard I-V protocol. From a -120mV holding potential, cells were stepped to a 100ms pre-pulse of -120mV, then stepped to test potentials ranging from -120mV to 60mV with 10mV increment, preceding by a 100ms post-pulse of -120mV. For steady-state inactivation, cells were held at test potential for 200ms, then tested availability by a depolarizing pulse of -20mV. Gating currents were recorded during test pulses from -150 to 50mV from a holding potential of -120mV. Capacitance and leak were compensated by P/4 leak subtraction with a subsweep potential of 40mV. Gating charge-voltage (QV) curves were constructed by integrating gating currents over 7ms after voltage step.

Voltage clamp fluorometry

Before recording, oocytes were labeled with 10 μmol/L methanethiosulfonate-carboxytetramethylrhodamine (MTS-TAMRA, Santa Cruz Biotechnology) in a depolarizing solution (mM: 110 KCl, 1.5 MgCl2, 0.8 CaCl2, 0.2 EDTA and 10 HEPES, pH 7.1) for 30 minutes on ice. Fluorescence data was collected simultaneously with ionic current on a custom rig (Varga et al., 2015), combining cut-open voltage clamp and an epifluorescence upright microscope (FN1, Nikon), using a 40X water-immersion objective with 0.8 NA (CFI Plan Fluor, Nikon). A green, high-powered LED (Luminus, PT-121) was used for illumination, controlled by a driver (Lumina Power, LDPC-30-6-24VDC) by Clampex software. The emission light was

measured with a photodiode (PIN-040A, United Detector Technology) mounted on the microscope epifluorescence port. The photocurrents generated by photodiode were then amplified by a patch clamp amplifier (Axopatch-200A, Molecular Devices). Each fluorescence trace is an average of 7-10 fluorescence recordings of the same cell.

Data analyses

Data analyses were performed using Clampfit (v10, Molecular Devices), Matlab (R2012a, Matlab), and Excel (Microsoft). For fluorescence data, signals were low-pass filtered at 1kHz offline, before analysis. To correct for photo-bleaching, the baseline fluorescence trace, which has no change in voltage, was fit and subtracted from the traces recorded when the voltage protocol was applied.

Steady state voltage dependence curves (G-V, F-V, SSI) were quantified by fitting a Boltzmann function: $y= 1/(1+\exp[(V-V1/2)/k])$. Sample sizes were chosen so that the standard error of mean was less than 0.1 for each data point, and a minimum sample size of 3 was determined to calculate the standard deviation. Each data point shown reflects n=3 or more from 2 or more batches of oocytes. Statistics for comparison between different constructs were performed using independent t-test (Excel, Microsoft). The ± symbols in the text/table, and error bars in the figures represent the standard errors of mean (S.E.M.).

Chapter 3

Predicting Patient Response to the Antiarrhythmic Mexiletine Based on Genetic Variation: Personalized Medicine for Long QT Syndrome

3.1 Summary

Background: Mutations in the *SCN5A* gene, encoding the α subunit of the Nav1.5 channel, cause a life-threatening form of cardiac arrhythmia, Long QT Syndrome Type 3 (LQT3). Mexiletine, which is structurally related to the Na^+ channel-blocking anesthetic lidocaine, is used to treat LQT3 patients. However, the patient response is variable, depending on the genetic mutation in *SCN5A*.

Objectives: The goal of this study is to understand the molecular basis of patients' variable responses and build a predictive statistical model that can be utilized to personalize mexiletine treatment based on patient's genetic variant.

Methods: We monitored the cardiac Na^+ channel voltage-sensing domain (VSD) conformational dynamics simultaneously with other gating properties for the LQT3 variants. To systematically identify the relationship between mexiletine block and channel biophysical properties, we used a system-based statistical modeling approach to connect the multivariate properties to patient phenotype.

Results: We found that mexiletine altered the conformation of the Domain-III VSD (DIII-VSD), which is the same VSD that many tested LQT3 mutations affect. Analysis of 15 LQT3 variants showed a strong correlation between the activation of the DIII-VSD and the strength of the inhibition of the channel by mexiletine. Based on this improved molecular-level understanding, we generated a systems-based model that successfully predicted the response of 7 out of 8 patients to mexiletine in a blinded, retrospective clinical trial.

Conclusions: Our results indicated that the modulated receptor theory of local anesthetic action, which confines local anesthetic binding effects to the channel pore, should be revised to include drug interaction with the DIII-VSD. Using an algorithm that incorporates this mode of action, we can predict patient-specific responses to mexiletine, improving therapeutic decision making.

3.2 Introduction

Class Ib antiarrhythmics are widely prescribed to treat patients with ventricular tachycardia, ventricular fibrillation(Priori, Blomström-Lundqvist, & Mazzanti, 2015), and Long QT (LQT) syndrome(Andrea Mazzanti et al., 2016). As a subset of the Class I agents that target the voltage-gated cardiac Na^+ channel, $Na_V1.5$, Class Ib drugs preferentially inhibit the late component of the Na^+ current (I_{Na}) to shorten action potential duration (APD) and prolong the effective refractory period (ERP)(Zipes & Jalife, 2013). Despite their ubiquitous clinical use, these drugs display high variability in efficacy and may cause a pro-arrhythmic response in some patients(Andrea Mazzanti et al., 2016; Ruan, Liu, Bloise, Napolitano, & Priori, 2007). For example, the classic Cardiac Arrhythmia Suppression Trial (CAST) showed that patients treated with Na_V channel inhibitors encainide or flecainide (Class Ic) were 2-3 times more likely to experience adverse events, compared to patients prescribed a placebo(Echt et al., 1991). Reasons for this stunning

clinical failure include an inability to predict which patients will be effectively treated with Class Ib molecules.

Recent clinical trials have shown that the class Ib drug mexiletine effectively shortens QT interval in a subset of LQT type 3 patients (LQT3)(A Mazzanti et al., 2016). LQT3 syndrome is caused by mutations in the SCN5A gene that encodes $Na_V1.5$, and accounts for approximately 10% of all LQT syndrome cases. Management of LQT3 has been challenging; beta-blockers, a mainstay of therapy for LQT1, have limited effectiveness for LQT3 patients and may be proarrhythmic(Shimizu & Antzelevitch, 2000). Despite mexiletine's overall efficacy, a spectrum of QT shortening was observed in patients that carry different SCN5A variants, effects that were reflected in single cell electrophysiology recordings(Ruan et al., 2007). A precise understanding of how $Na_V1.5$ mutations alter sensitivity to mexiletine would allow us to predict patient-specific response to mexiletine and develop better therapies.

Mexiletine is typically prescribed to patients who respond to intravenously administered lidocaine in the clinic, and its advantage is that it can be taken orally. Due to the structural similarity between mexiletine and lidocaine, it has generally been expected that these molecules interact with the Na_V channel via similar mechanisms. Mechanisms of lidocaine block have been studied for many years, and these reports show that it has a strong preference for the channels in the inactivated state(Bean, B.; Cohen, C J; Tsien, 1983; B Hille, 1977). This behavior is summarized by the modulated receptor theory proposed by Hille in 1977, which describes that the inhibitory action of local anesthetics is due to binding to a single receptor that is modulated by time and voltage dependent conformational changes within the channel such as those that cause inactivation(B Hille, 1977). Molecules may access this binding site in the channel pore

through both hydrophobic and hydrophilic pathways, where the hydrophilic pathway is only accessible when the pore opens, and the hydrophobic pathway through the cell membrane is accessible during both close and inactivated states of the channel (B Hille, 1977).

Recent advances in the understanding of the molecular structure of the alpha-subunit of Na_V sodium channels have shown that they are formed by a monomer with four homologous domains (DI-DIV), each composed by six transmembrane segments, S1-S6 (Gellens et al., 1992c). S1-S4 of each domain form the voltage sensing domain (VSD), and S5-S6 form the pore. Upon cell membrane depolarization, the VSDs activate and open the pore and allows Na^+ entry into the cell. Based on the observation that the replacement of phenylalanine with Lysine at position 1760 in the DIV-S6 segment eliminates use-dependent block by lidocaine (Hanck et al., 2009; D S Ragsdale, McPhee, Scheuer, & Catterall, 1996; David S Ragsdale, McPhee, Scheuer, & Catterall, 1994), it has been suggested that the drug binding site is within the pore region of the $Na_V1.5$ alpha-subunit.

More recent studies showed that VSD is part of the region that modulates binding of local-anesthetics to Nav1.5. The observation was prompted by the observation that the pore and VSDs are tightly coupled and therefore conformational changes induced by the binding of drugs within the pore can affect the voltage and time dependence of VSD conformation. Experiments that monitor VSD activation have shown that when lidocaine binds to the channel, it stabilizes the DIII-VSD in an activated conformation (Arcisio-Miranda et al., 2010b; Sheets & Hanck, 2003). This phenomenon is thought to be caused by lidocaine holding the pore-forming DIII-S6 in a partially open conformation even under hyperpolarized potentials, which then allosterically modulates the DIII-VSD to predispose its activated conformation (Arcisio-Miranda et al., 2010b).

We therefore hypothesized that the DIII-VSD plays an important role in the modulated receptor theory of local anesthetic block and it could contribute to the molecular mechanism underlying the heterogeneous response to mexiletine of different SCN5A variants that cause LQT3. Our results demonstrate the role of the DIII-VSD in the modulated receptor theory and create a systems-based model that predicts patient response to mexiletine therapy based on channel molecular gating properties.

3.3 Results:

Mexiletine stabilizes the active conformation of the DIII-VSD

We examined the effect of mexiletine on heterologously expressed Nav1.5 channels. The response to mexiletine was similar for some properties and different for others of the class Ib antiarrhythmics. Like other class Ib antiarrhythmics, mexiletine preferentially inhibited the late component of the Na^+ current (I_{Na}) compared with the effect on the peak current (D. W. Wang, Yazawa, Makita, George, & Bennett, 1997) (**Fig 3.1A**, top). Mexiletine also exhibited UDB (**Fig 3.1A**, bottom), which is a property of class Ib antiarrhythmics that is reflected by an increase in the inhibitory effect as the channels are repetitively activated by depolarizing voltage pulses.

Binding of class Ib drug lidocaine to the channel results in stabilization of the inactivated state, which is often reflected by a hyperpolarizing shift in the steady state inactivation (SSI) curve (D S Ragsdale et al., 1996). In contrast to lidocaine, mexiletine caused a minimal shift of the SSI curve (**Fig 3.1B)**. However, similar to lidocaine, mexiletine delayed recovery from inactivation, especially the slow component of recovery (**Fig 3.1C**). Thus, mexiletine appeared to influence the inactivated state through a mechanism different from that of lidocaine.

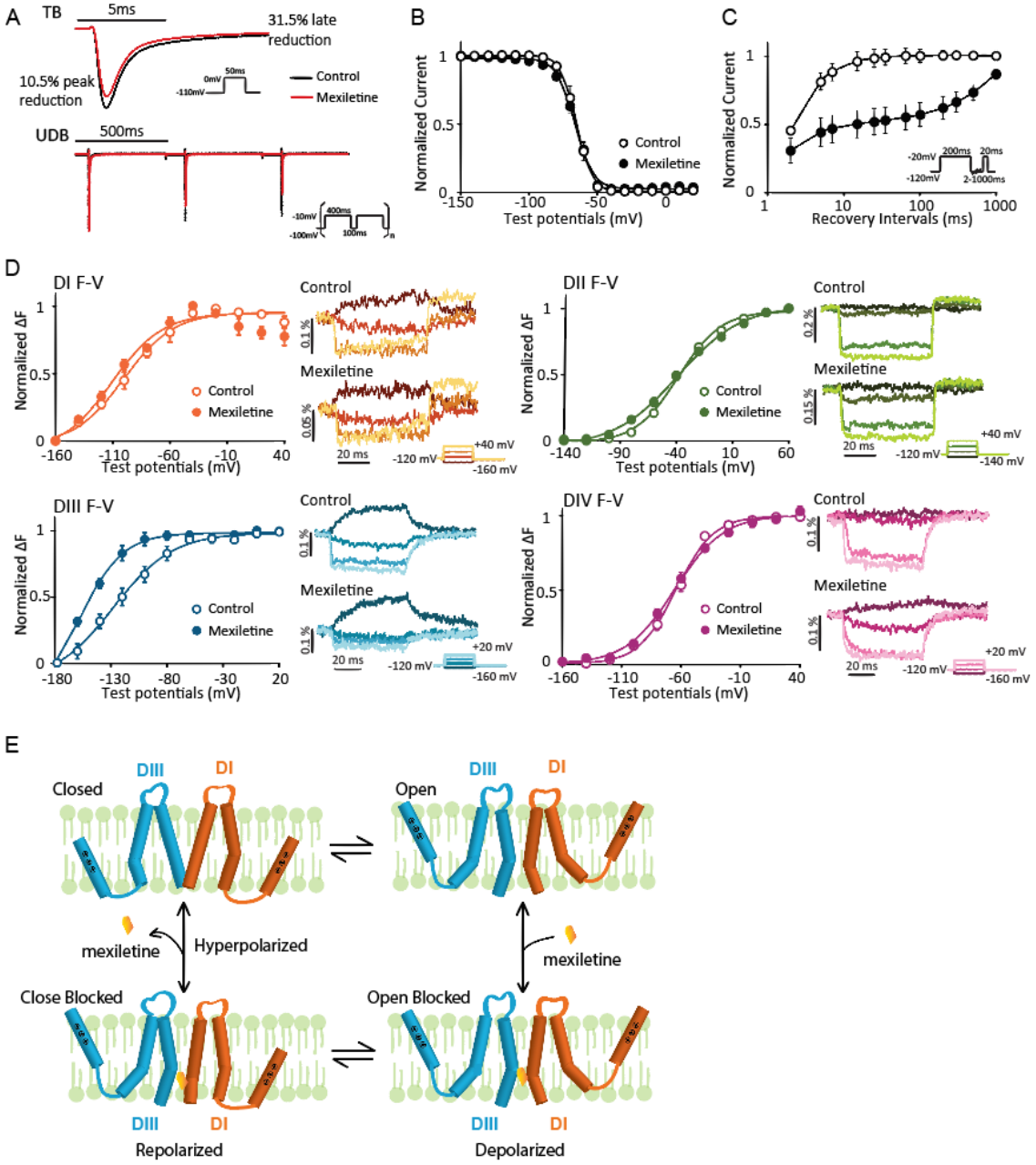

Figure 3.1 Mexiletine blockade of Nav1.5 channel stabilize the DIII-VSD at the activated position.
A. Representative current traces before and after 250 μM mexiletine tonic block (TB) and use-dependent block (UDB). B. Steady-state inactivation (SSI) curves before and after 2 mM mexiletine. Mexiletine induces minimal hyperpolarizing shift in SSI curve. C. Channel recovery from inactivation curves before and after 250 μM mexiletine. D. Left panels: Voltage dependence of steady-state fluorescence (F-V curves) from four domains (DI-V215C, DII-S805C, DIII-M1296C, DIV-S1618C) before and after 4 mM mexiletine. Fluorescence after mexiletine was measured after 80% tonic block. Right panels: representative fluorescence traces before and after mexiletine. Mexiletine only affects DIII-VSD by causing a hyperpolarizing shift in DIII F-V curve and slows down DIII-VSD deactivation, without affecting other three domains. E. Proposed schematic (adapted from Arcisio-Miranda lidocaine model[31]) showing the mechanism of mexiletine stabilization of activated DIII-VSD. Only DI and DIII are shown and the VSDs are represented by a single S4 segment for clarity.

Previously, multiple studies demonstrated that lidocaine block of Na_V channels enhances the stability of the DIII-VSD activated conformation (Arcisio-Miranda et al., 2010b; Sheets & Hanck, 2003). Here, we tested mexiletine interaction with the Nav1.5 VSDs by voltage-clamp fluorometry (VCF) (Varga et al., 2015). In these experiments, a fluorophore is tethered to the charged S4 segment of one of the four VSDs. As the VSD changes conformation, the environment around the fluorophore is altered, which changes emission from the fluorophore, enabling measurement of the time and voltage dependence of the VSD conformation. The steady-state fluorescence voltage (F-V) curves represent the voltage-dependence of the VSD activated conformation. Among four domains, only the DIII F-V curve displayed a large hyperpolarizing shift ($\Delta V_{1/2}$ = -32.5±7.5 mV, p = 0.04) after mexiletine block (**Fig 3.1D**), implying that the DIII-VSD remains in an activated conformation at more negative potentials upon mexiletine binding. Comparing the fluorescence traces before and after mexiletine block showed that both DIII and DIV-VSDs have slower activation and deactivation kinetics in the presence of mexiletine (**Fig 3.1D**). Because the DIII and DIV-VSDs are tightly coupled, the mexiletine-induced alteration of the DIV-VSD kinetics may be a consequence of its effects on the DIII-VSD.

To account for mexiletine's effects on the DIII-VSD, we proposed a model for its mechanism of action. Binding of mexiletine within the channel pore prevents the DIII-pore domain (S5-S6) from transitioning to a completely closed conformation during membrane repolarization (**Fig 3.1E**). The partially open conformation of the DIII-pore causes the DIII-VSD to remain in the activated conformation. This is like previously reported mechanisms of the interaction of lidocaine with Na_V channels.

LQT3 variants with different mexiletine sensitivities have distinct voltage dependence of DIII-VSD activation

To understand the molecular mechanisms underlying differences in mexiletine sensitivity among LQT variants, we tested channels with single point mutations R1626P or M1652R (**Fig 3.2A**), which exhibit different responses to mexiletine[4]. These two variants exhibited different responses to mexiletine under nonstimulated conditions, tonic block (TB), and under stimulated conditions, use-dependent block (UDB). Consistent with the previous studies, when compared to the effect of mexiletine on WT channels, the drug exerted TB of R1626P at lower concentrations (EC_{50} = 211.1 μM) and required higher concentrations to exert TB of M1652R (EC_{50} = 2035.3 μM). Mexiletine had an EC_{50}=760.8 μM for TB of WT channels (**Fig 3.2B**).

We assessed UDB by applying 400 ms depolarizing pulses at 2 Hz, mimicking conditions during ventricular tachycardia[4]. We found that WT and R1626P have comparable UDB (WT: EC_{50}=58.4 μM, R1626P: EC_{50}=56.6 μM), while M1652R has much lower UDB (EC_{50}=192.7 μM) (**Fig 3.2C**). We tested the UDB of mexiletine using the cut-open voltage clamp. The EC_{50} values that we observed with this method are higher than those reported using patch clamp analysis of HEK 293 cells[4]. We hypothesized that this difference is due to limited solution access to the cell membrane in the cut-open voltage clamp set-up during perfusion. To test this hypothesis, we measured dose responses using two-electrode voltage clamp (TEVC), which allows better access to the solution. TEVC recordings showed mexiletine EC_{50} values for each variant that were similar to previously reported values (**Table 3.1**), suggesting that, in the cut-open set-up, amount of mexiletine at the channel is approximately 3-fold lower than the perfused concentration (**Table 3.1**). With this information, we can account for the differences in EC_{50} values that relate to methodology.

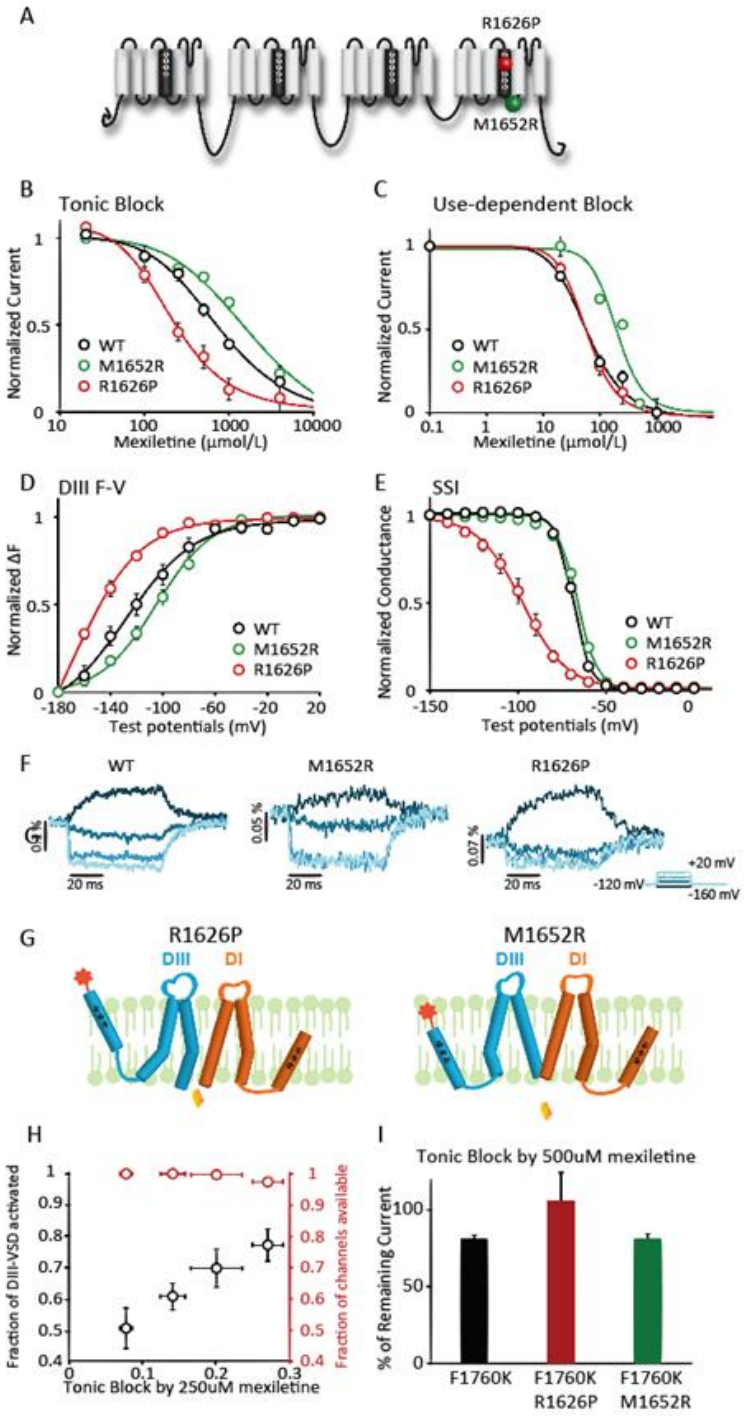

Figure 3.2 LQT variants with different sensitivities to mexiletine have distinct voltage dependence of DIII-VSD activation. A. Topology of Nav1.5 channel and location of the two LQT mutations with distinct mexiletine sensitivity, R1626P (red ball, sensitive) and M1652R (green ball, insensitive). B. Concentration dependence of tonic block (TB) by mexiletine for WT, R1626P, and M1652R channels expressed in Xenopus oocytes. EC50 values were 760.8 μM for WT, 2035.3 μM for M1652R, and 211.1 μM for R1626P channels. C. Concentration dependence of use-dependent block (UDB) by mexiletine. EC50 values were 58.4 μM for WT, 192.7 μM for M1652R, and 56.6

μM for R1626P channels. D. Voltage dependence of steady-state fluorescence of DIII. E.Steady-state inactivation (SSI) curves of WT, R1626P, and M1652R channels. F.Representative DIII fluorescence traces from WT-M1296C, M1652R-M1296C, and R1626P-M1296C. G.Proposed schematic showing possible mechanisms underlying the difference in mexiletine sensitivities between R1626P and M1652R. The DIII-VSD in the upward position represents the activated conformation. The lower position represents the inactivated conformation. At resting potential, R1626P has more activated DIII-VSD, which is coupled to the DIII pore domain (S5, S6), causing the pore to remain in a conformation with increase accessibility for mexiletine. In contrast, insensitive M1652R fewer activated DIII-VSDs, causing the DIII-pore to enter a conformation with less accessibility. H. The relationships between % of block and the fraction of DIII-VSD activated, or the fraction of current available for four different holding potentials (-120, -110, -100, -90 mV). I. TB by 500 μM mexiletine for F1760K, R1626P F1760K, M1652R F1760K channels.

To probe the link between the DIII-VSD conformation and mexiletine block, we assessed the correlation between DIII-VSD conformation and sensitivity of the channel to mexiletine. We hypothesized that, if mexiletine block of the pore caused the DIII-VSD to remain in the activated position, then channels with an activated DIII-VSD conformation would facilitate mexiletine accessibility to the pore. VCF experiments showed that both mutations significantly affected DIII-VSD conformation (**Fig 3.2D, 2F**), despite their locations in DIV-VSD, which is distant from DIII-VSD (**Fig 3.2A**). Compared to WT channels, the mexiletine-sensitive R1626P mutant exhibited a hyperpolarized DIII F-V curve ($\Delta V_{1/2}$ = -38.9 mV, p = 0.02), suggesting that more DIII-VSDs were in an activated conformation at the resting membrane potential. Conversely, the mexiletine-insensitive variant M1652R exhibited a depolarizing shift in the DIII F-V curve ($\Delta V_{1/2}$ = 28.2, p = 0.01), indicating that more DIII-VSDs were in deactivated conformation. The shifts in voltage dependence of the DIII-VSD activation mirrored the differences in block by mexiletine: The mutant with DIII-VSD in an activated conformation (R1626P) at the resting potential displayed higher TB. These results support our hypothesis of a reciprocal relationship between mexiletine block and DIII-VSD conformation of the mutants.

Conventionally, occupancy of the inactivated state has been considered the primary determinant of class Ib drug action. Consequently, the modulated receptor model describes preferential drug

binding to channels that are inactivated. To test this notion, we measured how variants affected the SSI curve. Although the most sensitive mutation R1626P shifted SSI prominently, the magnitude of the shifts by these two variants are not consistent with their differences in mexiletine block (**Fig 3.2E**).

	TB EC50 (μM)	UBD EC50 (μM)
cut-open voltage clamp		
WT	760	58.4
R1626P	211	56.6
M1652R	2035	192.7
two-electrode voltage clamp		
WT	449.9	36.7
R1626P	86.3	18.5
M1652R	633.3	96.7
patch clamp (HEK 293T) (reported in Ruan et al., 2007)		
WT	253	38.0
R1626P	153	8.8
M1652R	944	96.1

Table 3.1 Comparing EC50 for TB and UBD across different recording set-ups. Cut-open voltage clamp has 2 to 3-fold higher EC50 compared to two-electrode voltage clamp and patch clamp due to obstructed access to solution during perfusion.

To further test whether the conformation of DIII-VSD regulates mexiletine block independent of inactivation, we assessed TB of WT channels at various potentials ranging from -120 to -90 mV. At these holding potentials the WT channels exhibited full conductance (none in the inactivated state) (**Fig 3.2E**) and showed a range of DIII-VSD conformations (**Fig 3.2D**). At four different holding potentials, -120, -110, -100, and -90 mV, the channel showed altered TB by mexiletine (**Fig 3.2H**). Moreover, the amount of TB had a linear relationship with the fraction of DIII-VSDs in the activated conformation at those potentials (**Fig 3.2H**). This result showed that the

proportion of channels in the inactivated state is not the only factor that determines effectiveness of mexiletine block.

Based on our results, we proposed a model that explains the difference in mexiletine sensitivity between the two LQT variants (**Fig 3.2G**). At resting membrane potential, DIII-VSD of the sensitive variant R1626P tends to occupy the activated conformation. Because the activated conformation of DIII-VSD is coupled to conformation of the DIII-pore, the pore adopts a conformation that facilitates mexiletine accessibility. In contrast, fewer of the DIII-VSDs of the insensitive mutant M1652R are in the activated conformation at these potentials, causing the DIII-pore to remain in a conformation that prevents mexiletine from binding.

Voltage-dependent, not lipophilic, block accounts for differences in mexiletine response among LQT3 variants

The F1760K mutation eliminates UDB by lidocaine and prevents lidocaine from affecting gating currents. Based on this binding site, Hanck *et al*. categorized lidocaine block into two components: a voltage-independent lipophilic block and a voltage-dependent block. Lipophilic block is independent of the putative binding site F1760. We tested whether the difference in the EC_{50} for TB by mexiletine among the R1626P, M1652R, and WT channels is due to lipophilic or voltage-dependent block by monitoring their responses to mexiletine in the background of F1760K mutation.

We assessed the response of F1760K channels to mexiletine. Both TB and UDB by mexiletine are greatly reduced for the F1760K channel. Using VCF, we found that mexiletine did not alter the conformation of DIII-VSD of the F1760K mutant channel. We measured mexiletine-induced TB— at 500 μM, a concentration at which the difference in TB among the channels was evident

(**Fig 3.2B**), in WT, R1626P, and M1652R channels that also had the F1760K mutation. The TB achieved with 500 μM mexiletine in channels with F1760K was similar (**Fig 3.2I**). Thus, the differences in the EC_{50} values for mexiletine among these LQT variants appeared due to voltage-dependent block rather than lipophilic block.

Decoupling the DIII-VSD from the pore eliminates differences in mexiletine blockade among LQT3 variants

To further understand how the DIII-VSD affects mexiletine block, we utilized the A1326W mutation (**Fig 3.3A**), which decouples DIII-VSD from the pore (Muroi et al., 2010). In channels with A1326W, mexiletine no longer affects the conformation of DIII-VSD, demonstrating that a connection between the DIII-VSD and the pore is required to observe the mexiletine effect on DIII-VSD conformation. Our hypothesis is that R1626P and M1652R have distinct mexiletine sensitivities due to differences in the voltage dependence of DIII-VSD activation, consequently altering pore accessibility by mexiletine. From this hypothesis, we predict that channels in which the DIII-pore is decoupled from the DIII-VSD by A1326W will exhibit similar mexiletine block. Indeed, we observed that, upon the addition of A1326W, mexiletine caused similar TB and UDB for the R1626P, M1652R, and WT channels (**Fig 3.3B, C**).

In the presence of the A1326W mutation, the differences caused by R1626P or M1652R mutation in DIII-VSD activation and SSI are preserved (**Fig 3.3D, E**), suggesting that the A1326W mutation does not interfere with voltage-dependent DIII-VSD conformational changes. We proposed a model to explain the elimination of mexiletine sensitivity by the A1326W mutation in the two LQT3 variants (**Fig 3.3F**). Although R1626P stabilized and M1652R destabilized the activated conformation of DIII-VSD, the channel pore remains in the same conformation with the same mexiletine accessibility, because A1326W decoupled the DIII-pore

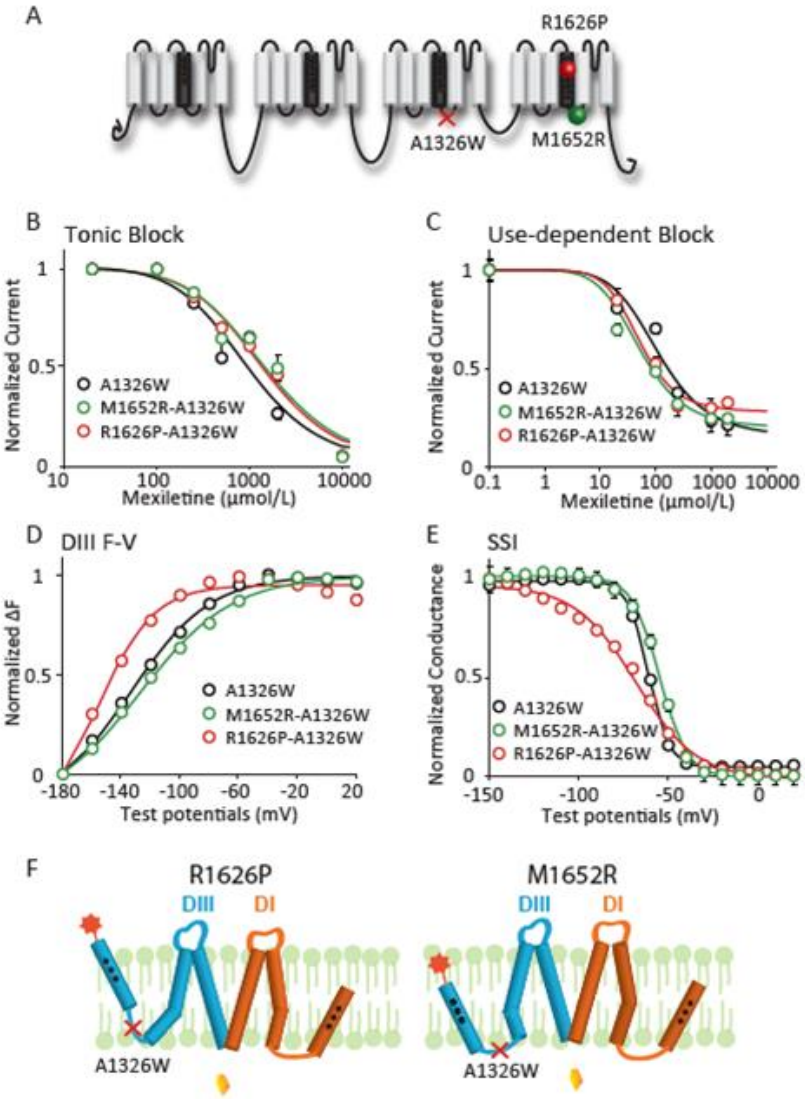

Figure 3.3 Mutation that decouples the DIII-VSD from DIII-pore eliminates differences in mexiletine sensitivity among LQT3 variants. A. Locations of the decoupling mutation A1326W and two LQT3 variant mutations, R1626P and M1652R. B. Concentration dependence of TB for A1326W, M1652R-A1326W, and R1626P-A1326W channels. EC50 values were 965.2 μM for WT, 1562.3 μM for M1652R, and 1440.7 μM for R1626P channels. C. Concentration dependence of UDB for M1652R-A1326W, and R1626P-A1326W channels. EC50 values were 113.0 μM for WT, 51.2 μM for M1652R, and 51.6 μM for R1626P channels. D. Voltage dependence of steady-state fluorescence of DIII for A1326W, M1652R-A1326W, and R1626P-A1326W channels. E. Steady-state inactivation (SSI) curves of WT, R1626P, and M1652R channels. The differences in SSI among different mutations are also preserved in presence of the A1326W background mutation. F. Proposed schematic showing a model of how A1326W eliminates the different sensitivities among LQT variants.

from the DIII-VSD. These results indicated that the differences in mexiletine sensitivity of R1626P and M1652R are a consequence of the effects of the mutations on DIII-VSD activation,

which are transmitted to the DIII-pore to increase accessibility to mexiletine. Thus, removing the coupling between the DIII-VSD and pore abolished the differences in mexiletine sensitivity.

Voltage dependence of DIII-VSD activation determines mexiletine-induced tonic block (TB)

By studying two LQT variants with extremely high or low mexiletine sensitivity, we showed that the voltage dependence of DIII-VSD activation strongly affects mexiletine block. We explored if this mechanism is generally applicable to common LQT3 variants. We first investigated how DIII-VSD activation modulates TB by mexiletine. TB is usually assessed at negative potentials (-100 mV), a voltage at which most LQT variants have similar level of inactivation. DIII-VSD activation occurs at much lower voltage range than closed-state inactivation. Consequently, at -100 mV, the variability in the proportion of channels with DIII-VSD in the activated conformation is high among LQT3 variants. We measured the gating properties of WT and 15 LQT3 variant channels and the mexiletine TB of these channels. Most variants that we analyzed are found in patients who were previously treated with mexiletine. Even though the LQT variants span the channel (**Fig 3.4A**), many of the variants exhibited altered DIII-VSD activation. We observed a strong correlation between the voltage dependence of DIII-VSD activation ($V_{1/2}$ of DIII F-V) and TB by (R^2=0.90, **Fig 3.4B**). Higher TB occurred for channels that had DIII-VSD activation at more negative potentials (**Fig 3.4B**). Instead of a linear relationship, we fitted the data to a Hill function, because we expected that TB will saturate at the ends of the curve. Intriguingly, we found that the minimum TB saturated at 15% block, suggesting that 15% of mexiletine-mediated TB is lipophilic block (low affinity, voltage-independent block).

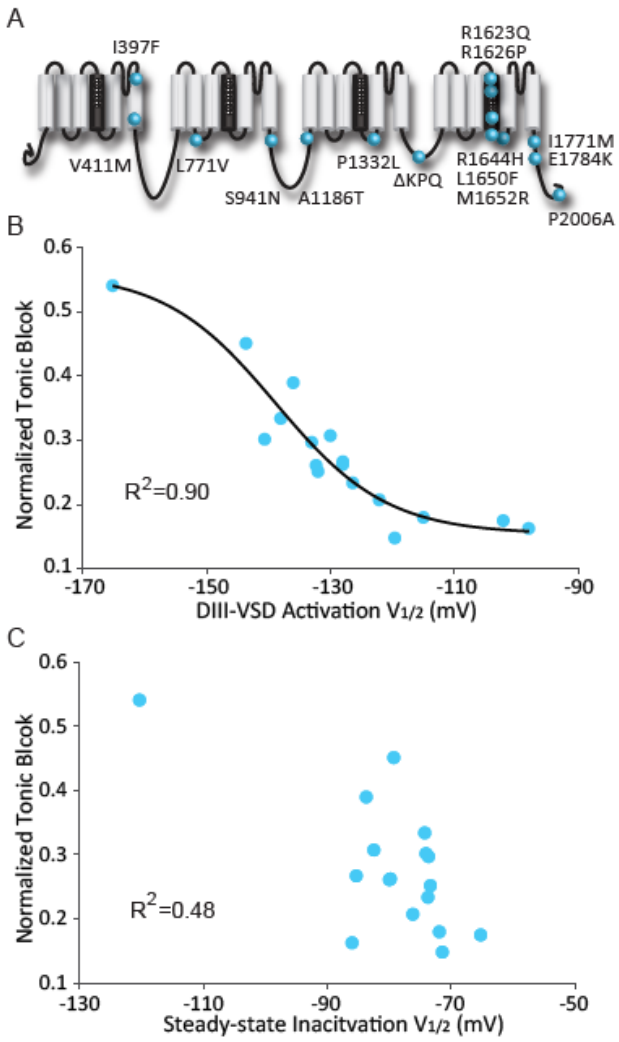

Figure 3.4 Voltage dependence of DIII-VSD activation strongly correlates with tonic block by mexiletine. A. Locations along the primary sequence and channel topology of 15 LQT3 variants tested. B. Relationship between the voltage dependence of DIII-VSD activation (V1/2 of DIII F-V) and normalized tonic block by mexiletine. The data were fitted with a Boltzmann function and the correlation calculated. A strong correlation (R2=0.9) between these two parameters were observed when fitted with a Boltzmann function. C. Relationship between the SSI (V1/2 of SSI) and normalized tonic block by mexiletine. The two parameters are not well-correlated, suggesting that channel inactivation is not a good predictor of mexiletine tonic block.

We also investigated the relationship between SSI and TB to test the classical theory that closed-state inactivation promotes class Ib block. In contrast to DIII-VSD activation, closed-state inactivation ($V_{1/2}$ of SSI) did not correlate well with mexiletine TB (R^2=0.48, **Fig 3.4C**). These results further support the hypothesis that voltage dependence of DIII-VSD activation rather than that of closed-state inactivation determines mexiletine TB.

Partial least-square regression model predicts mexiletine use-dependent block and patients' QT_C shortening

UDB is a critical feature of class Ib drugs, because this feature enables the drug to block channels during periods of heightened channel activity, as in tachycardia. Unlike TB, which occurs at resting potentials at which channels undergo limited conformational changes, UDB involves many complex gating transitions, including the activation of the other three VSDs, pore opening, pore closing, channel inactivation, and channel recovery from inactivation. Due to the complexity of the molecular movements that affect UDB, using a single gating parameter, such as SSI or DIII-VSD activation, to predict UDB is insufficient. To address this challenge, we applied a data-driven modeling approach to identify the multivariate relationship between channel gating parameters and UDB by mexiletine.

For each LQT variant, we quantified 14 gating parameters that describe gating processes, such as DIII-VSD, DIV-VSD activation, channel activation, and channel fast inactivation (**Fig 3.5A**). We also assessed UDB by 250 μM mexiletine for each variant. To understand how these gating phenomena related to drug block, we utilized the partial least-square (PLS) regression approach. Gating parameters were used as predictive inputs, and the measured UDB was used as an output for the PLS regression model. The PLS regression method has the ability to identify relationships between the measured gating parameters and UDB and can reduce redundancy amongst the input parameters.

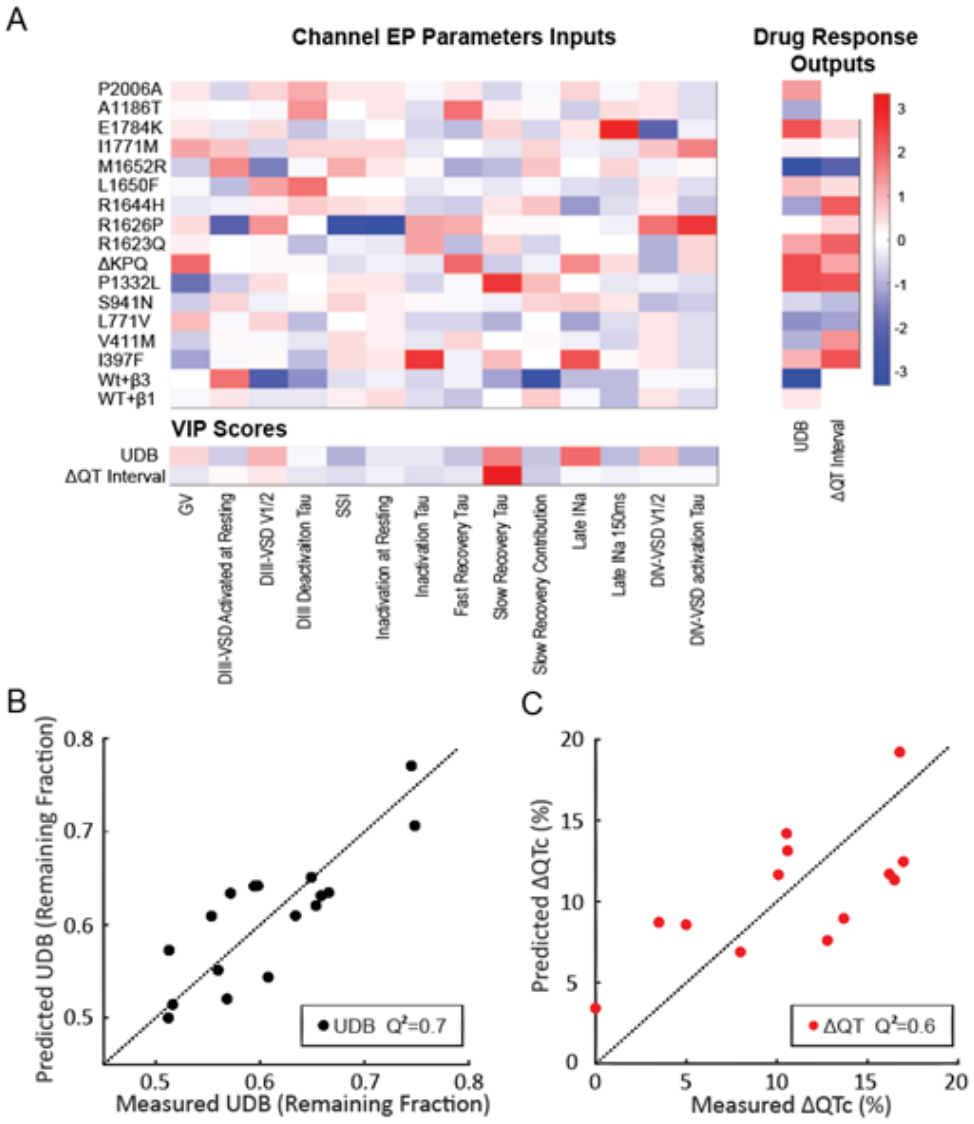

Figure 3.5 Partial least square (PLS) regression model can predict UDB and QTc shortening by mexiletine from channel gating parameters. A. Left: heatmap of 14 quantified electrophysiological parameters (EP) of the gating for 15 LQT3 variants and WT channels with β1 or β3 subunits. Right: heatmap of each channel's responses to mexiletine, including UDB and QTc shortening (ΔQTc) in LQT3 patients undergoing mexiletine treatment. Bottom: VIP scores for each gating parameter. VIP scores were ranked by each parameter's impact on model fitness. Each gating parameter is removed individually, and PLSR model was constructed with the rest of parameters. The corresponding model fitness was calculated based on Pearson correlation between measured block and predicted block with leave-one-out cross-validation. Higher VIP score (red) suggests that the gating parameter is more important for improving the model fitness. B-C. Relationship between measured and predicted UDB or ΔQTc. The predictions were made using the PLS regression model with parameters with high VIP scores. Model stability was tested with leave-one-out cross validation.

We applied feature selection among the 14 gating parameters to identify the most important parameters in determining mexiletine UDB. Feature selection was based on the VIP (variable

importance in projection) score of each parameter (See Materials and Methods), which describes parameter impact on model fitness. Gating parameters with high VIP scores (**Fig 3.5A** bottom, red squares) were then extracted to build the final PLS regression model for prediction. The VIP scores suggest that 5 gating parameters are crucial for determining UDB, including voltage dependence of channel conductance ($V_{1/2}$ of G-V), DIII-VSD activation ($V_{1/2}$ of DIII F-V), DIV-VSD activation ($V_{1/2}$ of DIV F-V), time constant of slow recovery from inactivation (slow recovery τ), and late I_{Na}. By reducing the number of gating parameters used in the model, feature selection not only helps prevent overfitting but also improves our understanding of the relationship between channel gating processes and drug response.

To reduce data dimensionality, we also decreased the number of principal components to 3, because 3 principal components were sufficient to explain 90% variants in our data. With the selected features and reduced components, the PLS regression model predicts the UDB with a R-squared (R^2) of 0.9. We further validated the model with "leave one out" cross-validation, as described in Methods. The cross-validated PLS regression model predicts the UDB with a Q-squared (Q^2) of 0.7 (**Fig 3.5B**). Compared to the best prediction using a single gating parameter (DIII-VSD activation), which has a Q^2 of 0.3, the PLS regression approach improved the prediction accuracy.

We also built a PLS regression model to predict mexiletine-induced corrected QT_c shortening (ΔQT_c) in patients with the LQT3 variants for which we measured channel gating parameters. We obtained QT_c interval data before and after mexiletine for 32 patients with 13 different genetic variants from a previously published study[6]. The VIP scores for ΔQT_c showed that only two gating parameters are important for determining the ΔQT_c: DIII-VSD activation and τ of slow recovery from inactivation (**Fig 3.5A** bottom). With these two parameters as inputs, the

cross-validated PLS regression model predicted QT_c shortening in patients with a Q-square (Q^2) of 0.6 (**Fig 3.5C**), demonstrating that the model has significant predictive value. Our results indicated that the clinical efficacy of mexiletine can be predicted from measurements of gating parameters of the $Na_V1.5$ variants, supporting the proposal that in vitro testing may help predict a patient's specific response to mexiletine[4]. We extended this observation by building a precise model for predicting patient specific QT_c shortening by mexiletine based on detailed biophysical parameters.

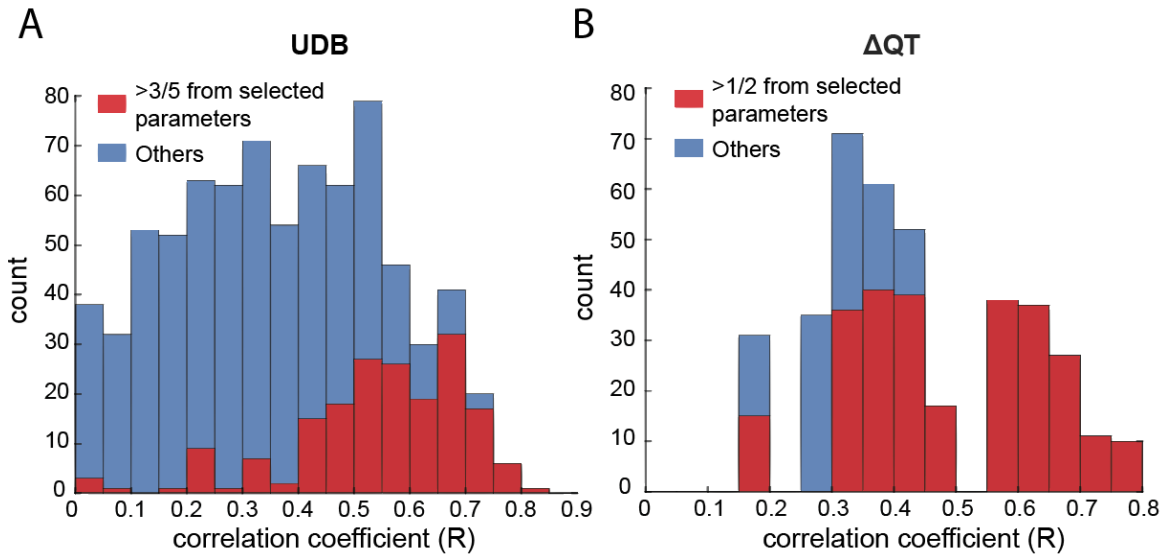

Figure 3.6 Test if gating parameter based on VIP scores can improve prediction by comparing with models generated with randomly selected gating parameters. A-B. Histogram of model fitness (R) for predicting UDB and ΔQT of 1000 PLSR models with 5 or 2 random selected parameters (blue) respectively. The fraction of models that contains 3 out of 5 (UDB) or 1 out of 2 (ΔQT) parameters with high VIP scores are shown in red. Those models have higher fitness than the rest of models, suggesting parameter selection based on VIP scores increases the model prediction accuracy.

To validate if the gating parameters selected based on the VIP scores improved the prediction accuracy (model fitness) of the PLS regression models, we evaluated 1000 models with randomly selected parameters (blue bars, **Fig 3.6**). Among these models, those that contain most of the preselected parameters (more than 3 out of 5 for UDB and 1 out 2 for ΔQT_c) had overall

improved prediction accuracy, implying that VIP score is an effective method to rank gating parameter importance.

Finally, to facilitate utilization of our predictive model, we built a mexiletine QT_c shortening calculator user interface (**Fig 3.7**). Users can select from a list of previously tested LQT3 variants or enter the channel gating parameters for a new variant, and then input the patient's baseline QT_c. The calculator will predict mexiletine shortening of QT_c based on the PLS regression model and output patient's predicted QT_c after mexiletine therapy. If the patients' predicted QT_c after mexiletine is still above 500 ms (high-risk QT_c[6]), the warning light will illuminate, indicating that mexiletine is unlikely to be a sufficiently effective therapy in preventing arrhythmia events.

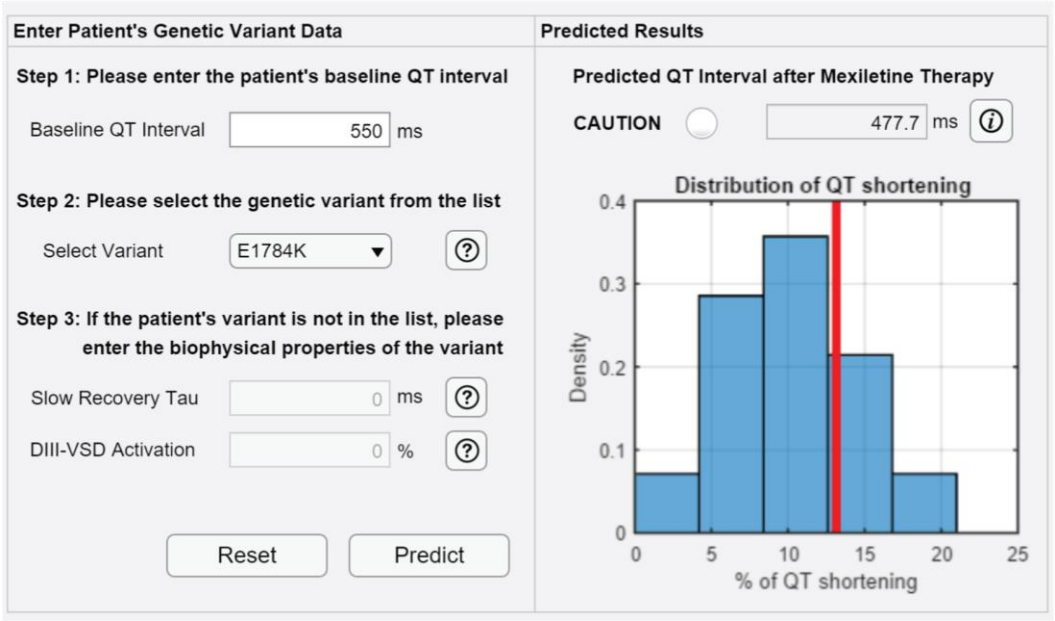

Figure 3.7 Mexiletine QTc calculator: user-interface for the PLS regression model. Users can enter the patient's baseline QT, select patient's genetic variant or enter a new variant. The predict button runs the PLS regression model based on our training set data containing 13 LQT3 mutations. The calculator output the patient's predicted QTc after mexiletine therapy. A red line that shows the predicted percentage of QTc shortening for the patient is displayed in the background of the histogram of all LQT3 variants in our database, which indicates the variant's relative sensitivity to mexiletine

Test QTc shortening calculator performance with a blind clinical trial

To test the accuracy of our ΔQT_c predictions using the PLS regression model, we conducted a blind retrospective clinical trial that involved 8 LQT3 patients carrying 5 distinct SCN5A variants (**Table 3.2, Fig 3.8**), which were not variants included in the training dataset. The 8 patients were previously treated with mexiletine and their electrocardiograms were recorded before and after treatment. Evaluators were blinded from these clinical data during prediction. We expressed the $Na_V1.5$ channel variants from those patients and tested them in vitro to obtain the two essential electrophysiological parameters for the prediction: DIII-VSD activation and slow recovery τ. We generated the predicted post-mexiletine QT_c is with the mexiletine QT_c shortening calculator, with an upper and lower bound based on the 95% confidence interval calculated from the cross-validated model.

Genetic Variants	*baseline QT_c*	*Measured post mex QT_c*	*Predicted post mex QT_c*	*Prediction lower bound*	*Prediction upper bound*
F1473S	550	491	488	452	523
I1768V	520	503	499	465	520
K1500del	478	434	415	384	446
K1500del	500	430	434	401	466
K1500del	493	463	428	396	460
K1500del	494	434	429	397	461
L1608P	604	480	518	479	558
N1774D	814	610	750	697	803

Table 3.2 Mexiletine QTc calculator trial outcomes. 7 out of 8 patients have clinical measured QTc post mexiletine that fall into the predicted range.

Strikingly, 7 out 8 patients had post-mexiletine QT_c that aligned with our predictions (**Table 3.2, Fig 3.8**). We noted that the one outlier (N1774D) patient that we failed to predict had a baseline QTc of 814 ms, which is higher than most of the training data. Assembling patient data from

both training and trial datasets, we observed a trend that patients with very high QTc baselines (> 650 ms) tend to have higher percentage of QT_c shortening by mexiletine, independent of their genetic variants. As a result, our current model is not suitable for predicting patients with very high baseline QT_c (> 650 ms). From this blind clinical trial, we validated that our PLS model accurately predicted patients' response to mexiletine therapy for those patients with a baseline lower than 650 ms.

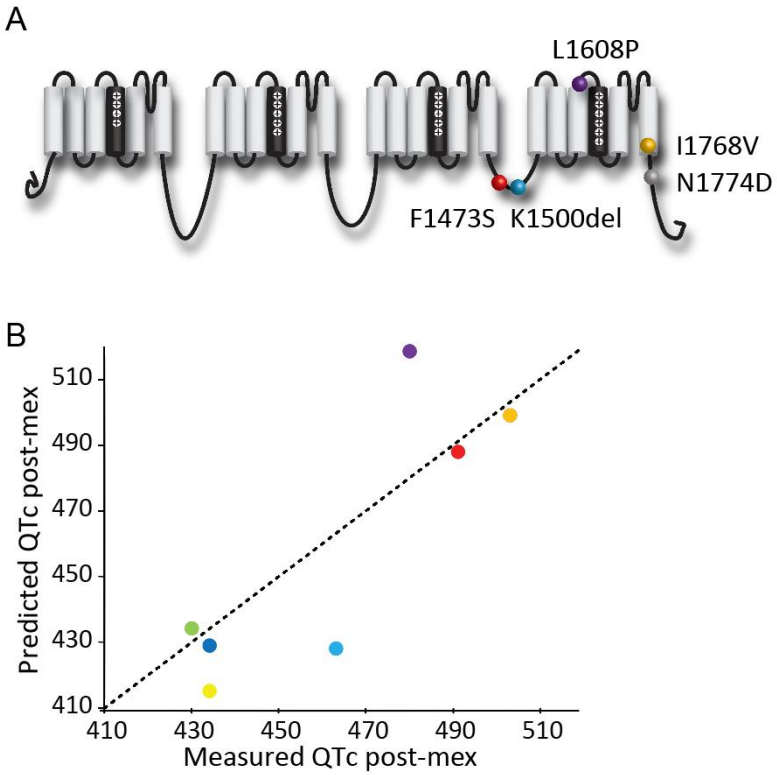

Figure 3.8 PLS regression model predicts QTc shortening by mexiletine for genetic variants A. Locations of 5 LQT3 variants that are included in the clinical trial and were not used for training the model. B. Comparison of the measured patients' QTc after mexiletine therapy and the predicted QTc after mexiletine using the PLS regression model.

We also tested the ability of PLS regression model to predict UDB with LQT3 variants that were not used for training the model. Using the critical gating parameters that we identified, the model accurately predicted UDB by mexiletine with Pearson correlation R of 0.82.

3.4 Discussion

Mexiletine, as an oral Class Ib agent, is commonly prescribed to patients suffering from ventricular tachycardia (VT) and with a predisposition to sudden cardiac death, but who have a suboptimal response to β-blockers and the multitargeted antiarrhythmic amiodarone. Studies have shown that the efficacy of mexiletine is patient specific. However, the reason behind the patient specificity is poorly understood, resulting an inability to predict drug outcomes for a given patient. A better understanding of class Ib drug action is needed to develop precision medicine for management of ventricular tachycardia. A well-defined example of mexiletine's variable efficacy is the LQT3 syndrome, an inherited arrhythmia syndrome caused by mutations in the *SCN5A* gene. Unlike other LQT syndromes, LQT3 patients usually experience episodes of ventricular tachycardia during rest and bradycardia (Ruan et al., 2007). Mexiletine is an effective therapy in suppressing arrhythmia events in some of these patients (A Mazzanti et al., 2016). However, patients carrying different SCN5A variants show varying QT interval shortening with mexiletine therapy, suggesting that the genetic variants perturb the channel in diverse ways to alter the mexiletine-channel interaction and thus drug efficacy.

In this study, we investigated the molecular mechanism of drug action by determining how $Na_V1.5$ mutations alter the sensitivity to mexiletine. We showed that DIII-VSD conformation is essential for determining mexiletine blockade. We propose a model where an activated DIII-VSD causes the channel pore to remain in a partially open conformation that promotes mexiletine TB. Among the 15 common LQT3 variants tested, many variants altered the DIII-VSD conformation, despite their distal locations to the DIII-VSD. We observed that mexiletine TB strongly correlated with the voltage dependence of DIII-VSD activation but not with SSI,

which further suggests that the DIII-VSD conformation rather than closed state inactivation of the channel controls the sensitivity to mexiletine TB.

To predict patient-specific response to mexiletine, we used a systems biology approach, PLS regression. With data collected from 15 LQT3 variants and WT channels, we built a PLS model that accurately predicted mexiletine UDB and patients' QT_c shortening from measured channel gating parameters. Two gating processes, DIII-VSD activation and slow recovery from inactivation, greatly influenced both predictions, suggesting that they are important in modulating the dynamic interactions of mexiletine with the channel.

An updated modulated receptor model describing Class Ib molecular drug action

The modulated receptor theory proposed by Hille has been applied for 40 years to describe class Ib drug interaction with Na_V channels (B Hille, 1977). This theory includes three basic and modulated channel states that illustrate drug interactions with the channel pore: closed, open, and inactivated. The modulated receptor theory emphasizes the primary role of the inactivation gate in promoting and stabilizing drug blockade. As more information regarding channel structure has become available, it is apparent that many conformational changes that are spread throughout the channel work together to cause channel gating. The four VSDs exhibit varied behavior during gating, and each is coupled to the channel pore. Thus, subtle changes in VSD dynamics can affect pore conformation and vice versa.

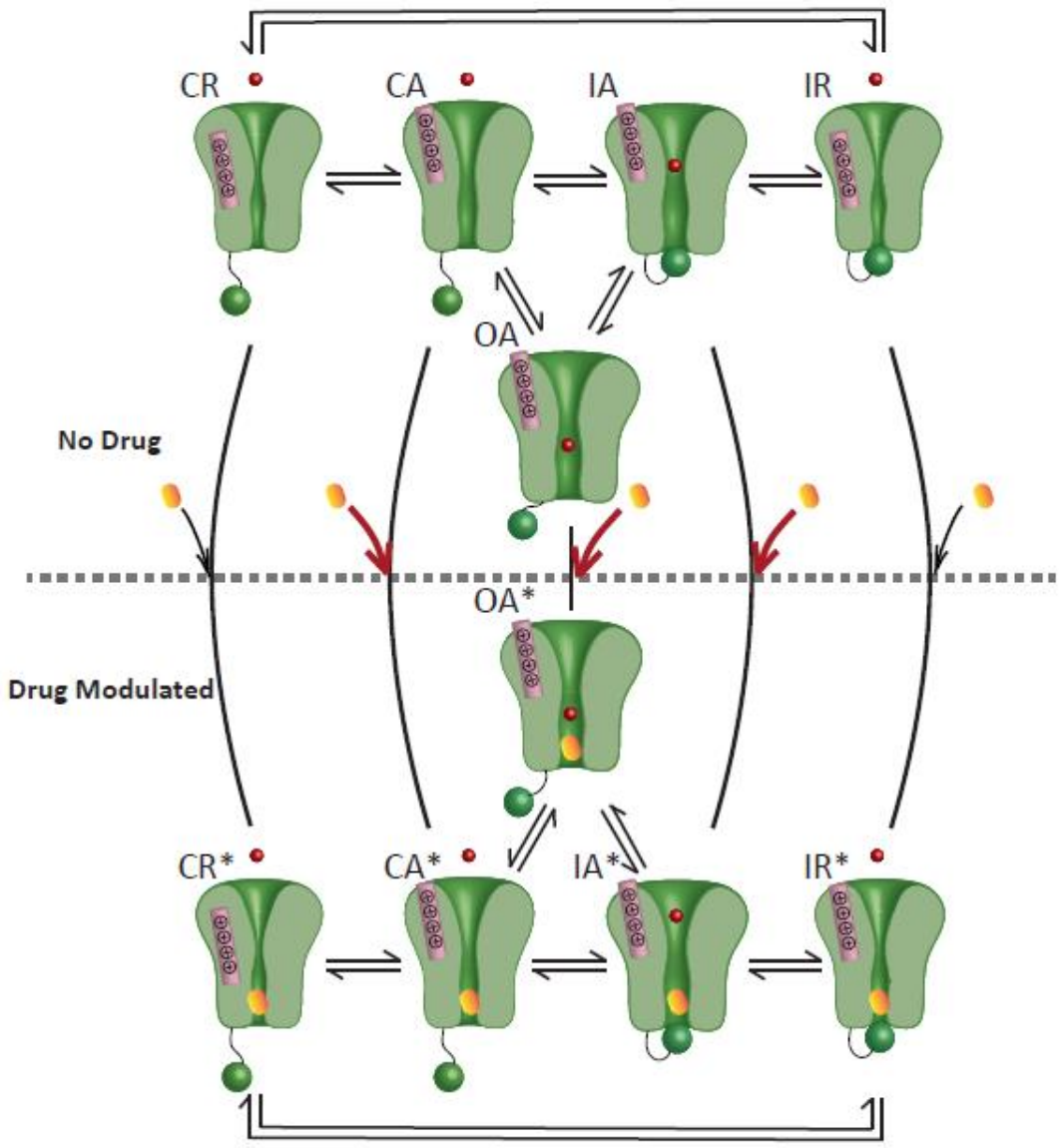

Figure 3.9 Proposed updated modulated receptor model for class Ib antiarrhythmics. The model comprises five states, CR, CA, OA, IA, and IR. R and A represent the DIII-VSD at resting and activated positions, respectively. C, O, and I represent closed, open and inactivated states of the pore. Mexiletine has different binding affinity to each state. Thick red arrows represent high binding affinity, and the thin black arrows represent low binding affinity. After mexiletine blocks the pore, channels enter five drug modulated states, CR*, CA*, OA*, IA*, and IR*. The transition rates between modulated states change compared to those between the unmodulated states. This model provides a molecular basis for how mexiletine preferentially blocks the channel when the DIII-VSD is activated (CA, OA, IA).

Previous studies showed that lidocaine binding to the pore affected DIII-VSD dynamics

(Arcisio-Miranda et al., 2010b; Sheets & Hanck, 2003). We demonstrated that LQT3 variants

alter the voltage dependence of the DIII-VSD activation, and channels that populated an activated DIII-VSD conformation exhibit increased mexiletine block. To form a more complete understanding of channel and class Ib drug interactions, we considered various components of the channel. Based on these results, we propose an updated modulated receptor model that describes how conformations of the DIII-VSD, the pore, and the inactivation gate alter class Ib drug blockade. In this updated model, we included 5 states: CR (pore closed, DIII-VSD resting), CA (pore closed, DIII-VSD activated), OA (pore open, DIII-VSD activated), IA (pore inactivated, DIII-VSD activated), and IR (pore inactivated, DIII-VSD resting (**Fig 3.9**). Drugs can block the channel from each state, but with different binding and unbinding affinities. When channels are in the CR state, drugs have a low binding rate, because the hydrophilic pathway is unavailable. When the DIII-VSD activates, channels enter the CA state, in which drugs have much higher accessibility to the pore. Finally, in the channel open (OA) and inactivated (IA) states drugs exhibit very high binding rates. After membrane repolarization, channel recovery from inactivation has slower kinetics compare to the DIII-VSD deactivation, causing the channel to enter the IR state. Drugs have both low binding and unbinding rates when the channel occupies this state. When channels are in CR and IR states, only the hydrophobic pathway is accessible.

Mexiletine interacts with the channel differently than lidocaine

Due to the structural similarity between lidocaine and mexiletine, patients with ventricular tachycardia that respond well to intravenous lidocaine are often prescribed mexiletine for long-term treatment. However, mexiletine fails to prevent arrhythmia in a large fraction (50%) of these patients (Zehender et al., 1988), and even induces severe arrhythmia in some cases (Cocco, Strozzi, Chu, & Pansini, 1980). This clinical outcome suggests that mexiletine and lidocaine

have distinct interactions with the channel that were not previously defined. Notably, mexiletine (pK_a 9.52) is mostly hydrophilic, whereas lidocaine (pK_a 7.6) is partly hydrophobic at physiological pH. Here, our results showed that the activated conformation of the DIII-VSD is required for hydrophilic drug, not for hydrophobic drugs, to access the channel pore. Many LQT3 variants stabilize the DIII-VSD in its activated position, promoting mexiletine block through the hydrophilic voltage-dependent pathway, which explains why mexiletine is effective in managing LQT3 syndrome. In contrast, for treating ventricular tachycardia patients with normal $Na_V1.5$ channels that do not have activated DIII-VSDs, mexiletine may be less effective than lidocaine. These results suggest that response to lidocaine may not be a good predictor of the clinical response to mexiletine therapy.

A better understanding of the drug mechanism suggests a novel therapeutic strategy

We demonstrated several LQT3 variants are insensitive to mexiletine due to the less activated DIII-VSD conformation of the channel. To rescue their insensitivity, a new therapeutic strategy that uses a combination of drugs can potentially be employed. A drug that promotes DIII-VSD activation can be used in combination with mexiletine to improve antiarrhythmic efficacy in the insensitive variants. Several combination therapies of Na^+ channel blockers have been tested in clinical settings (Duff, Mitchell, Manyari, & Wyse, 1987; Jordaens et al., 1990). For instance, an early study suggested that a combination of oral mexiletine and flecainide prevents recurrence of ventricular tachycardia in patients that are nonresponsive to monotherapy. From the present study, one may conjecture that flecainide may improve mexiletine efficacy by promoting DIII-VSD activation. However, the mechanism of why certain combinations improve efficacy is not known. More work must be done to systematically evaluate how different combination therapies alter channel conformations and gating to improve drug outcomes.

For more general ventricular arrhythmias other than LQT3 syndrome, mexiletine is commonly prescribed to patients with recurrent ventricular tachycardia post myocardial infarction and ischemic heart diseases that are resistant to other conventional antiarrhythmic agents (H J Duff, Roden, Primm, Oates, & Woosley, 1983). Although mexiletine effectively suppress episodes of premature ventricular contraction (PVC), it induces adverse side effects in some patients resulting in them withdrawing from therapy (Group, 1984). Side effects include severe nausea and tremor. The incidence of side effects is dosage dependent. It is possible that higher doses are needed to suppress ventricular tachycardia in these patients, because they have wild-type $Na_V1.5$ channels, which are not as sensitive as some LQT variants. The patient-specific responses can be attributed to disparity in expression of $Na_V1.5$ isoforms (polymorphisms) and accessory Na_V β subunits(Yuan et al., 2014; Zhu et al., 2017). To reduce the side effects of mexiletine, the dose must be lowered while preserving its blocking efficiency. A combined antiarrhythmic therapy that promotes DIII-VSD activation could resolve this challenge.

Understanding channel electrophysiology data with a systems biology approach

Data-driven modeling is commonly applied in the field of systems biology, due to the large-scale nature of non-intuitive experimental data from biological assays, such as microarray and gene sequencing (Janes & Yaffe, 2006). Although the scale of data from channel electrophysiology recordings is much smaller, data-driven modeling can still be very useful, because ion channels themselves are complex systems, in which many parts of the channel work in concert to generate time- and voltage-dependent gating. Different voltage protocols can isolate different channel gating processes. Although effective, these voltage protocols are not ideal, because the properties they measure overlap. For example, an inactivation change can affect protocols that measure activation by shutting down channels before the channels open maximally. Statistical tools that

can reduce data dimensionality, such as principal component analysis and partial least square regression can reduce redundant information in data recorded with different voltage protocols.

In addition to dimensionality reduction, the methods that we applied in this study has the advantage of recognizing the multivariate relationships between input (independent) and output (dependent) variables. It rotates the input data to new optimal dimensions that maximize the covariance between input and output data. Thus, PLS regression models can be trained with existing data, and then used to predict output of new input data. In this study, we built PLS regression models that predict mexiletine response using channel gating parameters. This approach can also be applied to predict other class I drug responses. In the future, if a series of PLS regression models for common class I drugs is established, this series could be used to predict a patient's response to available drugs. When a patient is identified with a new genetic variant, a patient's response to various drugs could be predicted with the established PLS regression models. Moreover, a systems biology approach has the advantage of testing the outcomes of a combination of scenarios (Fitzgerald, Schoeberl, Nielsen, & Sorger, 2006). Different drug prediction models can be combined to discover an optimal therapy for a certain patient.

Clinical perspective

With our new findings of how channel gating dynamics determine mexiletine blockade, we built a PLS regression model that uses channel gating parameters to predict patient-specific response to mexiletine. We incorporated this regression model into a mexiletine QT_c calculator that can output the patient's predicted QT_c after mexiletine therapy. The calculator gives users a warning if the patient is predicted to still have high-risk QT_c (> 500ms) after therapy. In a blind clinical trial, we validated that the calculator accurately predicted the majority of patients' post-

mexiletine QT_c. Overall, our understanding of the mexiletine molecular mechanism can be applied to predict patient-specific response to mexiletine, which can improve clinical outcomes of LQT3 management through a precision medicine approach.

Study Limitations

Since LQT3 is a rare disease and only a fraction of patients were treated with mexiletine, we have limited patient data for training the predictive model. The model performance can be improved as more patient data are added. In future studies, we hope to conduct a multicenter trial, to increase the sample size. We also noticed that our model underestimated mexiletine effects for patient with very long baseline QT_c (> 650ms) in the clinical trial. However, it is important to consider that even though mexiletine reduces QT_c in these patients, they still have high-risk QT_c post therapy, suggesting it is necessary to apply mexiletine in conjunction with therapies, such as implantable cardioverter-defibrillator.

Conclusions

Mexiletine is widely used as an antiarrhythmic drug for patients with LQT syndrome and ventricular tachycardia. Patient-specific responses to mexiletine have been observed in clinical studies. However, the underlying mechanism is not well defined due to the lack of understanding of mexiletine's molecular interactions with the $Na_V1.5$ channel. We demonstrate that the conformation of the DIII-VSD of the $Na_V1.5$ channel is crucial for determining mexiletine blockade. Using biophysical data and a systems biology approach, we built a model that can predict LQT3 patient QT_c shortening with mexiletine therapy based on channel gating parameters. Our findings also suggest a new antiarrhythmic strategy of combination therapies that target molecular conformations of the channel to increase mexiletine efficacy.

3.5 Materials and Methods

Molecular Biology

cRNA for human Nav1.5 α subunit was produced from the pMAX vector. All mutagenesis was achieved using overlap extension PCR reaction, followed by In-fusion cloning (Clonetech). All mutations were confirmed with sequencing (Genewiz). Each plasmid was then linearized with PacI restriction enzyme. Capped mRNA was synthesized using the mMESSAGE mMACHINE T7 Transcription Kit (Life Technologies) and purified via phenol-chloroform extraction.

Voltage Clamp Fluorometry

Four previously developed constructs for VCF were used in recordings (DI: V215C, DII: S805C, DIII: M1296C, and DIV: S1618C). mRNA of the NaV1.5 channel constructs were co-injected with the NaV β1 subunit in Xenopus oocytes. Voltage clamp recordings were performed 4-5 days after injection. The recording set-up, solutions, and recording protocols for VCF are the same as described previously16. Mexiletine hydrochloride powder (Sigma) was dissolved in extracellular recording solution to a stock concentration of 4 mM. pH for the solution is adjusted to 7.4. Mexiletine was further diluted from the stock solution to various concentrations (2-1000 μM). During recordings, measurements were made from the same cell before and after addition of the indicated concentration of mexiletine. Mexiletine was manually perfused into the extracellular solution chamber in the cut-open voltage clamp set-up.

Electrophysiology Data Analysis

Data analyses were performed with Clampfit (v10; Molecular Devices), MATLAB (R2012a; MATLAB), and Excel (Microsoft). G-V, fluorescence-voltage (F-V), and SSI curves were quantified by fitting a Boltzmann function: y=1/(1+exp⁡〖((V-V_(1/2))/k)〗. DIII-VSD

deactivation rate was quantified based on the time to 50% decay. Channel recovery from inactivation was fitted with a sum of exponents function: y=C-Af*exp(-t/τf)-As*exp(-t/τs), which accounts for both fast and slower components of recovery17. Comparison between conditions or constructs were performed using paired or independent student t test, respectively (Microsoft Excel). The error bars shown in the figures represent the standard errors of mean (SEM).

Partial Least-Squares Regression

Channel parameters (predictor variables) and channel responses to mexiletine (response variables) were standardized using z-score transformation. Partial least-square (PLS) regression was performed using MATLAB function "plsregress". Model stability was examined with leave-one-out cross validation. Each perturbation (channel variant) is individually removed from the dataset, and a PLS regression model is built on the rest of the variants. Using this model, mexiletine responses are predicted for the removed variant and compared with the measured responses. The model's general ability to predict left-out data was measured by calculating the Q-squared (Q2) values, which is the sum of squares of the difference between predicted and real values, normalized by the total variability in data. Variable importance in the projection (VIP) scores for each gating parameter is ranked by its impact on model fitness (Q2). One gating parameter is removed at a time, and cross-validated model fitness Q2 is calculated for the model based on the rest of parameters. The lower the is, the higher VIP score the gating parameter has.

Mexiletine QTc shortening calculator

The final model containing all training dataset with reduced features for predicting QTc shortening (DIII-VSD activation and slow recovery τ) was implemented in a user-interface.

When the gating parameters for a new variant are entered into the calculator, they are normalized with the training dataset. The predicted percentage of QTc shortening is multiplied with patient's baseline QTc for calculating predicted post-mexiletine QTc.

Blind Retrospective Clinical Trial

All predictions were made without prior knowledge of clinical outcomes. Predictions were made based on patient QTc baseline and their genetic variants. After measuring mutant channel gating properties, parameters were inputted into the mexiletine QTc shortening calculator, which then predicted post-mexiletine QTc intervals. The predicted values were then compared to clinical data.

Chapter 4

Noncovalent β subunit modulation of interactions between Na_V channel and Class Ib antiarrhythmics: a mechanism for chamber-specific response to drug therapy

4.1 Summary

The sodium channel β subunits form a macromolecular complex with the cardiac sodium channel ($Na_V1.5$) to regulate channel expression and gating. In human hearts, β1 expresses at levels that are 3-fold higher in the atria compared to ventricles. Given that β subunits can modulate $Na_V1.5$ pharmacology, this differential expression could be exploited to target drugs to chamber-specific diseases (e.g. atrial fibrillation).

We investigated how β1, through its interaction with the voltage-sensing domains (VSDs), differentially regulates NaV1.5 channel interaction with two commonly prescribed Class Ib drugs, lidocaine and ranolazine. Our results reveal that both lidocaine and ranolazine stabilize the Domain III VSD (DIII-VSD) in the activated position. However, in the presence of β1, the lidocaine DIII-VSD effect was enhanced, while ranolazine interaction was abolished. Consistently, use-dependent block by ranolazine was also impaired. To test whether this mechanism was operative in native myocytes, block by both drugs was measured in WT and β1 (scn1b) knockout mouse ventricular myocytes. Consistent with our molecular observations, in β1

KO, lidocaine EC50 shows approximately 3-fold increase, while ranolazine EC50 was reduced to half compared to the WT. In vivo experiments show that IP injection of ranolazine prolongs PR interval and P wave duration in scn1b knockout mice, but not in WT mice, suggesting that β1 expression reduces the ranolazine's effect on peak I_{Na} in atria.

We demonstrate that the β1 subunit differentially modulates lidocaine and ranolazine blockade of NaV1.5. The molecular mechanism underlying this phenomenon is due to altered drug interaction with the DIII-VSD. This molecular difference can be targeted to develop chamber specific antiarrhythmic therapies.

4.2 Introduction

Na^+ currents (I_{Na}) carried by the Na_V channels cause initiation and propagation of action potentials in atria and ventricles (Zipes & Jalife, 2013). Na_V channels are formed by four homologous domains that are connected by intracellular linkers. Each domain contains six transmembrane segments (S1-S6). The S1-S4 form the voltage sensing domains (VSDs). VSDs undergo conformational changes upon membrane potential change, which then affects the pore (S5-S6) conformation, determining Na^+ flux (Gellens et al., 1992b).

Na_V channels present in the cardiomyocytes as macromolecular complexes, which contain many regulatory and anchoring proteins that precisely control channel function and localization based on the cell type (Abriel, 2010). β subunits are essential members of this macromolecular complex. Five types of β subunits present in heart, β1, β1b, β2, β3, and β4. β1, β1b and β3 interact with the channel non-covalently, while β2 and β4 modulates the channel by forming disulfide bonds (Calhoun & Isom, 2014). As β subunits play crucial roles in maintaining normal heart function, genetic mutations in β subunits have been shown to be associated with severe

arrhythmias, including Brugada syndrome, long QT syndrome, and sick sinus syndrome (Calhoun & Isom, 2014). β1 and β1b are the dominant isoforms in heart, as previous studies showed that their mRNA express at the highest level among all the β subunits.

Although β subunits were first identified in the 90s, when they were co-immunoprecipitated with the Na_V channel from the cardiac tissue (Isom et al., 1992b), the molecular interactions between α-β subunits were not clear until recently. Recent cryo-EM structure of the eel $Na_V1.4$-β1 complex suggests that β1 co-assemble with the $Na_V1.4$ around the domain III VSD (DIII-VSD) (Yan et al., 2017). Concurrently, optically tracking of the Na_V VSDs using voltage clamp fluorometry (VCF) revealed that the β1 and β3 subunits differentially modulate the DIII and DIV-VSD movements (Zhu et al., 2017). Both structural and functional studies suggest that non-covalently linked β subunits regulate channel function by interacting with the VSDs.

The conformational changes of the VSDs are not only important for regulating channel gating, but also essential for modulating channel interactions with drugs, even for those that bind to the pore domain, such as local anesthetics (Muroi & Chanda, 2009a). Previously, VCF and gating currents recordings showed that when lidocaine blocks the channel, it stabilizes the DIII-VSD at its activated conformation (Arcisio-Miranda et al., 2010a). Moreover, in Chapter 3, we demonstrated that the alterations of DIII-VSD conformational changes by long QT syndrome 3 variants, cause channels to have different sensitivities to Class Ib antiarrhythmic mexiletine.

Class I antiarrhythmics modulate cardiomyocytes excitability through targeting the Na_V channels. Class Ib drugs, such as lidocaine, ranolazine and mexiletine, specifically modulates the late component of I_{Na}, resulting in shortening of the action potential duration in ventricular cardiomyocytes (D S Ragsdale et al., 1996). It was previously observed in expression systems

that β subunits could alter pharmacological responses of the Na_V channel. However, the underlying mechanism and physiological impact of such alteration is poorly understood.

In this study, we aim to understand the molecular mechanisms, whereby non-covalently bound β subunits modulate Class-Ib antiarrhythmics interaction with the $Na_V1.5$ channel. We further investigated the physiological significance of this modulation by studying the scn1b knock-out mice.

4.3 Results

Both lidocaine and ranolazine alter the DIII-VSD conformation

Previous work has shown that a local anesthetic, lidocaine, shifts the activation of the DIII-VSD in muscle isoform $Na_V1.4$ to hyperpolarized potentials (Muroi and Chanda 2009; Arcisio-Miranda et al. 2010; Hanck et al. 2009). Consistently, a class Ib antiarrhythmic mexiletine that shares similar structure as lidocaine also affects the DIII-VSD conformation upon binding. This interaction highly affects the use-dependence of the drug interaction (Hanck et al. 2009), and its alteration is therefore likely to have a significant therapeutic impact.

Here, we tested two Class Ib antiarrhythmics, lidocaine and ranolazine's (**Fig 4.1A**) effects on the DIII-VSD in the cardiac isoform $Na_V1.5$ with VCF (**Fig 4.1B**). We observed a hyperpolarizing shift in the DIII F-V by 10mM lidocaine ($\Delta V1/2$=-24.8±9.4 mV, p=0.03), and a similar shift by 2.5mM ranolazine ($\Delta V1/2$=-30.7±7.5 mV, p=0.05), suggesting that both lidocaine and ranolazine stabilize the DIII-VSD in its activated conformation when bound to the channel. The similar effects on the DIII-VSD caused by both drugs are not surprising, since they share some common chemical functional groups.

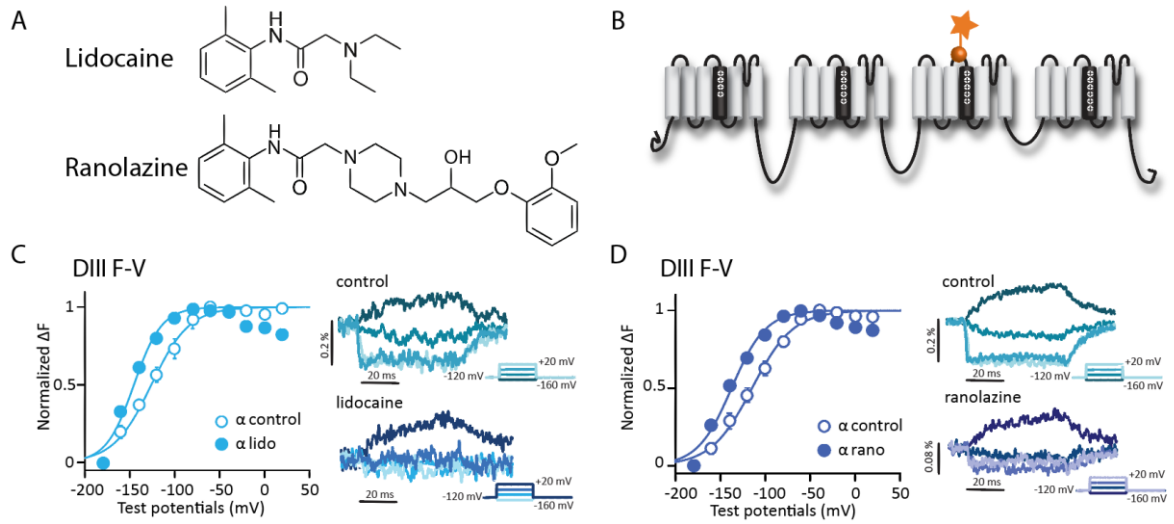

Figure 5.1 Class Ib antiarrhythmics lidocaine and ranolazine stabilize the DIII-VSD to its activated conformation. A. Ranolazine is a derivative of lidocaine. They share similar chemical structure and common binding sites on the NaV1.5 channel. However, they modulate channel current differently in use-dependent manner. B. The conformational changes of the DIII-VSD is tracked by attaching a fluorophore to the DIII S3-S4 linker. C. When bound to the channel, both lidocaine and ranolazine cause hyperpolarizing shifts in the DIII F-V curves, suggesting a stabilization of the DIII-VSD at its activated conformation.

β1 and β3 differentially modulates lidocaine and ranolazine's interactions with the DIII-VSD

Recent cryo-EM structure of eukaryotic Na^+ channel revealed that the β1 subunit is proximal to the DIII-VSD (Yan et al., 2017). We also showed previously that both β1 and β3 alter the DIII-VSD dynamics during channel gating. Given that both structural and functional insights suggest that non-covalently bound β subunits modulate the DIII-VSD, we hypothesized that β subunit can also alter Class Ib antiarrhythmics' interactions with the DIII-VSD. To test this hypothesis, we co-expressed NaV1.5 with the β1 or β3 subunit and measure the DIII-VSD conformational changes with or without lidocaine or ranolazine.

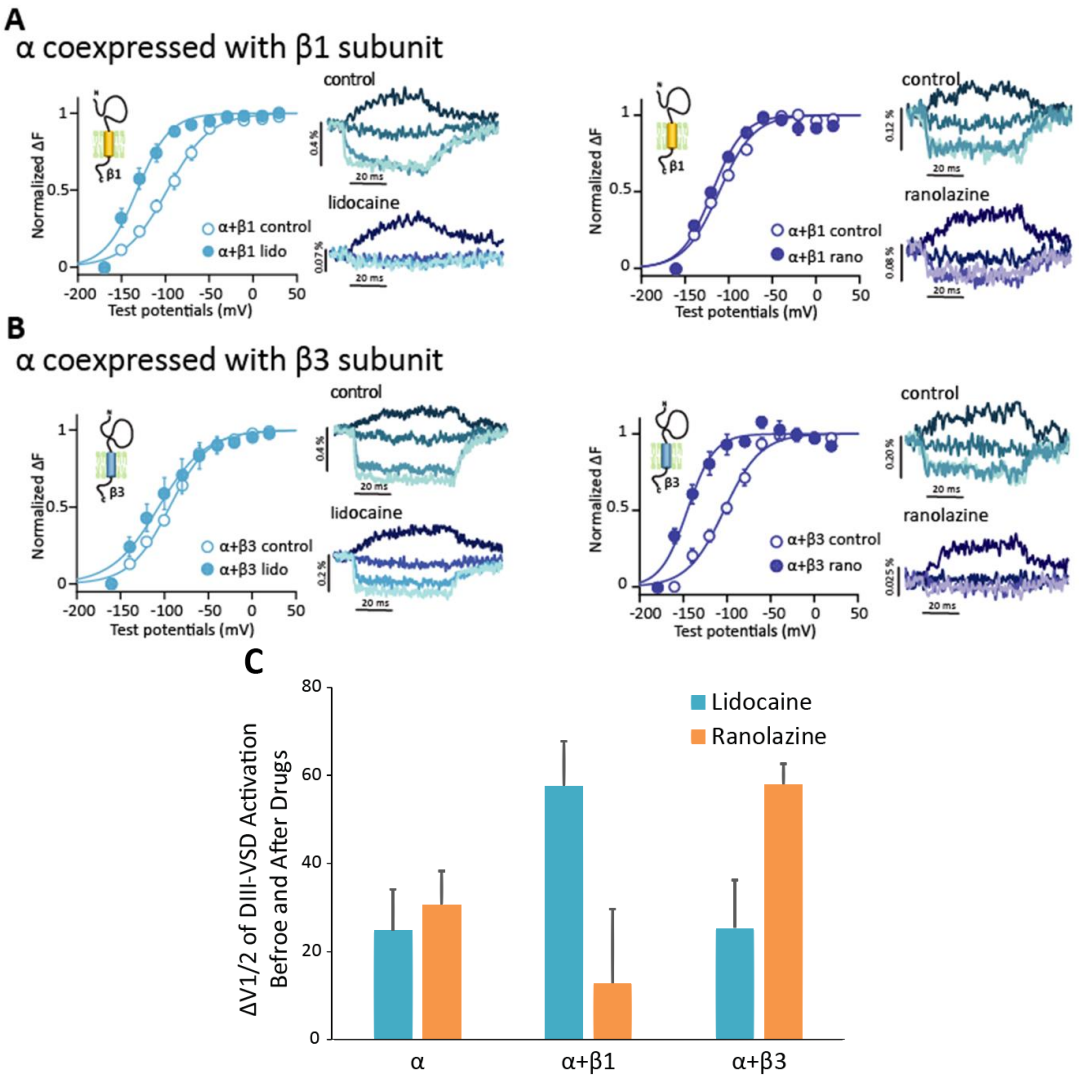

Figure 4.2 β1 and β3 differentially regulate lidocaine and ranolazine interactions with the DIII-VSD.
A. Coexpressing $Na_V1.5$ with β1 subunit enhances the DIII F-V shift by lidocaine but reduced the shift by ranolazine. B. Coexpressing NaV1.5 with β3 subunit increases the DIII F-V shift by ranolazine but almost abolishes the shift by lidocaine. C. Change in DIII F-V V1/2 after lidocaine or ranolazine application for α alone, α co-expressed with β1 or β3.

When we co-expressed the NaV1.5 channel with β1, we observed distinct DIII-VSD responses to lidocaine and ranolazine. Lidocaine block induced a greater hyperpolarizing shift in DIII-FV (ΔV1/2=-57.6±10.2 mV, p=0.01) (**Fig 4.2A**) when β1 was present, compared to the α subunit alone, while ranolazine block caused only a marginal DIII-FV shift (ΔV1/2=-12.8±16.8 mV,

p=0.53) (**Fig 4.2A**), suggesting that even when the channel pore is blocked by ranolazine, the DIII-VSD is still free to recover to its resting state, in contrast to the action of lidocaine.

Co-expression with the WT β3 subunit caused an opposite effect on DIII-VSD. Upon lidocaine block, the DIII-FV was minimally shifted to hyperpolarized potentials (ΔV1/2=-25.3±10.9 mV, p=0.13) (**Fig 4.2B**), while the ranolazine effect on the DIII-VSD was potentiated, causing a larger hyperpolarizing shift in the DIII F-V (ΔV1/2=58.0±4.7 mV, p<0.001) (**Fig 4.2B**). Strikingly, even though ranolazine is a derivative of lidocaine and shares part of its chemical structure, expression of the β subunits differentially regulates the drug interaction with the DIII-VSD (**Fig 4.2C**).

Loss of β1 expression in mouse cardiomyocytes does not affect Na_V channel gating

To further investigated how non-covalent β subunits affects cardiomyocytes' response to Class Ib antiarrhythmics, we utilized the cardiac specific scn1b Knockout (KO) mouse. First, we characterized the I_{Na} from ventricular cardiomyocytes acutely dissociated from the scn1b KO The peak I_{Na} is increased by 13% in scn1b KO cardiomyocyte compared to WT cardiomyocytes (scn1b KO: 81.3±3.6pA/pF, WT: 63.9±5.2pA/pF). A similar increase in peak current was also reported in the global scn1b KO. Other than the peak current amplitude, losing β1 expression in ventricular cardiomyocyte did not significantly alter other channel gating properties, including voltage dependence of activation (g-V) (**Fig 4.3**), steady-state inactivation (SSI) (**Fig 4.3**), and channel recovery from inactivation (**Fig 4.3**). This result is in contrary of previously reported β1's modulation of I_{Na} recorded from heterologous expression systems, but consistent with results from global scn1b KO. Given that Na_V channel form a macromolecular complex that involves many other regulatory proteins in cardiomyocytes, it is not unusual that losing one regulatory protein does not directly perturb channel function.

mouse heart.

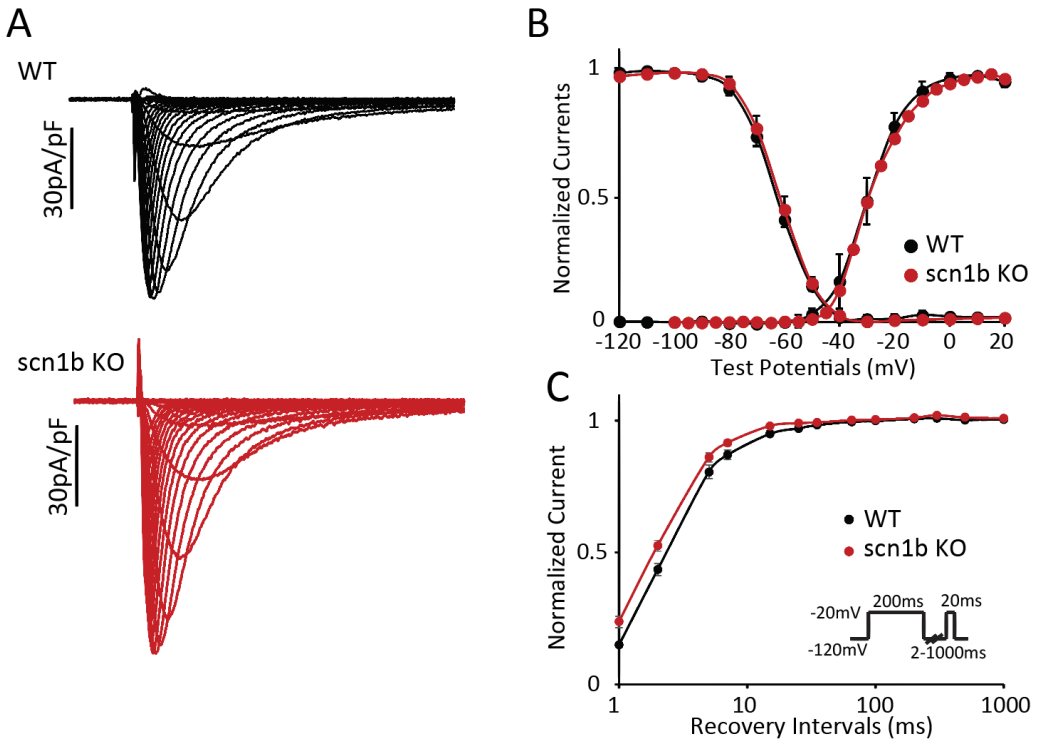

Figure 4.3 INa from scn1b KO and WT mouse cardiomyocytes have similar gating properties. A. Representative INa recorded from WT and scn1b KO mouse cardiomyocytes. B-C. loss of β1 in scn1b KO mouse cardiomyocytes did not affect channel GV, SSI, or recovery properties.

I_{Na} exhibits increased block by ranolazine, but reduced block by lidocaine in scn1b KO mouse cardiomyocytes

Even though loss of β1 in mouse cardiomyocyte does not significantly perturb Na_V gating, we continued to investigate whether it still affects channels' responses to the Class Ib drugs. We tested both lidocaine and ranolazine tonic block (TB) and use-dependent (UDB) of I_{Na} in WT and scn1b KO ventricular cardiomyocytes. Compared to WT, scn1b KO shows about 3-fold reduction in lidocaine UDB (WT: EC50=9.3uM, scn1b KO EC50=24.8uM), but significant increase in ranolazine UDB (WT: EC50=53.3uM, scn1b KO EC50=36.0uM) (**Fig 4.4C, D**). Ranolazine also exhibits more tonic block of I_{Na} in scn1b KO than WT (**Fig 4.4B**).

In mouse ventricular cardiomyocytes, we found that loss of β1 causes decreased lidocaine block, but increased ranolazine block. This result is consistent with our VCF data that suggest β1 enhances lidocaine, but reduces ranolazine interactions with the DIII-VSD. The reduced effects on the DIII-VSD conformation could result in a lessened UDB.

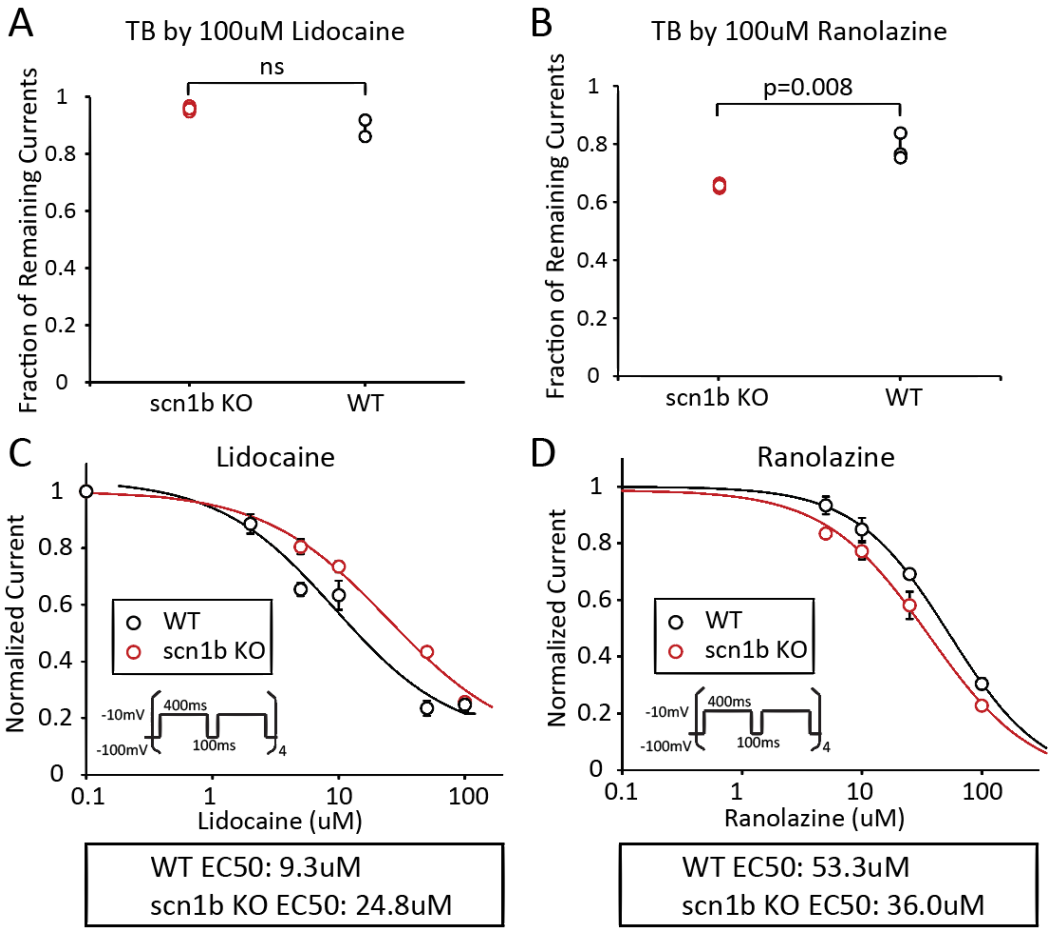

Figure 4.4 scn1b Knock-out show reduced lidocaine, but enhanced lidocaine response
A.Tonic block (TB) of INa by 100uM lidocaine is slightly reduced in scn1b KO mouse cardiomyocytes, but not significantly B. Tonic block of INa by 100uM ranolazine is significantly enhanced in scn1b KO mouse cardiomyocytes. C. Use-dependent block (UDB) is measured by applying 8 repetitive depolarizing pulses of 400ms at 2Hz frequency, a protocol that mimics tachycardia. INa from WT mouse cardiomyocytes is more sensitive to lidocaine, compared to the scn1b KO. D. Opposite to lidocaine, INa from WT mouse cardiomyocyte is more sensitive to ranolazine, compared to the scn1b KO.

β1 differentially express in human atria and ventricles

Since β1 alters Class Ib antiarrhythmics block of Na_V channel, the expression level of β1 in cardiac tissue can play an important role in regulating drug responses. We quantified mRNA expression levels of all β isoforms in human heart tissue with RNA sequencing (**Fig 4.5**). We found that scn1b has the highest expression among all isoforms at the transcript level. Moreover, scn1b is expressed 3-fold more in atria compared to ventricles (**Fig 4.5**). In contrast, both scn2b and scn4b express significantly higher in ventricles compare to atria (**Fig 4.5**). This result shows that there is a chamber heterogeneity in β subunits expression.

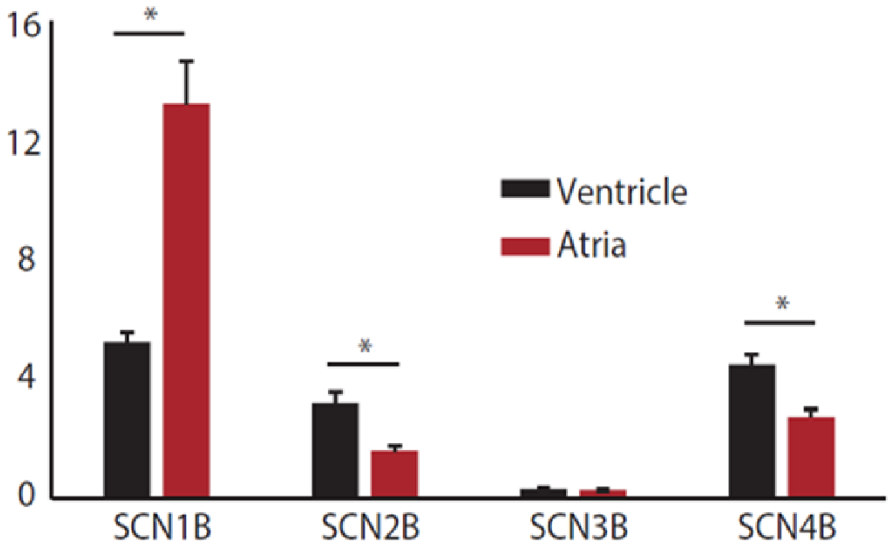

Figure 4.6 Scn1b has differential expression in human atria and ventricles. RNAseq data from human ventricular and atrial tissue. Scn1b has the highest expression among different β isoforms. The β1 expression at transcript level is ~3 fold higher in atria, compared to ventricles, suggesting a spatial heterogeneity of β1 regulation of NaV channel function in heart.

Ranolazine and lidocaine induce distinct ECG phenotypes in WT and scn1b KO mice

To further understand how β1 modulates antiarrhythmic responses at the whole heart level, we measured ECG for WT and scn1b KO mice before and after IP injections of lidocaine or

ranolazine (**Fig 4.6**). From the ECG measurements, we quantified several parameters that describe the heart electrical activities, including P wave interval (**Fig 4.6**) that represent atrial conduction, PR interval (**Fig 4.6**) that characterizes atrial-ventricular conduction, and QRS interval (**Fig 4.6**) that describes ventricle conduction. We found that both lidocaine and ranolazine significantly reduced the QRS interval for both WT and scn1b KO mice (**Fig 4.6D**), consistent with their function of reducing I_{Na}. Intriguingly, ranolazine significantly shortened the PR and P wave interval in the scn1b KO mice, but not in the WT mice (**Fig 4.6B, C**). This result suggests that loss of β1 enhances ranolazine's inhibition of I_{Na} in atria.

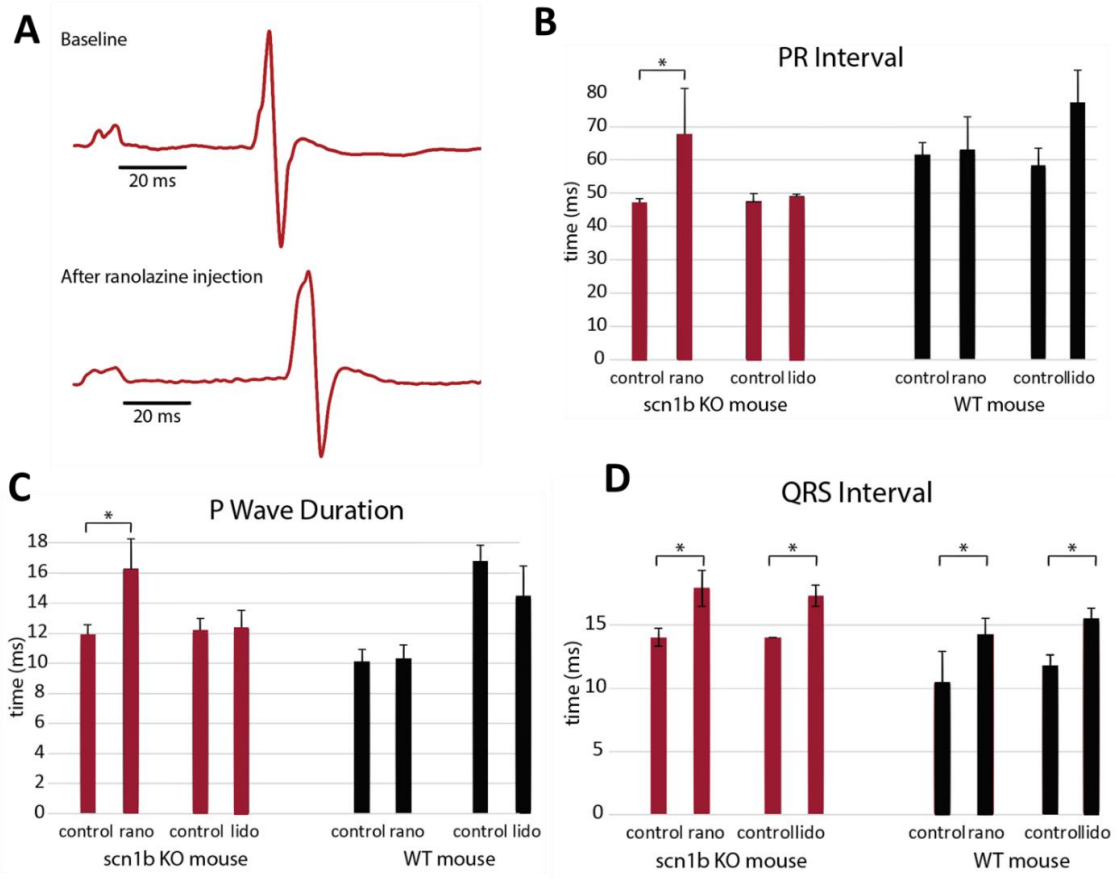

Figure 4.7 ECG recordings of WT and scn1b KO mice before and after lidocaine or ranolazine injection. A. Sample ECG recordings before and 20 minutes after IP ranolazine injection for scn1b KO mice. B-C. PR interval and P wave are significantly prolonged by ranolazine in scn1b KO mice, but not WT mice.

4.4 Discussion

Although class Ib antiarrhythmics have great therapeutic potentials, they are not broadly used in clinics because of their proarrhythmic risks in some patients (Zimetbaum, 2012). Patient or disease variability of class Ib drug response suggests that there are external factors that modulate drug interactions with the channel (A Mazzanti et al., 2016). In this study, we investigated the role of Na^+ channel accessory subunits β1 and β3 in regulating class Ib antiarrhythmics' interaction with the channel. We demonstrated at a molecular level that expression of β1 and β3 subunits differentially alter lidocaine and ranolazine's effects on the DIII-VSD, where β1 enhances lidocaine's, but inhibit ranolazine's interaction with the DIII-VSD. Conversely, β3 eliminates lidocaine's, but increases ranolazine's effect on the DIII-VSD. This difference in molecular interactions between NaV1.5 DIII-VSD and class Ib antiarrhythmic drugs caused by β subunit result in distinct drug blockade of Na_V channels in WT and scn1b KO cardiomyocytes.

The β1 and β3 subunits alter Na_V1.5 pharmacology via the DIII-VSD

The DIII-VSD plays an important role in regulating channel gating. It is involved in both activation and inactivation processes(Albert Cha et al., 1999; Hsu et al., 2017a). However, it is not clear how DIII-VSD conformation modulates inactivation. Recent studies showed a correlation between DIII-VSD deactivation and slow component of recovery from inactivation, which suggest that an activated form DIII-VSD stabilizes inactivation. As Class Ib antiarrhythmics promote DIII-VSD to activate, it can subsequently increase the inactivation, which induce more UDB.

Our results show that the presence of the β1 or β3 subunit can potently modulate the ability of Class 1b antiarrhythmics to stabilize of DIII-VSD in the activated conformation. This DIII-VSD effect of lidocaine has been previously shown to regulate use-dependent block, a critical feature

of Class-Ib drugs, which renders them most potent when myocytes are being excited repeatedly during an arrhythmic event. We observed that ranolazine and lidocaine similarly affect the Nav1.5 α subunit, when it is expressed on its own. However, with the β1 subunit present, the lidocaine effect on the DIII-VSD was significantly enhanced, while the ranolazine effect was blunted. Conversely, β3 enhanced ranolazine-induced DIII-VSD stabilization while inhibiting the lidocaine effect. Thus, despite the similarity of their chemical structures, the therapeutic response is drastically modified by the co-expression of the β1 and β3 subunits.

Differential expressions of β1 in human atria and ventricle contributes to chamber-specific drug responses

Ranolazine was proposed as a candidate for atrial specific therapy for atrial fibrillation (Burashnikov, Di Diego, Zygmunt, Belardinelli, & Antzelevitch, 2007; Zygmunt et al., 2011). Studies in canine heart illustrated that atrial and ventricular cardiomyocytes had distinct responses to ranolazine. In atria, ranolazine prolongs the APD90 and effective refractory period (ERP) (Burashnikov et al., 2007). In contrast, in ventricle, ranolazine shortens APD90. Here, we demonstrated a higher expression of β1 and β1b subunit in atria compared to ventricles. We also showed that β1 coexpression attenuated I_{Na} block. Notably, ranolazine is also blocker for HERG channel that conduct I_{Kr}, a repolarizing current (Antzelevitch, Burashnikov, Sicouri, & Belardinelli, 2011). If ranolazine's blocking effect on I_{Na} is reduced in atria, its modulation of I_{Kr} current will dominant, resulting in prolongation of APD in atria. We think that the heterogeneous expression of β1 across different chambers is one of the underlying mechanisms for ranoalzine's chamber-specific response.

In this chapter, we demonstrated the role of non-covalently linked β subunits in regulating anti-arrhythmic drug effects from molecular interactions to whole heart phenotypes.

Chapter 5

Conclusions

Heart diseases is the leading cause of death. Antiarrhythmic drug therapies were first used over 100 years ago. However, the development of the field was discouraged by catastrophic failures of several early clinical trials. In the last decades, surgical procedure and devices had great success in treating arrhythmias. Nevertheless, those procedures are invasive and associated with high cost. Moreover, reoccurrence of arrhythmia after treatment is also fairly common for those procedures.

In theory, the antiarrhythmia drugs that modulate different ion channels can directly target the fundamental pathologies of arrhythmia. Given the complexity of how different ionic currents interplay to control cardiac excitability, the antiarrhythmics need to precisely modulate channel functions temporally and spatially. When the Class I antiarrhythmics were first used in clinics, there was no information on the drug mechanisms, other than that they are Na_V channel blockers. In the last few decades, great advances have been made in understanding the ion channel functions and structures, which are essential knowledge for understanding drug actions.

We decided to revisit some of the antiarrhythmia drugs that were first used in the 70s. We aimed to probe the molecular interactions between Na_V channel and Class Ib agents, and use that information to precisely guide Class Ib usage based on disease mechanism.

As the Na_V channels present in cardiomyocytes as macromolecular complexes, the drugs do not simply interact with channel alone. We first investigated how accessary β subunits modulate channel functions. We found that non-covalently linked β1 and β3 subunit alter the dynamics of

the DIII and DIV-VSD. Our functional results suggest that β1 and β3 reside on the opposite sides of the DIII-VSD.

The DIII-VSD is also the domain that allosterically interacts with the Class Ib antiarrhythmics drugs. From studying over 20 LQT3 variants, we found that conformation of the DIII-VSD altered by different variant determines channel's sensitivities to Class Ib drug mexiletine. Further, using this information, we build a system-based model that successfully predicted the LQT3 patients' responses to mexiletine therapy in a retrospective blind clinical trial.

We also wanted to understand the spatial heterogeneity of antiarrhythmic responses in heart. We studied how β subunits alter Class Ib interactions with the channel. We found that β1 and β3 subunits have opposite effects on lidocaine and ranoalzine's interaction with the DIII-VSD. This molecular difference resulted in different levels of block by these two compounds in WT and scn1b KO mouse cardiomyocytes. Since we also observed that β1 express 3-fold higher in the human atira,compared to the ventricles, we tested lidocaine and ranoalzine in vivo by injecting them in WT and scn1b KO mice. From measuring ECG before and after drug injection, we found that β1 specifically protect NaV channel from ranoalzine block in atria. The differential expression of β1 in different chamber can potentially be targeted for developing drugs for chamber specific diseases, such as atrial fibrillation.

I believe that our studies are only the beginning of fully understand antiarrhythmic therapy from a molecular level. More future studies need to done in order to develop disease and patient specific therapeutic strategies with antiarrhythmics. I think the adverse effects by some drugs can be prevented with a complete understanding of drug mechanisms. Antiarrhythmic can eventually be beneficial for patients when we understand how to use them properly.

References

Abriel, H. (2010). Cardiac sodium channel Nav1.5 and interacting proteins: Physiology and pathophysiology. *Journal of Molecular and Cellular Cardiology*. https://doi.org/10.1016/j.yjmcc.2009.08.025

Aggarwal, S. K., & MacKinnon, R. (1996). Contribution of the S4 segment to gating charge in the Shaker K+ channel. *Neuron*, *16*(6), 1169–1177. https://doi.org/10.1016/S0896-6273(00)80143-9

An, R. H., Wang, X. L., Kerem, B., Benhorin, J., Medina, A., Goldmit, M., & Kass, R. S. (1998). Novel LQT-3 mutation affects Na+ channel activity through interactions between alpha- and beta1-subunits. *Circulation Research*, *83*(2), 141–146. https://doi.org/10.1161/01.RES.83.2.141

Antzelevitch, C., Burashnikov, A., Sicouri, S., & Belardinelli, L. (2011). Electrophysiologic basis for the antiarrhythmic actions of ranolazine. *Heart Rhythm*. https://doi.org/10.1016/j.hrthm.2011.03.045

Arcisio-Miranda, M., Muroi, Y., Chowdhury, S., & Chanda, B. (2010a). Molecular mechanism of allosteric modification of voltage-dependent sodium channels by local anesthetics. *The Journal of General Physiology*, *136*(5), 541–554. https://doi.org/10.1085/jgp.201010438

Arcisio-Miranda, M., Muroi, Y., Chowdhury, S., & Chanda, B. (2010b). Molecular mechanism of allosteric modification of voltage-dependent sodium channels by local anesthetics. *The Journal of General Physiology*, *136*(5), 541–554. https://doi.org/10.1085/jgp.201010438

Armstrong, C. M., & Bezanilla, F. (1977). Inactivation of the sodium channel. II. Gating current experiments. *The Journal of General Physiology*, *70*(5), 567–590. https://doi.org/10.1085/jgp.70.5.567

Barro-Soria, R., Rebolledo, S., Liin, S. I., Perez, M. E., Sampson, K. J., Kass, R. S., & Larsson, H. P. (2014). KCNE1 divides the voltage sensor movement in KCNQ1/KCNE1 channels into two steps. *Nature Communications*, *5*, 3750. https://doi.org/10.1038/ncomms4750

Bean, B.; Cohen, C J; Tsien, R. W. (1983). Lidocaine block of cardiac sodium channels. *The Journal of General Physiology*, *81*(5), 613–642. https://doi.org/10.1085/jgp.81.5.613

Bezanilla, F. (2008). How membrane proteins sense voltage. *Nature Reviews. Molecular Cell Biology*, *9*(4), 323–332. https://doi.org/10.1038/nrm2376

Blunck, R. (2015). Investigation of Ion Channel Structure Using Fluorescence Spectroscopy. In J. Zheng & M. C. Trudeau (Eds.), *Handbook of Ion Channels* (pp. 113–133). CRC Press. https://doi.org/10.1201/b18027-12

Blunck, R., Starace, D. M., Correa, A. M., & Bezanilla, F. (2004). Detecting rearrangements of shaker and NaChBac in real-time with fluorescence spectroscopy in patch-clamped

mammalian cells. *Biophysical Journal*, *86*(6), 3966–3980. https://doi.org/10.1529/biophysj.103.034512

Brugada, P., & Brugada, J. (1992). Right bundle branch block, persistent ST segment elevation and sudden cardiac death: a distinct clinical and electrocardiographic syndrome. A multicenter report. *Journal of the American College of Cardiology*, *20*(6), 1391–1396. https://doi.org/0735-1097(92)90253-J [pii]

Burashnikov, A., Di Diego, J. M., Zygmunt, A. C., Belardinelli, L., & Antzelevitch, C. (2007). Atrium-selective sodium channel block as a strategy for suppression of atrial fibrillation: Differences in sodium channel inactivation between atria and ventricles and the role of ranolazine. *Circulation*, *116*(13), 1449–1457. https://doi.org/10.1161/CIRCULATIONAHA.107.704890

Burton, F. L., & Cobbe, S. M. (2001). Dispersion of ventricular repolarization and refractory period. *Cardiovascular Research*. https://doi.org/10.1016/S0008-6363(01)00197-3

Calhoun, J. D., & Isom, L. L. (2014). The Role of Non-pore-Forming β Subunits in Physiology and Pathophysiology of Voltage-Gated Sodium Channels. In *Voltage Gated Sodium Channels* (Vol. 221, pp. 51–89). https://doi.org/10.1007/978-3-642-41588-3

Campos, F. V, Chanda, B., Beirão, P. S. L., & Bezanilla, F. (2007). beta-Scorpion toxin modifies gating transitions in all four voltage sensors of the sodium channel. *The Journal of General Physiology*, *130*(3), 257–268. https://doi.org/10.1085/jgp.200609719

Campos, F. V, Chanda, B., Beirão, P. S. L., & Bezanilla, F. (2008). Alpha-scorpion toxin impairs a conformational change that leads to fast inactivation of muscle sodium channels. *The Journal of General Physiology*, *132*(2), 251–263. https://doi.org/10.1085/jgp.200809995

Capes, D. L., Goldschen-Ohm, M. P., Arcisio-Miranda, M., Bezanilla, F., & Chanda, B. (2013). Domain IV voltage-sensor movement is both sufficient and rate limiting for fast inactivation in sodium channels. *The Journal of General Physiology*, *142*(2), 101–112. https://doi.org/10.1085/jgp.201310998

Cha, A., Peter C., R., Alfred L., G., Esther, F., & Francisco, B. (1999). Voltage sensors in domains III and IV, but not I and II, are immobilized by Na+ channel fast inactivation. *Neuron*, *22*(1), 73–87. https://doi.org/10.1016/S0896-6273(00)80680-7

Cha, A., Snyder, G. E., Selvin, P. R., & Bezanilla, F. (1999). Atomic scale movement of the voltage-sensing region in a potassium channel measured via spectroscopy. *Nature*, *402*(6763), 809–813. https://doi.org/10.1038/45552

Chanda, B., & Bezanilla, F. (2002). Tracking voltage-dependent conformational changes in skeletal muscle sodium channel during activation. *The Journal of General Physiology*, *120*, 629–645. https://doi.org/10.1085/jgp.20028679

Chen, H., Ahsan, S. S., Santiago-Berrios, M. B., Abruña, H. D., & Webb, W. W. (2010). Mechanisms of quenching of alexa fluorophores by natural amino acids. *Journal of the American Chemical Society*, *132*(21), 7244–7245. https://doi.org/10.1021/ja100500k

Cocco, G., Strozzi, C., Chu, D., & Pansini, R. (1980). Torsades de pointes as a manifestation of mexiletine toxicity. *American Heart Journal*, *100*(6 PART 1), 878–880. https://doi.org/10.1016/0002-8703(80)90070-8

Das, S., Gilchrist, J., Bosmans, F., & Van Petegem, F. (2016). Binary architecture of the Nav1.2-β2 signaling complex. *ELife*, *5*, 1–21. https://doi.org/10.7554/eLife.10960

Domínguez, J. N., Navarro, F., Franco, D., Thompson, R. P., & Aránega, A. E. (2005). Temporal and spatial expression pattern of beta1 sodium channel subunit during heart development. *Cardiovascular Research*, *65*(4), 842–850. https://doi.org/10.1016/j.cardiores.2004.11.028

Doose, S., Neuweiler, H., & Sauer, M. (2005). A close look at fluorescence quenching of organic dyes by tryptophan. *Chemphyschem : A European Journal of Chemical Physics and Physical Chemistry*, *6*(11), 2277–2285. https://doi.org/10.1002/cphc.200500191

Doose, S., Neuweiler, H., & Sauer, M. (2009). Fluorescence quenching by photoinduced electron transfer: A reporter for conformational dynamics of macromolecules. *ChemPhysChem*, *10*(9–10), 1389–1398. https://doi.org/10.1002/cphc.200900238

Duff, H. J., Mitchell, L. B., Manyari, D., & Wyse, D. G. (1987). Mexiletine-quinidine combination: Electrophysiologic correlates of a favorable antiarrhythmic interaction in humans. *Journal of the American College of Cardiology*, *10*(5), 1149–1156. https://doi.org/10.1016/S0735-1097(87)80360-1

Duff, H. J., Roden, D., Primm, R. K., Oates, J. A., & Woosley, R. L. (1983). Mexiletine in the treatment of resistant ventricular arrhythmias: enhancement of efficacy and reduction of dose-related side effects by combination with quinidine. *Circulation*, *67*(5), 1124–1128.

Echt, D. S., Liebson, P. R., Mitchell, L. B., Peters, R. W., Obias-Manno, D., Barker, A. H., … Richardson, D. W. (1991). Mortality and Morbidity in Patients Receiving Encainide, Flecainide, or Placebo. *New England Journal of Medicine*, *324*(12), 781–788. https://doi.org/10.1056/NEJM199103213241201

Fahmi, A. I., Patel, M., Stevens, E. B., Fowden, A. L., John, J. E., Lee, K., … Vandenberg, J. I. (2001). The sodium channel beta-subunit SCN3b modulates the kinetics of SCN5a and is expressed heterogeneously in sheep heart. *The Journal of Physiology*, *537*, 693–700. https://doi.org/10.1111/j.1469-7793.2001.00693.x

Ferrera, L., & Moran, O. (2006). Beta1-subunit modulates the Nav1.4 sodium channel by changing the surface charge. *Experimental Brain Research*, *172*(2), 139–150. https://doi.org/10.1007/s00221-005-0323-4

Fitzgerald, J. B., Schoeberl, B., Nielsen, U. B., & Sorger, P. K. (2006). Systems biology and combination therapy in the quest for clinical efficacy. *Nature Chemical Biology*. https://doi.org/10.1038/nchembio817

Gandhi, C. S., & Olcese, R. (2008). The voltage-clamp fluorometry technique. *Methods in Molecular Biology*, *491*, 213–231. https://doi.org/10.1007/978-1-59745-526-8-17

Ganetzky, B., Robertson, G. a, Wilson, G. F., Trudeau, M. C., & Titus, S. a. (1999). The eag family of K+ channels in Drosophila and mammals. *Annals of the New York Academy of Sciences*, *868*, 356–369. https://doi.org/10.1111/j.1749-6632.1999.tb11297.x

Gellens, M. E., George, a L., Chen, L. Q., Chahine, M., Horn, R., Barchi, R. L., & Kallen, R. G. (1992a). Primary structure and functional expression of the human cardiac tetrodotoxin-insensitive voltage-dependent sodium channel. *Proceedings of the National Academy of Sciences of the United States of America*, *89*(2), 554–558. https://doi.org/10.1073/pnas.89.2.554

Gellens, M. E., George, A. L., Chen, L. Q., Chahine, M., Horn, R., Barchi, R. L., & Kallen, R. G. (1992b). Primary structure and functional expression of the human cardiac tetrodotoxin-insensitive voltage-dependent sodium channel. *Proceedings of the National Academy of Sciences of the United States of America*, *89*, 554–558. https://doi.org/10.1073/pnas.89.2.554

Gellens, M. E., George, A. L., Chen, L. Q., Chahine, M., Horn, R., Barchi, R. L., & Kallen, R. G. (1992c). Primary structure and functional expression of the human cardiac tetrodotoxin-insensitive voltage-dependent sodium channel. *Proceedings of the National Academy of Sciences of the United States of America*, *89*(2), 554–558. https://doi.org/10.1073/pnas.89.2.554

Gilchrist, J., Das, S., Van Petegem, F., & Bosmans, F. (2013). Crystallographic insights into sodium-channel modulation by the β4 subunit. *Proceedings of the National Academy of Sciences of the United States of America*, *110*(51), E5016-24. https://doi.org/10.1073/pnas.1314557110

Greene, H. L., Roden, D. M., Katz, R. J., Woosley, R. L., Salerno, D. M., & Henthorn, R. W. (1992). The cardiac arrhythmia suppression trial: First CAST ... then CAST-II. *Journal of the American College of Cardiology*. https://doi.org/10.1016/0735-1097(92)90267-Q

Group, I. R. (1984). International mexiletine and placebo antiarrhythmic coronary trial: I. Report on arrhythmia and other findings. *Journal of the American College of Cardiology*, *4*(6), 1148–1163. https://doi.org/10.1016/S0735-1097(84)80133-3

Hakim, P., Brice, N., Thresher, R., Lawrence, J., Zhang, Y., Jackson, A. P., … Huang, C. L. H. (2010). Scn3b knockout mice exhibit abnormal sino-atrial and cardiac conduction properties. *Acta Physiologica*, *198*, 47–59. https://doi.org/10.1111/j.1748-1716.2009.02048.x

Hakim, P., Gurung, I. S., Pedersen, T. H., Thresher, R., Brice, N., Lawrence, J., … Huang, C. L. H. (2008). Scn3b knockout mice exhibit abnormal ventricular electrophysiological properties. *Progress in Biophysics and Molecular Biology*, *98*, 251–266. https://doi.org/10.1016/j.pbiomolbio.2009.01.005

Hanck, D. A., Nikitina, E., McNulty, M. M., Fozzard, H. A., Lipkind, G. M., & Sheets, M. F. (2009). Using lidocaine and benzocaine to link sodium channel molecular conformations to state-dependent antiarrhythmic drug affinity. *Circulation Research*, *105*(5), 492–499. https://doi.org/10.1161/CIRCRESAHA.109.198572

Hartshorne, R. P., & Catterall, W. A. (1984). The sodium channel from rat brain. Purification and subunit composition. *J Biol Chem, 259*(3), 1667–1675. Retrieved from http://www.ncbi.nlm.nih.gov/pubmed/6319405

Hille, B. (1977). Local anesthetics: hydrophilic and hydrophobic pathways for the drug-receptor reaction. *The Journal of General Physiology*, *69*(4), 497–515. https://doi.org/10.1085/jgp.69.4.497

Hille, B. (2001). Ion Channel Excitable Membranes. In *Sunderland Massachusetts USA* (pp. 1–37). https://doi.org/10.1007/3-540-29623-9_5640

Hondeghem, L. M., & Katzung, B. G. (1984). Antiarrhythmic agents: the modulated receptor mechanism of action of sodium and calcium channel-blocking drugs. *Annual Review of Pharmacology and Toxicology*, *24*, 387–423. https://doi.org/10.1146/annurev.pa.24.040184.002131

Hsu, E. J., Zhu, W., Schubert, A. R., Voelker, T., Varga, Z., & Silva, J. R. (2017a). Regulation of Na(+) channel inactivation by the DIII and DIV voltage-sensing domains. *The Journal of General Physiology*, *149*(3), 389–403. https://doi.org/10.1085/jgp.201611678

Hsu, E. J., Zhu, W., Schubert, A. R., Voelker, T., Varga, Z., & Silva, J. R. (2017b). Regulation of Na+ channel inactivation by the DIII and DIV voltage-sensing domains. *The Journal of General Physiology*. Retrieved from http://jgp.rupress.org/content/early/2017/02/22/jgp.201611678.abstract

Hu, D., Barajas-Martínez, H., Medeiros-Domingo, A., Crotti, L., Veltmann, C., Schimpf, R., … Antzelevitch, C. (2012). A novel rare variant in SCN1Bb linked to Brugada syndrome and SIDS by combined modulation of Nav1.5 and Kv4.3 channel currents. *Heart Rhythm*, *9*, 760–769. https://doi.org/10.1016/j.hrthm.2011.12.006

Hughes, L. D., Rawle, R. J., & Boxer, S. G. (2014). Choose your label wisely: water-soluble fluorophores often interact with lipid bilayers. *PLOS ONE*, *9*, e87649. https://doi.org/10.1371/journal.pone.0087649

Isom, L. L., De Jongh, K. S., Patton, D. E., Reber, B. F., Offord, J., Charbonneau, H., … Catterall, W. A. (1992a). Primary structure and functional expression of the beta 1 subunit of the rat brain sodium channel. *Science (New York, N.Y.)*, *256*(5058), 839–842. Retrieved from http://www.ncbi.nlm.nih.gov/pubmed/1375395

Isom, L. L., De Jongh, K. S., Patton, D. E., Reber, B. F., Offord, J., Charbonneau, H., … Catterall, W. A. (1992b). Primary structure and functional expression of the beta 1 subunit of the rat brain sodium channel. *Science (New York, N.Y.)*, *256*, 839–842.

Isom, L. L., Ragsdale, D. S., De Jongh, K. S., Westenbroek, R. E., Reber, B. F. X., Scheuer, T., & Catterall, W. A. (1995a). Structure and function of the beta2 subunit of brain sodium channels, a transmembrane glycoprotein with a CAM motif. *Cell*, *83*(3), 433–442. https://doi.org/10.1016/0092-8674(95)90121-3

Isom, L. L., Ragsdale, D. S., De Jongh, K. S., Westenbroek, R. E., Reber, B. F. X., Scheuer, T.,

& Catterall, W. A. (1995b). Structure and function of the β2 subunit of brain sodium channels, a transmembrane glycoprotein with a CAM motif. *Cell*, *83*, 433–442. https://doi.org/10.1016/0092-8674(95)90121-3

Isom, L. L., Scheuer, T., Brownstein, a B., Ragsdale, D. S., Murphy, B. J., & Catterall, W. a. (1995). Functional co-expression of the beta 1 and type IIA alpha subunits of sodium channels in a mammalian cell line. *The Journal of Biological Chemistry*.

Itoh, T., Tanaka, T., Nagai, R., Kikuchi, K., Ogawa, S., Okada, S., … Nakamura, Y. (1998). Genomic organization and mutational analysis of KVLQT1, a gene responsible for familial long QT syndrome. *Human Genetics*, *103*(3), 290–294. Retrieved from http://www.ncbi.nlm.nih.gov/pubmed/9799083

Janes, K. A., & Yaffe, M. B. (2006). Data-driven modelling of signal-transduction networks. *Nature Reviews Molecular Cell Biology*. https://doi.org/10.1038/nrm2041

JORDAENS, L. J., TAVERNIER, R., VANMEERHAEGHE, X., ROBBENS, E., & CLEMENT, D. L. (1990). Combination of Flecainide and Mexiletine for the Treatment of Ventricular Tachyarrhythmias. *Pacing and Clinical Electrophysiology*, *13*(9), 1127–1135. https://doi.org/10.1111/j.1540-8159.1990.tb02170.x

Kazen-Gillespie, K. a, Ragsdale, D. S., D'Andrea, M. R., Mattei, L. N., Rogers, K. E., & Isom, L. L. (2000). Cloning, localization, and functional expression of sodium channel beta1A subunits. *The Journal of Biological Chemistry*, *275*(2), 1079–1088. https://doi.org/10.1074/jbc.275.2.1079

Lenkowski, P. W., Shah, B. S., Dinn, A. E., Lee, K., & Patel, M. K. (2003). Lidocaine block of neonatal Nav1.3 is differentially modulated by co-expression of ??1 and ??3 subunits. *European Journal of Pharmacology*, *467*, 23–30. https://doi.org/10.1016/S0014-2999(03)01595-4

Li, R. G., Wang, Q., Xu, Y. J., Zhang, M., Qu, X. K., Liu, X., … Yang, Y. Q. (2013). Mutations of the SCN4B-encoded sodium channel ??4 subunit in familial atrial fibrillation. *International Journal of Molecular Medicine*, *32*(1), 144–150. https://doi.org/10.3892/ijmm.2013.1355

Liman, E. R., Hess, P., Weaver, F., & Koren, G. (1991). Voltage-sensing residues in the S4 region of a mammalian K+ channel. *Nature*, *353*(6346), 752–756. https://doi.org/10.1038/353752a0

Makita, N., Bennett, P. B., & George Jr, A. L. (1996). Molecular determinants of beta 1 subunit-induced gating modulation in voltage-dependent Na+ channels. *Journal.of.Neuroscience*, *16*(22), 7117–7127.

Malhotra, J. D., Chen, C., Rivolta, I., Abriel, H., Malhotra, R., Mattei, L. N., … Isom, L. L. (2001). Characterization of sodium channel alpha- and beta-subunits in rat and mouse cardiac myocytes. *Circulation*, *103*(9), 1303–1310. https://doi.org/10.1161/01.cir.103.9.1303

Malhotra, J. D., Kazen-Gillespie, K., Hortsch, M., & Isom, L. L. (2000a). Sodium channel beta subunits mediate homophilic cell adhesion and recruit ankyrin to points of cell-cell contact. *Journal of Biological Chemistry*, *275*(15), 11383–11388. https://doi.org/10.1074/jbc.275.15.11383

Malhotra, J. D., Kazen-Gillespie, K., Hortsch, M., & Isom, L. L. (2000b). Sodium channel β subunits mediate homophilic cell adhesion and recruit ankyrin to points of cell-cell contact. *Journal of Biological Chemistry*, *275*, 11383–11388. https://doi.org/10.1074/jbc.275.15.11383

Malhotra, J. D., Koopmann, M. C., Kazen-Gillespie, K. A., Fettman, N., Hortsch, M., & Isom, L. L. (2002). Structural requirements for interaction of sodium channel ??1 subunits with ankyrin. *Journal of Biological Chemistry*, *277*(29), 26681–26688. https://doi.org/10.1074/jbc.M202354200

Maltsev, V. A., Kyle, J. W., & Undrovinas, A. (2009a). Late Na+ current produced by human cardiac Na+ channel isoform Nav1.5 is modulated by its ??1 subunit. *Journal of Physiological Sciences*, *59*(3), 217–225. https://doi.org/10.1007/s12576-009-0029-7

Maltsev, V. A., Kyle, J. W., & Undrovinas, A. (2009b). Late Na+ current produced by human cardiac Na+ channel isoform Nav1.5 is modulated by its beta1 subunit. *Journal of Physiological Sciences*, *59*(3), 217–225. https://doi.org/10.1007/s12576-009-0029-7

Mannuzzu, L. M., Moronne, M. M., & Isacoff, E. Y. (1996). Direct physical measure of conformational rearrangement underlying potassium channel gating. *Science (New York, N.Y.)*, *271*(5246), 213–216. https://doi.org/10.1126/science.271.5246.213

Mansoor, S. E., Dewitt, M. A., & Farrens, D. L. (2010). Distance mapping in proteins using fluorescence spectroscopy: The tryptophan-induced quenching (TrIQ) method. *Biochemistry*, *49*(45), 9722–9731. https://doi.org/10.1021/bi100907m

Mansoor, S. E., Mchaourab, H. S., & Farrens, D. L. (2002). Mapping proximity within proteins using fluorescence spectroscopy. A study of T4 lysozyme showing that tryptophan residues quench bimane fluorescence. *Biochemistry*, *41*(8), 2475–2484. https://doi.org/10.1021/bi011198i

Marmé, N., Knemeyer, J. P., Sauer, M., & Wolfrum, J. (2003). Inter- and Intramolecular Fluorescence Quenching of Organic Dyes by Tryptophan. *Bioconjugate Chemistry*, *14*(6), 1133–1139. https://doi.org/10.1021/bc0341324

Mazzanti, A., Maragna, R., Faragli, A., Monteforte, N., Bloise, R., Memmi, M., … Priori, S. G. (2016). Gene-specific therapy with mexiletine reduces arrhythmic events in patients with long QT syndrome type 3. *Journal of the American College of Cardiology*, *67*(9), 1053–1058. https://doi.org/10.1016/j.jacc.2015.12.033

Mazzanti, A., Maragna, R., Faragli, A., Monteforte, N., Bloise, R., Memmi, M., … Priori, S. G. (2016). Gene-specific therapy with mexiletine reduces arrhythmic events in patients with long QT syndrome type 3. *Journal of the American College of Cardiology*, *67*(9), 1053–1058. https://doi.org/10.1016/j.jacc.2015.12.033

Medeiros-Domingo, A., Kaku, T., Tester, D. J., Iturralde-Torres, P., Itty, A., Ye, B., … Ackerman, M. J. (2007). SCN4B-encoded sodium channel beta4 subunit in congenital long-QT syndrome. *Circulation*, *116*(2), 134–142. https://doi.org/10.1161/CIRCULATIONAHA.106.659086

Messner, D. J., & Catterall, W. A. (1985). The sodium channel from rat brain. Separation and characterization of subunits. *J Biol Chem*, *260*(19), 10597–10604. Retrieved from http://www.ncbi.nlm.nih.gov/entrez/query.fcgi?cmd=Retrieve&db=PubMed&dopt=Citation&list_uids=2411726

Moreno, J. D., Zhu, Z. I., Yang, P.-C., Bankston, J. R., Jeng, M.-T., Kang, C., … Clancy, C. E. (2011). A computational model to predict the effects of class I anti-arrhythmic drugs on ventricular rhythms. *Science Translational Medicine*, *3*(98), 98ra83. https://doi.org/10.1126/scitranslmed.3002588

Morgan, K., Stevens, E. B., Shah, B., Cox, P. J., Dixon, a K., Lee, K., … Jackson, a P. (2000a). Beta 3: an Additional Auxiliary Subunit of the Voltage-Sensitive Sodium Channel That Modulates Channel Gating With Distinct Kinetics. *Proceedings of the National Academy of Sciences of the United States of America*, *97*(5), 2308–2313. https://doi.org/10.1073/pnas.030362197

Morgan, K., Stevens, E. B., Shah, B., Cox, P. J., Dixon, A. K., Lee, K., … Jackson, A. P. (2000b). beta 3: an additional auxiliary subunit of the voltage-sensitive sodium channel that modulates channel gating with distinct kinetics. *Proceedings of the National Academy of Sciences of the United States of America*, *97*, 2308–2313. https://doi.org/10.1073/pnas.030362197

Muroi, Y., Arcisio-Miranda, M., Chowdhury, S., & Chanda, B. (2010). Molecular determinants of coupling between the domain III voltage sensor and pore of a sodium channel. *Nature Structural & Molecular Biology*, *17*(2), 230–237. https://doi.org/10.1038/nsmb.1749

Muroi, Y., & Chanda, B. (2009a). Local anesthetics disrupt energetic coupling between the voltage-sensing segments of a sodium channel. *The Journal of General Physiology*, *133*(1), 1–15. https://doi.org/10.1085/jgp.200810103

Muroi, Y., & Chanda, B. (2009b). Local anesthetics disrupt energetic coupling between the voltage-sensing segments of a sodium channel. *The Journal of General Physiology*, *133*(1), 1–15. https://doi.org/10.1085/jgp.200810103

Namadurai, S., Yereddi, N. R., Cusdin, F. S., Huang, C. L. H., Chirgadze, D. Y., & Jackson, A. P. (2015). A new look at sodium channel β subunits. *Open Biology*, *5*(1), 140192. https://doi.org/10.1098/rsob.140192

Nerbonne, J. M., & Kass, R. S. (2005). Molecular physiology of cardiac repolarization. *Physiological Reviews*. https://doi.org/10.1152/physrev.00002.2005

Okata, S., Yuasa, S., Suzuki, T., Ito, S., Makita, N., Yoshida, T., … Fukuda, K. (2016). Embryonic type Na+ channel β-subunit, SCN3B masks the disease phenotype of Brugada syndrome. *Scientific Reports*, *6*, 34198. Retrieved from http://dx.doi.org/10.1038/srep34198

Olesen, M. S., Jespersen, T., Nielsen, J. B., Liang, B., Moller, D. V, Hedley, P., … Svendsen, J. H. (2011). Mutations in sodium channel beta-subunit SCN3B are associated with early-onset lone atrial fibrillation. *Cardiovasc.Res.*, *89*(1755–3245 (Electronic)), 786–793. https://doi.org/10.1093/cvr/cvq348

Olesen, M. S., Nielsen, M. W., Haunsø, S., & Svendsen, J. H. (2014). Atrial fibrillation: the role of common and rare genetic variants. *European Journal of Human Genetics : EJHG*, *22*, 297–306. https://doi.org/10.1038/ejhg.2013.139

Pantazis, A., & Olcese, R. (2012). Relative transmembrane segment rearrangements during BK channel activation resolved by structurally assigned fluorophore-quencher pairing. *The Journal of General Physiology*. https://doi.org/10.1085/jgp.201210807

Pantazis, A., & Olcese, R. (2013). Cut-open Oocyte Voltage Clamp Technique. In *In Encyclopedia of Biophysics. Roberts GCK, ed.* (pp. 406–413). Springer Berlin Heidelberg.

Patino, G. A., Brackenbury, W. J., Bao, Y., Lopez-Santiago, L. F., O'Malley, H. A., Chen, C., … Isom, L. L. (2011). Voltage-Gated Na+ Channel 1B: A Secreted Cell Adhesion Molecule Involved in Human Epilepsy. *Journal of Neuroscience*. https://doi.org/10.1523/JNEUROSCI.0361-11.2011

Priori, S. G., Blomström-Lundqvist, C., & Mazzanti, A. (2015). 2015 ESC Guidelines for the management of patients with ventricular arrhythmias and the prevention of sudden cardiac death. *European Heart Journal*, *8*(9), 746–837. https://doi.org/10.1093/europace/eul108

Qin, N., Yagel, S., Momplaisir, M.-L., Codd, E. E., & D'Andrea, M. R. (2002). Molecular cloning and characterization of the human voltage-gated calcium channel alpha(2)delta-4 subunit. *Molecular Pharmacology*, *62*(3), 485–496. https://doi.org/10.1016/0896-6273(91)90072-8

Ragsdale, D. S., McPhee, J. C., Scheuer, T., & Catterall, W. A. (1994). Molecular determinants of state-dependent block of Na+ channels by local anesthetics. *Science (New York, N.Y.)*, *265*(5179), 1724–1728. https://doi.org/10.1126/science.8085162

Ragsdale, D. S., McPhee, J. C., Scheuer, T., & Catterall, W. A. (1996). Common molecular determinants of local anesthetic, antiarrhythmic, and anticonvulsant block of voltage-gated Na+ channels. *Proceedings of the National Academy of Sciences of the United States of America*, *93*, 9270–9275. https://doi.org/10.1073/pnas.93.17.9270

Riuró, H., Campuzano, O., Arbelo, E., Iglesias, A., Batlle, M., Pérez-Villa, F., … Brugada, R. (2014). A missense mutation in the sodium channel β1b subunit reveals SCN1B as a susceptibility gene underlying long QT syndrome. *Heart Rhythm : The Official Journal of the Heart Rhythm Society*, *11*(7), 1202–1209. https://doi.org/10.1016/j.hrthm.2014.03.044

Ruan, Y., Liu, N., Bloise, R., Napolitano, C., & Priori, S. G. (2007). Gating properties of SCN5A mutations and the response to mexiletine in long-QT syndrome type 3 patients. *Circulation*, *116*(10), 1137–1144. https://doi.org/10.1161/CIRCULATIONAHA.107.707877

Rudokas, M. W., Varga, Z., Schubert, A. R., Asaro, A. B., & Silva, J. R. (2014). The Xenopus

Oocyte Cut-open Vaseline Gap Voltage-clamp Technique With Fluorometry. *Journal of Visualized Experiments*, *85*, 1–11. https://doi.org/10.3791/51040

Schwartz, P. J., Priori, S. G., Spazzolini, C., Moss, A. J., Vincent, G. M., Napolitano, C., … Coumel, P. (2001). Genotype-phenotype correlation in the long-QT syndrome: gene-specific triggers for life-threatening arrhythmias. *Circulation*, *103*(1), 89–95. https://doi.org/10.1161/01.CIR.103.1.89

Seoh, S. A., Sigg, D., Papazian, D. M., & Bezanilla, F. (1996). Voltage-sensing residues in the S2 and S4 segments of the Shaker K+ channel. *Neuron*, *16*(6), 1159–1167. https://doi.org/10.1016/S0896-6273(00)80142-7

Sheets, M. F., Fozzard, H. A., & Hanck, D. A. (2015). Important Role of Asparagines in Coupling the Pore and Votage-Sensor Domain in Voltage-Gated Sodium Channels. *Biophysical Journal*, *109*(11), 2277–2286. https://doi.org/10.1016/j.bpj.2015.10.012

Sheets, M. F., & Hanck, D. A. (2003). Molecular Action of Lidocaine on the Voltage Sensors of Sodium Channels. *The Journal of General Physiology*, *121*(2), 163–175. https://doi.org/10.1085/jgp.20028651

Sheets, M. F., & Hanck, D. a. (2005). Charge immobilization of the voltage sensor in domain IV is independent of sodium current inactivation. *The Journal of Physiology*, *563*(Pt 1), 83–93. https://doi.org/10.1113/jphysiol.2004.077644

Shen, H., Zhou, Q., Pan, X., Li, Z., Wu, J., & Yan, N. (2017). Structure of a eukaryotic voltage-gated sodium channel at near-atomic resolution. *Science (New York, N.Y.)*, *355*(6328). https://doi.org/10.1126/science.aal4326

Shimizu, W., & Antzelevitch, C. (2000). Differential effects of beta-adrenergic agonists and antagonist in LQT1, LQT2 and LQT3 models of the long QT syndrome. *Journal of the American College of Cardiology*, *35*(3), 778–786. https://doi.org/10.1016/S0735-1097(99)00582-3

Siefani, E., & Bezanilla, F. (1998). Cut-open oocyte voltage-clamp technique. *Methods in Enzymology*. https://doi.org/10.1016/S0076-6879(98)93020-8

Silva, J. R., & Goldstein, S. a N. (2013a). Voltage-sensor movements describe slow inactivation of voltage-gated sodium channels I: wild-type skeletal muscle Na(V)1.4. *The Journal of General Physiology*, *141*(3), 309–321. https://doi.org/10.1085/jgp.201210909

Silva, J. R., & Goldstein, S. a N. (2013b). Voltage-sensor movements describe slow inactivation of voltage-gated sodium channels I: Wild-type skeletal muscle NaV1.4. *The Journal of General Physiology*, *141*(3), 309–321. https://doi.org/10.1085/jgp.201210909

Silva, J. R., & Goldstein, S. a N. (2013c). Voltage-sensor movements describe slow inactivation of voltage-gated sodium channels II: a periodic paralysis mutation in Na(V)1.4 (L689I). *The Journal of General Physiology*, *141*(3), 323–334. https://doi.org/10.1085/jgp.201210910

Spampanato, J., Kearney, J. a, de Haan, G., McEwen, D. P., Escayg, a, Aradi, I., … Meisler, M.

H. (2004a). A novel epilepsy mutation in the sodium channel SCN1A identifies a cytoplasmic domain for beta subunit interaction. *The Journal of Neuroscience : The Official Journal of the Society for Neuroscience*, *24*(44), 10022–10034. https://doi.org/10.1523/JNEUROSCI.2034-04.2004

Spampanato, J., Kearney, J. a, de Haan, G., McEwen, D. P., Escayg, A., Aradi, I., … Meisler, M. H. (2004b). A Novel Epilepsy Mutation in the Sodium Channel SCN1A Identifies a Cytoplasmic Domain for Subunit Interaction. *The Journal of Neuroscience : The Official Journal of the Society for Neuroscience*, *24*(44), 10022–10034. https://doi.org/10.1523/JNEUROSCI.2034-04.2004

Uebachs, M., Opitz, T., Royeck, M., Dickhof, G., Horstmann, M.-T., Isom, L. L., & Beck, H. (2010). Efficacy loss of the anticonvulsant carbamazepine in mice lacking sodium channel beta subunits via paradoxical effects on persistent sodium currents. *The Journal of Neuroscience : The Official Journal of the Society for Neuroscience*, *30*(25), 8489–8501. https://doi.org/10.1523/JNEUROSCI.1534-10.2010

Vaiana, A. C., Neuweiler, H., Schulz, A., Wolfrum, J., Sauer, M., & Smith, J. C. (2003). Fluorescence Quenching of Dyes by Tryptophan: Interactions at Atomic Detail from Combination of Experiment and Computer Simulation. *Journal of the American Chemical Society*, *125*(47), 14564–14572. https://doi.org/10.1021/ja036082j

Varga, Z., Zhu, W., Schubert, A. R., Pardieck, J. L., Krumholz, A., Hsu, E. J., … Silva, J. R. (2015). Direct Measurement of Cardiac Na^+ Channel Conformations Reveals Molecular Pathologies of Inherited Mutations. *Circulation: Arrhythmia and Electrophysiology*, CIRCEP.115.003155. https://doi.org/10.1161/CIRCEP.115.003155

Vaughan Williams, E. M. (1970). The experimental basis for the choice of an anti-arrhythmic drug. *Advances in Cardiology*, *4*, 275–289.

Wang, D. W., Yazawa, K., Makita, N., George, A. L., & Bennett, P. B. (1997). Pharmacological targeting of long QT mutant sodium channels. *Journal of Clinical Investigation*, *99*(7), 1714–1720. https://doi.org/10.1172/JCI119335

Wang, H.-G., Zhu, W., Kanter, R. J., Silva, J. R., Honeywell, C., Gow, R. M., & Pitt, G. S. (2016). A Novel NaV1.5 Voltage Sensor Mutation Associated with Severe Atrial and Ventricular Arrhythmias. *Journal of Molecular and Cellular Cardiology*, *92*, 52–62. https://doi.org/10.1016/j.yjmcc.2016.01.014

Watanabe, H., Darbar, D., Kaiser, D. W., Jiramongkolchai, K., Chopra, S., Donahue, B. S., … Roden, D. M. (2009). Mutations in Sodium Channel β1- and β2-Subunits Associated With Atrial Fibrillation. *Circulation: Arrhythmia and Electrophysiology*, *2*(3). https://doi.org/10.1161/CIRCEP.108.779181

Watanabe, H., Darbar, D., Kaiser, D. W., Jiramongkolchai, K., Chopra, S., Donahue, B. S., … Roden, D. M. (2009). Mutations in Sodium Channel β1- and β2-Subunits Associated With Atrial Fibrillation. *Circulation: Arrhythmia and Electrophysiology*, *2*(3), 268–275. https://doi.org/10.1161/CIRCEP.108.779181

Watanabe, H., Koopmann, T. T., Le Scouarnec, S., Yang, T., Ingram, C. R., Schott, J.-J., … Bezzina, C. R. (2008). Sodium channel β1 subunit mutations associated with Brugada syndrome and cardiac conduction disease in humans. *The Journal of Clinical Investigation*, *118*(6), 2260–2268. https://doi.org/10.1172/JCI33891

West, J. W., Patton, D. E., Scheuer, T., Wang, Y., Goldin, A. L., & Catterall, W. A. (1992). A cluster of hydrophobic amino acid residues required for fast Na(+)-channel inactivation. *Proceedings of the National Academy of Sciences of the United States of America*, *89*(22), 10910–10914. https://doi.org/10.1073/pnas.89.22.10910

Xu, R., Thomas, E. A., Gazina, E. V., Richards, K. L., Quick, M., Wallace, R. H., … Petrou, S. (2007). Generalized epilepsy with febrile seizures plus-associated sodium channel ??1 subunit mutations severely reduce beta subunit-mediated modulation of sodium channel function. *Neuroscience*, *148*(1), 164–174. https://doi.org/10.1016/j.neuroscience.2007.05.038

Yan, Z., Zhou, Q., Wang, L., Wu, J., Zhao, Y., Huang, G., … Yan, N. (2017). Structure of the Nav1.4-β1 Complex from Electric Eel. *Cell*. https://doi.org/10.1016/j.cell.2017.06.039

Yereddi, N. R., Cusdin, F. S., Namadurai, S., Packman, L. C., Monie, T. P., Slavny, P., … Jackson, A. P. (2013). The immunoglobulin domain of the sodium channel beta3 subunit contains a surface-localized disulfide bond that is required for homophilic binding. *FASEB Journal*, *27*(2), 568–580. https://doi.org/10.1096/fj.12-209445

Yu, F. H., Westenbroek, R. E., Silos-Santiago, I., McCormick, K. A., Lawson, D., Ge, P., … Curtis, R. (2003). Sodium channel beta4, a new disulfide-linked auxiliary subunit with similarity to beta2. *The Journal of Neuroscience : The Official Journal of the Society for Neuroscience*, *23*, 7577–7585. https://doi.org/23/20/7577 [pii]

Yuan, L., Koivumäki, J. T., Liang, B., Lorentzen, L. G., Tang, C., Andersen, M. N., … Jespersen, T. (2014). Investigations of the Navβ1b sodium channel subunit in human ventricle; functional characterization of the H162P Brugada syndrome mutant. *American Journal of Physiology. Heart and Circulatory Physiology*, *306*(8), H1204-12. https://doi.org/10.1152/ajpheart.00405.2013

Zehender, M., Geibel, A., Treese, N., Hohnloser, S., Meinertz, T., & Just, H. (1988). Prediction of efficacy and tolerance of oral mexiletine by intravenous lidocaine application. *Clinical Pharmacology and Therapeutics*, *44*(4).

Zhu, W., Varga, Z., & Silva, J. R. (2016). Molecular motions that shape the cardiac action potential : Insights from voltage clamp fl uorometry. *Progress in Biophysics and Molecular Biology*, 1–15. https://doi.org/10.1016/j.pbiomolbio.2015.12.003

Zhu, W., Voelker, T. L., Varga, Z., Schubert, A. R., Nerbonne, J. M., & Silva, J. R. (2017). Mechanisms of noncovalent β subunit regulation of Na $_V$ channel gating. *The Journal of General Physiology*, *149*(8), 813–831. https://doi.org/10.1085/jgp.201711802

Zimetbaum, P. (2012). Antiarrhythmic drug therapy for atrial fibrillation. *Circulation*. https://doi.org/10.1161/CIRCULATIONAHA.111.019927

Zipes, D. P., & Jalife, J. (2013). *Cardiac Electrophysiology: From Cell to Bedside: Sixth Edition*. *Cardiac Electrophysiology: From Cell to Bedside: Sixth Edition*. https://doi.org/10.1016/C2011-0-06826-6

Zygmunt, a. C., Nesterenko, V. V., Rajamani, S., Hu, D., Barajas-Martinez, H., Belardinelli, L., & Antzelevitch, C. (2011). Mechanisms of atrial-selective block of Na+ channels by ranolazine: I. Experimental analysis of the use-dependent block. *AJP: Heart and Circulatory Physiology*, *301*(4), H1606–H1614. https://doi.org/10.1152/ajpheart.00242.2011